VOLUME 37 SEPTEMBER 1959 NUMBER 9

Canadian Journal of Physics

Editor: H. E. DUCKWORTH

Associate Editors:

L. G. ELLIOTT, *Atomic Energy of Canada, Ltd., Chalk River*
J. S. FOSTER, *McGill University*
G. HERZBERG, *National Research Council of Canada*
L. LEPRINCE-RINGUET, *Ecole Polytechnique, Paris*
B. W. SARGENT, *Queen's University*
G. M. VOLKOFF, *University of British Columbia*
W. H. WATSON, *University of Toronto*
G. A. WOONTON, *McGill University*

Published by THE NATIONAL RESEARCH COUNCIL

OTTAWA CANADA

V37 I9 SEP 59

UMI

CANADIAN JOURNAL OF PHYSICS

Under the authority of the Chairman of the Committee of the Privy Council on Scientific and Industrial Research, the National Research Council issues THE CANADIAN JOURNAL OF PHYSICS and five other journals devoted to the publication, in English or French, of the results of original scientific research. Matters of general policy concerning these journals are the responsibility of a joint Editorial Board consisting of: members representing the National Research Council of Canada; the Editors of the Journals; and members representing the Royal Society of Canada and four other scientific societies.

EDITORIAL BOARD

Representatives of the National Research Council

I. McT. Cowan, *University of British Columbia*
A. Gauthier, *University of Montreal*
H. G. Thode (Chairman), *McMaster University*
D. L. Thomson, *McGill University*

Editors of the Journals

D. L. Bailey, *University of Toronto*
T. W. M. Cameron, *Macdonald College*
H. E. Duckworth, *McMaster University*
K. A. C. Elliott, *Montreal Neurological Institute*
Léo Marion, *National Research Council*
R. G. E. Murray, *University of Western Ontario*

Representatives of Societies

D. L. Bailey, *University of Toronto*
Royal Society of Canada
T. W. M. Cameron, *Macdonald College*
Royal Society of Canada
H. E. Duckworth, *McMaster University*
Royal Society of Canada
Canadian Association of Physicists
K. A. C. Elliott, *Montreal Neurological Institute*
Canadian Physiological Society
P. R. Gendron, *University of Ottawa*
Chemical Institute of Canada
R. G. E. Murray, *University of Western Ontario*
Canadian Society of Microbiologists
T. Thorvaldson, *University of Saskatchewan*
Royal Society of Canada

Ex officio

Léo Marion (Editor-in-Chief), *National Research Council*
J. B. Marshall (Administration and Awards), *National Research Council*

Manuscripts for publication should be submitted to Dr. H. E. Duckworth, Editor, Canadian Journal of Physics, Hamilton College, McMaster University, Hamilton, Ontario.
For instructions on preparation of copy, see **NOTES TO CONTRIBUTORS** (back cover).

Proof, correspondence concerning proof, and orders for reprints should be sent to the Manager, Editorial Office (Research Journals), Division of Administration and Awards, National Research Council, Ottawa 2, Canada.

Subscriptions, renewals, requests for single or back numbers, and all remittances should be sent to Division of Administration and Awards, National Research Council, Ottawa 2, Canada. Remittances should be made payable to the Receiver General of Canada, credit National Research Council.

The journals published, frequency of publication, and prices are:

Canadian Journal of Biochemistry and Physiology	Monthly	$9.00 a year
Canadian Journal of Botany	Bimonthly	$6.00 a year
Canadian Journal of Chemistry	Monthly	$12.00 a year
Canadian Journal of Microbiology	Bimonthly	$6.00 a year
Canadian Journal of Physics	Monthly	$9.00 a year
Canadian Journal of Zoology	Bimonthly	$5.00 a year

The price of regular single numbers of all journals is $2.00.

Canadian Journal of Physics

Issued by THE NATIONAL RESEARCH COUNCIL OF CANADA

VOLUME 37 SEPTEMBER 1959 NUMBER 9

SCATTERING FACTORS FOR SOME OF THE HEAVIER ATOMS[1]

BEATRICE H. WORSLEY

ABSTRACT

A program for calculating X-ray atomic scattering factors from the radial wave functions has been written for the IBM 650 installation at the University of Toronto. It has been applied to the results of self-consistent field calculations previously performed at this University on the FERUT computer. Results are given for Ne, V^{++}, Kr, Ag^{+}, and Pb^{+++}. The results for Ne and V^{++} are compared with those calculated by Freeman using Allen's wave functions for Ne and Hartree's approximate wave functions for V^{++}.

INTRODUCTION

As new Hartree–Fock radial wave functions become available, it becomes possible to derive functions which can more readily be compared with experimental results. Such a function is the X-ray scattering factor for coherent radiation, which is of particular interest to crystallographers. It has been described by Hoerni and Ibers (1954). This function has been calculated for several specific cases by hand and also with the aid of automatic digital computers. Just recently it has been calculated for 45 different atoms and ions by Freeman (1959) using the Whirlwind computer at M.I.T.

A program has been written at the University of Toronto for the IBM 650 installation to calculate the atomic scattering factor for a spherical charge distribution, given the appropriate set of radial wave functions. This program has been applied to the self-consistent fields with exchange for Ne (Worsley 1958*a*) and for V^{++}, Kr, and Ag^{+} (Worsley 1958*b*). It has also been applied to the less accurate self-consistent field without exchange for Pb^{+++} (Hart and Worsley 1959).

THE PROGRAM

Assuming that the electron density is spherically symmetric and averaging over all orientations, Hoerni and Ibers (1954) give, for the definition of the atomic scattering factor:

$$f(s) = \int_0^{\infty} \sum_{\substack{\text{all} \\ \text{electrons}}} \{P^2(r) \sin sr/sr\} dr,$$

[1]Manuscript received April 30, 1959.
Contribution from the Computation Centre, McLennan Laboratory, University of Toronto, Toronto, Ontario.

where the $P(r)$'s are the radial wave functions and $s = 4\pi\lambda^{-1} \sin\theta$ is the magnitude of the radiation vector in reciprocal space, s being treated as a parameter.

To be readily applicable to the wave functions calculated by FERUT, the present program was designed to evaluate this function in the form

$$f(s) = \int_{\rho=0}^{100\delta\rho} \sum_{\substack{\text{all} \\ \text{electrons}}} \{P^2(\rho) \sin sr/s\} d\rho,$$

where the P's are supplied at equal intervals of the logarithmic variable $\rho = \ln cr$. For each application it should be verified that $\rho = 0$ is an adequate approximation to $\rho = -\infty$, and $\rho = 100\delta\rho$ to $\rho = +\infty$ in the sense that contributions to the integral outside the range $0 \leqslant \rho \leqslant 100\delta\rho$ are negligible. Provision is made for introducing c and $\delta\rho$ as well as s into the program as parameters. Furthermore, the program will handle a configuration with as many as 16 different wave functions. Newton's three-eighth's rule is used to evaluate the integral. It is modified in such a way that, in effect, the half-interval is used, the values of the integrand at the mid-points being evaluated by linear interpolation.

RESULTS

Results of the current application of this program are given in Table I. The errors are indicated, on the assumption that the input wave functions

TABLE I

Values of the atomic scattering factors

$\sin\theta/\lambda$ Å^{-1}	Ne, $f\pm0.003$	V^{++}, $f\pm0.01$	Kr, $f\pm0.01$	Ag^{+}, $f\pm0.01$	Pb^{+++},* $f\pm0.1$
0.00	10.000	21.00	36.00	46.00	79.0
0.05	9.832	20.70	35.30	45.38	78.3
0.10	9.351	19.86	33.45	43.68	76.0
0.15	8.643	18.62	31.00	41.20	72.6
0.20	7.804	17.15	28.47	38.31	68.8
0.25	6.926	15.60	26.15	35.33	64.8
0.30	6.077	14.10	24.12	32.48	60.9
0.35	5.300	12.72	22.37	29.89	57.2
0.40	4.614	11.51	20.83	27.63	53.8
0.50	3.531	9.61	18.15	24.02	47.9
0.60	2.786	8.33	15.81	21.42	43.1
0.70	2.292	7.47	13.73	19.48	39.0
0.80	1.968	6.86	11.95	17.89	35.5
0.90	1.754	6.38	10.46	16.48	32.3
1.00	1.607	5.94	9.26	15.14	29.4
1.10	1.500	5.52	8.32	13.86	26.7
1.20	1.416	5.10	7.59	12.63	24.4
1.30	1.344	4.69	7.03	11.48	22.3
1.50	1.216	3.91	6.25	9.50	19.1
1.70	1.099	3.24	5.69	7.98	16.8
1.90	0.981	2.69	5.23	6.90	15.2

*Wave functions without exchange.

are correct. It should be noted that the sine term modulates somewhat rapidly for the higher values of s. Nevertheless, it seemed worth while to include these in the calculations.

In all cases of functions derived from atomic wave functions, the accuracy of the latter should be taken into account. This accuracy depends upon the closeness of the formulation to the physics of the system and upon the numerical errors introduced in the course of the calculation. In the case of the results in Table I, the errors of calculation of the wave functions are overridden by the errors in the calculation of the scattering factors, so that the results should reflect the closeness of the Hartree–Fock formulation to the physical picture.

The values for Ne and V^{++} have been compared with those recently published by Freeman (1959). In the case of Ne, Freeman used L. C. Allen's unpublished wave functions, and the maximum discrepancy in the scattering factors is 0.4%. For V^{++}, Freeman used the approximate wave functions published by Hartree (1956), and the discrepancies are correspondingly greater. These amount to as much as 7% at $\sin\theta/\lambda = 1.00$, or as much as 0.80 $Å^{-1}$ units at $\sin\theta/\lambda = 0.40$. The present values reflect the higher accuracy of the FERUT wave functions. Finally, it has been reported by Ibers (1959) that the results for Pb^{+++} are in good agreement with values based on calculations for the Thomas–Fermi–Dirac model.

ACKNOWLEDGMENTS

These calculations were performed at the suggestion of Dr. James A. Ibers of the Shell Development Company, Emeryville, California, to supplement the work currently being done by Freeman (1959) and others. The results are being contributed to Volume III of the *International Tables for X-Ray Crystallography*. The author wishes to thank Dr. Ibers for his continued interest, and also to express gratitude for the facilities made available by the Director of the Computation Centre.

REFERENCES

FREEMAN, A. J. 1959. Acta Cryst. **12**, 261.
HART, J. F. and WORSLEY, B. H. 1959. Can. J. Phys. **37**, 983.
HARTREE, D. R. 1956. J. Opt. Soc. Am. **46** (5), 350.
HOERNI, J. A. and IBERS, J. A. 1954. Acta Cryst. **7**, 744.
IBERS, J. A. 1959. Private communication.
WORSLEY, B. H. 1958*a*. Can. J. Phys. **36**, 289.
——— 1958*b*. Proc. Roy. Soc. A, **247**, 390.

THE ONSET TIMES OF FORBUSH-TYPE COSMIC RAY INTENSITY DECREASES[1]

A. G. FENTON,[2] K. G. MCCRACKEN,[2] D. C. ROSE, AND B. G. WILSON[3]

ABSTRACT

The onset times of a number of Forbush-type decreases observed at four widely spaced stations are compared, and it is shown that appreciable differences occur. The stations selected were Hobart, Mawson, Ottawa, and Sulphur Mountain. It was found that a consistent pattern is obtained for the events studied when the onset times are plotted as a function of the direction of maximum sensitivity of the recorders relative to the earth–sun line. This is interpreted as being due to a directional anisotropy that exists in the mechanism producing the decreases, at least in the early stages. The depression occurs first for particles arriving from directions between 30° and 120° west of the earth–sun line. The relation between these observations and geomagnetic disturbances and the quiet-day daily variation is discussed.

INTRODUCTION

It was mentioned briefly in a recent paper (Fenton, McCracken, Rose, and Wilson 1959) that an examination of the hourly intensities at widely separated stations has revealed obvious differences in response to Forbush-type decreases, and that these differences appear to be at least partly due to primary anisotropies which are detected at different times and directions in space as the earth rotates. In this report we shall consider in some detail the time dependency of the commencements of a number of events of this type observed at the stations operated by the Ottawa and Hobart groups during recent years of high solar activity. During this period data were obtained from high counting rate recorders developed for the International Geophysical Year 1957–58, enabling the analysis of individual events at reasonable counting statistics, thus avoiding recourse to the procedure of averaging over a number of events.

Data from four widely spaced stations, namely, Hobart, Mawson, Ottawa, and Sulphur Mountain, will be presented and examined for evidence of a consistent pattern in the intensity–time changes at the commencement of Forbush-type decreases. If it exists, such a pattern would be expected to provide important information concerning the space–time behavior of the agency responsible for these transient cosmic ray intensity decreases. At the present state of knowledge of the mechanisms involved we are of the opinion that much can be gained by a phenomenological approach to these problems, using the currently available data of adequate statistical accuracy in hourly values, in order to establish firmly the essential features upon which a sound physical explanation may be based.

[1]Manuscript received June 2, 1959.
Contribution from the Department of Physics, University of Tasmania, Hobart, and the Division of Pure Physics, National Research Council, Ottawa, Canada.
Issued as N.R.C. No. 5274.
[2]Department of Physics, University of Tasmania, Hobart, Tasmania.
[3]National Research Council Sulphur Mountain Laboratory, Banff, Alberta.

THE DEPENDENCE OF ONSET TIMES UPON STATION CO-ORDINATES

Examination of the hourly intensities from widely separated stations, plotted as a function of universal time, reveals that there are obvious differences in the observed onset time of many Forbush-type decreases. Also, these differences seem to depend more on the station longitudes than on their latitudes. Sample events to illustrate this are shown in Fig. 1, in which are plotted the intensities observed at a number of stations. The co-ordinates of

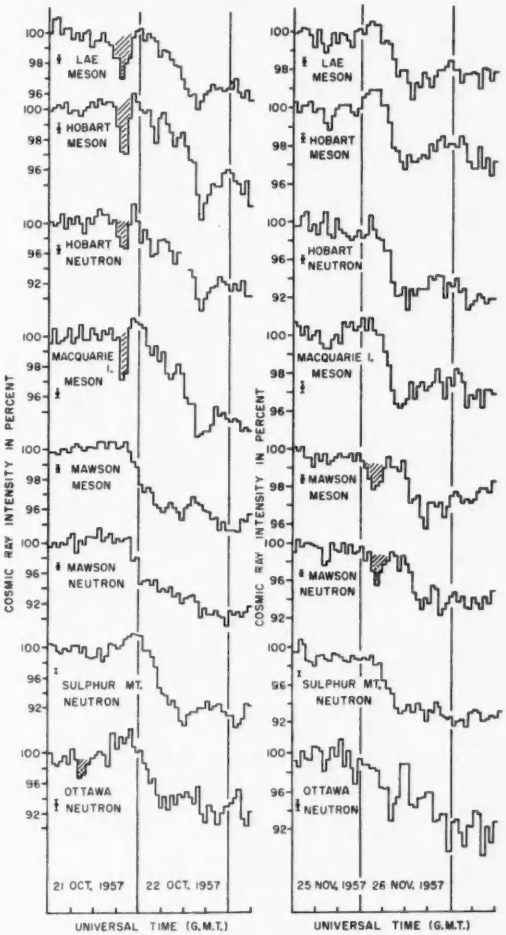

FIG. 1. The pressure-corrected data obtained during the initial phases of the Forbush-type decreases occurring on 21 October, 1957, and 26 November, 1957.

stations* operated by the Ottawa and Hobart cosmic ray groups have been set out previously (Fenton, McCracken, Rose, and Wilson 1959). It may be noted that there is a close similarity between intensity–time plots for data from the stations lying within a narrow longitude zone, namely, Hobart, Macquarie Island, and Lae. On the other hand, the Mawson, Ottawa, and Sulphur Mountain results have quite a different appearance.

Associated with some events there is a clearly distinguishable short-lived decrease which occurs before the main decrease. Cases of this phenomenon are included in Fig. 1; for example, it occurred at Hobart during the October 21 event and at Mawson during the November 26 event. One of these short-lived transient decreases has been described recently (McCracken and Parsons 1958) as a "preliminary decrease" associated with the October 21 event. As will be pointed out below, this type of intensity change has been observed on a number of occasions at one or more of our stations, so it is by no means a rare phenomenon. In fact, it seems likely that the mechanism responsible for this type of variation is present, to a greater or lesser extent, during the early stages of all Forbush-type events.

Following the technique used previously (Fenton, McCracken, Rose, and Wilson 1959) to study the superposition of transient decreases, the event of November 26, 1957, has been examined as it appears in the average of the intensities recorded at Hobart, Mawson, Ottawa, and Sulphur Mountain. This procedure is expected to give an approximation to the decrease that would be observed by an omnidirectional (4π) detector placed at the position of the earth, and thus able to detect temporal changes in the depressive mechanism, independently of scanning effects. In the averaging process each station was allotted equal weight, irrespective of counting rate. No allowance was made for the effect of the different station altitudes upon the observed event amplitude. Although recent work has shown that correction for altitude is desirable for some studies (McCracken and Johns 1959), neglect of this is not serious in the present analysis. The average response at the four stations during the November 26 event is plotted in Fig. 2, which shows that the

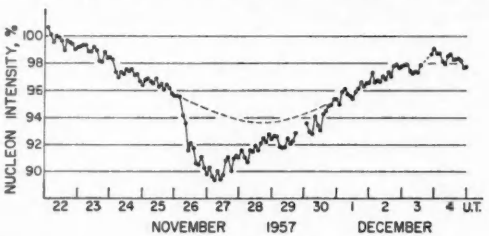

FIG. 2. Average nucleon intensities observed at four stations during November 26 event, 1957, expressed as percentages of the mean intensity observed on November 21.

*Co-ordinates of stations reported here:

	Latitude	Longitude
Ottawa	45.4 N.	75.6 W.
Sulphur Mountain	51.1 N.	115.6 W.
Hobart	42.8 S.	147.5 E.
Mawson	67.6 S.	62.9 E.

event may be regarded as a rather slow change upon which is superimposed a more rapid short-lived event. This type of analysis has been made for other events, and generally leads to a smoothing of the intensity–time plot. This suggests that the variation in the time of commencement, the rate of change of intensity, and the general appearance of the intensity–time plot for Forbush-type decreases are due to the directional sensitivity of the recorders and asymmetries in the agency responsible for the decreases, made evident by the rotation of the earth. In other words, the integral effect at the earth due to the cosmic ray intensity-reducing agency varies more smoothly with time than is apparent from the records at a single station.

Intensity–time plots similar to those of Fig. 1 have been prepared for events observed between August 1956 and December 1958. Information from events of amplitude about 4% or greater is summarized in Table I. During

TABLE I

The times of commencement of Forbush-type decreases (or of the preliminary phases of these events when identified) are given for four stations, together with the magnetic storm sudden commencements to which the decreases may be related

	Hour of commencement, U.T.					
Date of event	Hobart	Ottawa	Mawson	Sulphur Mt.	S.S.C., U.T.	Preliminary decrease observed at:
20 Aug. 1956	16	09 (T)	01 (21st) (T)			Hobart, Mawson, Ottawa
9 Nov. 1956	02 (10th)	23	22 (T)		2000	
25 Dec. 1956	11	03	12 (T)		0800	
21 Jan. 1957	21	21	19 (T)		1230	
10 Mar. 1957	09	05	00 (T)		0030	
17 Apr. 1957	08	00	11		1130	
22 June 1957	08	04	04	07		
3 Aug. 1957	13	24	16	15	1600	Four stations
29 Aug. 1957	21	23	20	21	1930	
29 Sept. 1957	04	06 (28th)	02	04	0030	Mawson, Ottawa
21 Oct. 1957	19	09	23	02 (22nd)	2330	Hobart, Ottawa
26 Nov. 1957	07	05	04	06		Mawson
11 Feb. 1958	03	02	03	02	0130	
25 Mar. 1958	12	16	14	19	1630	
9 May 1958	10	08	05	09		
29 May 1958	12 (28th)	04	07	04		Hobart
28 June 1958	14	09	15	01		
8 July 1958	12 (7th)	10 (7th)	21 (7th)	10	0800	Hobart, Ottawa, Mawson
17 Aug. 1958	06	05	06	01	0730	Hobart, Ottawa, Sulphur Mt.
24 Aug. 1958	19 (23rd)	04	01	03	0300	Hobart
15 Sept. 1958	16	09	23	03 (16th)		Ottawa
22 Oct. 1958	24	23	03 (23rd)	23	0330	

NOTE: Times corresponding to neutron monitor data are given except where indicated by the letter T for meson telescope. Blank spaces indicate equipment not operating, S.S.C. not observed or preliminary decrease not identified. Hour 24 refers to the intensity observed between 2300 and 2400 hours U.T. Hour 00 indicates hour 24 of the previous day.

preparation of this table the onset time of a Forbush-type decrease has been defined as the first hour of the decreasing phase of the event during which the intensity was more than two standard deviations below the pre-event level. The onset time listed is that of the preliminary decrease where such a decrease is clearly connected with the event. It is sometimes difficult to decide

upon a pre-event level if there are concurrent intensity changes other than statistical fluctuations. In such cases a smooth curve was drawn through the points prior to the first obviously decreasing phase of the event. On some occasions there is a pronounced maximum intensity just before the decrease begins. It is not known whether this is a significant feature or whether it arises simply because of recovery from earlier transient decreases. Throughout the present investigation nucleon intensity data corrected for pressure have been used in preference to meson data, although the latter have been employed to provide supporting evidence when determining onset times, or to permit the use of events that occurred before neutron monitors were in operation at all four stations. There is an indication that the onset times at a given station are not always the same for the nucleon and meson components, but the time difference is small, if genuine, and is not likely to influence the conclusions of this paper.

Onset-time differences amounting to many hours are apparent from Table I and Fig. 1. Errors in the determination of onset time have not been assigned, but would appear to vary from 0 to 2 or 3 hours depending on the abruptness of the event and the counting rate.

THE DIRECTIONAL SENSITIVITY OF THE RECORDERS

In what follows, we take the view that the asymmetries resulting in the rapid changes in intensity, as the earth rotates, are situated outside the region occupied by the earth's magnetic field. The justification for this assumption is the observation of a number of preliminary depressions and Forbush decreases beginning prior to the commencement of the accompanying magnetic storm. This suggests that the corpuscular matter responsible for the magnetic storm, while outside the region occupied by the geomagnetic field, is able to affect the cosmic ray intensity at the earth.

The particles detected by a neutron monitor are due to primaries arriving from within a cone of acceptance of rather small solid angle compared with 4π, so that as the earth rotates the recorder scans a region of space determined by the location of the recording station and geophysical factors. Thus a daily survey of the intensity arriving from different directions relative to the earth–sun line is obtained by selecting data from stations at different latitudes. If sufficient stations at different longitudes as well as latitudes are selected, a practically continuous survey of all regions is possible.

When determining the cone of acceptance of a recorder it is necessary to take into account the shape of the primary spectrum and the deflection of charged particles in the earth's magnetic field. In addition there are effects due to the properties of the nucleon cascades in the atmosphere (the specific yield function) and geometrical factors.

Taking all these factors into account, the dependence of counting rate upon direction has been determined for a number of stations, the dependence of counting rate upon geographic longitude for the stations considered in this paper being given in Fig. 3. In the calculation of these curves, the published data on the deflection of cosmic rays in a dipole field (Brunberg 1953; Brunberg and Dattner 1953; Jory 1956), and the coupling constants appropriate

to the neutron component (Dorman 1957), have been used. A description of the derivation of these curves will be given in a later paper.

It will be seen from Fig. 3 that the direction of maximum response of a neutron monitor is not at a fixed angular distance from the meridian plane

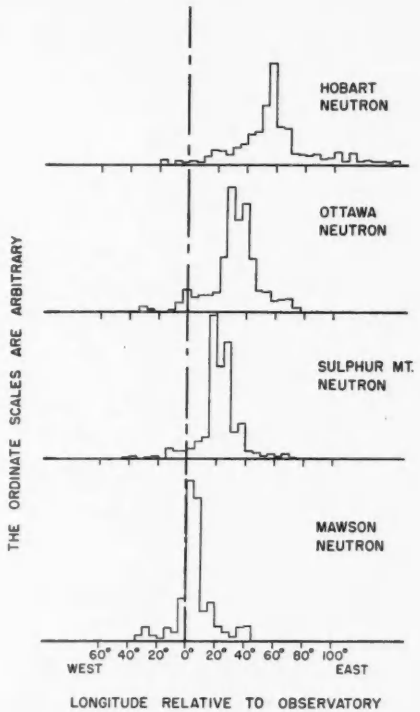

FIG. 3. The contributions made to the total counting rates of four different neutron monitors as functions of asymptotic longitude. Longitude is measured relative to the meridians through the monitors. The ordinate scales are arbitrary.

through the station. The longitude of the directions of maximum response relative to the station meridian is set out in Table II for the four stations of

TABLE II

Geographic longitudes of observatories and directions of maximum response measured east from the Greenwich meridian

Station \ Longitudinal	Observatory	Direction of maximum response
Mawson	63° E.	68° E.
Hobart	147	207
Sulphur Mt.	245	270
Ottawa	284	319

interest. It is clear that a region in space from which the intensity is depressed will be scanned at different local times by different stations. For this reason we prefer to express the results presented in this paper in universal time rather than local time, and to relate the observations to directions in space as described below.

THE TIME AND DIRECTIONAL DEPENDENCE OF THE FORBUSH-TYPE DECREASE MECHANISM

Three well-defined Forbush events are represented in Fig. 4 as follows:

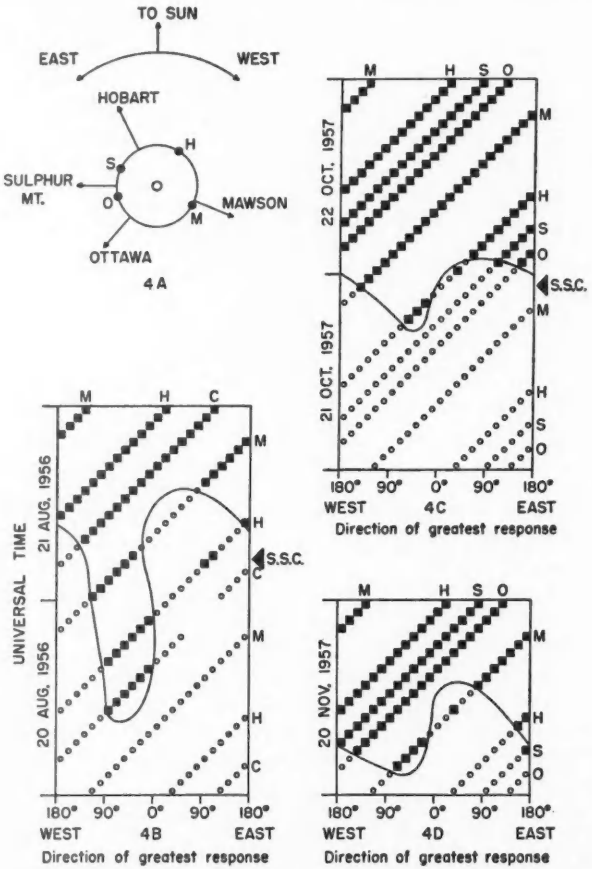

FIG. 4. (A) Showing the directions of greatest response of four neutron monitors at 0000 U.T. The positions of the recorders themselves are indicated by the solid circles. The convention whereby directions are designated as being west or east of the earth–sun line is illustrated.
(B, C, D) Surveys of the directional and temporal dependence of intensity during three Forbush-type decreases. The letters indicate from which recorder the adjacent data were obtained. Thus M—Mawson, H—Hobart, S—Sulphur Mountain, O—Ottawa, C—Climax. The times at which magnetic storm sudden commencements occurred are indicated.

In these diagrams the ordinates represent the progress of time and the abscissae denote asymptotic directions east or west of the earth–sun line (see Fig. 4A and Table II for a definition of these directions). As the intensities are sampled hour by hour while the earth rotates a small square representing the direction of maximum sensitivity of a given recorder moves across the diagram from the lower left to upper right. An open square indicates no significant depression below the pre-event level, while a blackened square identifies times and directions for which the intensity was depressed below this level by more than two standard deviations. The contour lines serve to distinguish depressed from non-depressed zones of the diagrams.

It is clear that on the three occasions represented in Fig. 4 the onset behavior of the events had similar features. The most striking feature is that the radiation arriving from directions out to about 120° west of the earth–sun line is depressed first, while that from 0 to 120° east is depressed last.

IDEALIZED TIME-DIRECTION DIAGRAM FOR FORBUSH-TYPE DECREASES

Two of the events depicted in Fig. 4 have been examined in greater detail. These occurred on October 21 and November 26, 1957, and were well-defined cases of variable onset behavior from station to station. Instead of the "depressed" or "not depressed" representation we shall now indicate the extent of depression below the pre-event level. This is illustrated in Fig. 5 in which different symbols are used for each 2% interval between 2% and 12% depressed intensity. To allow for the altitude dependence (McCracken and Johns 1959) the Sulphur Mountain data have been multiplied by the factor 0.8 to make them comparable with those from the other stations. Figure 5 points to a systematic behavior for these two events, the values of greatest depression avoiding the directions between 0 and 90° east. The intensity due to particles arriving from east was the last to be depressed and it suffered the least depression during the events.

On the basis of these two well-defined events the idealized time–direction diagram shown in Fig. 5C was prepared. From this diagram we may predict the following features to be expected on other occasions:

(*a*) When they occur, short-lived preliminary depressions will be observed at times characteristic of the station. According to the diagram these times are centered about: Hobart 1800–2000 U.T., Mawson 0400–0600 U.T., Ottawa 1100–1300 U.T., Sulphur Mountain 1400–1600 U.T. The duration of the preliminary depression will be determined to an extent by the shape of the directional sensitivity curve appropriate to the station.

(*b*) Intensity maxima occurring during the progress of the decrease will be observed at characteristic times. These are: Hobart 2300–0400 U.T., Mawson 0800–1300 U.T., Ottawa 1500–2000 U.T., Sulphur Mountain 1900–2400 U.T.

In Table III these predicted features are compared with the observations for five well-defined but less striking events than those used in Fig. 4. The good agreement leads us to conclude that the idealized time–direction diagram adequately describes the structure of at least eight of the Forbush-type decreases examined.

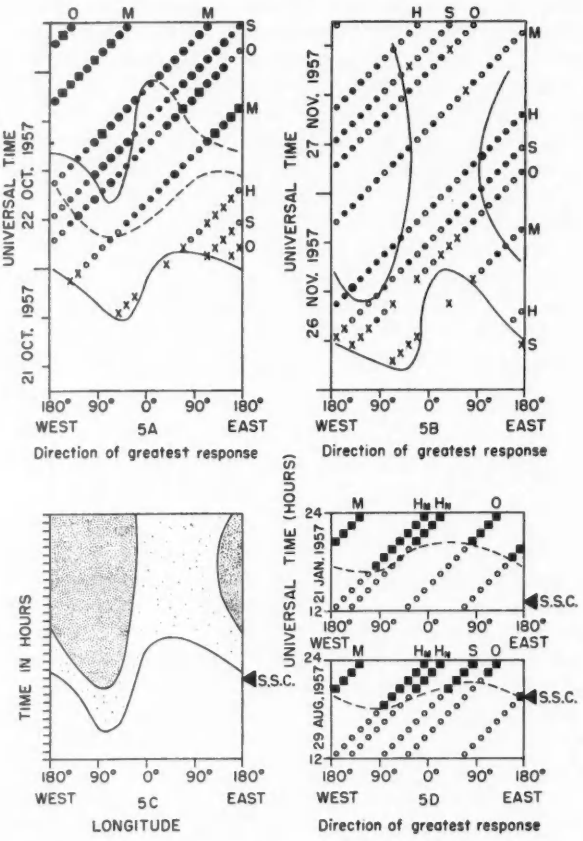

FIG. 5. (A, B) Detailed surveys of two Forbush-type decreases. The symbols are: cross = 2 to 4% intensity depression; open circle = 4 to 6% depression; small solid circle = 6 to 8% depression; large solid circle = 8 to 10% depression; solid square = 10 to 12% depression.
(C) Survey of the idealized Forbush-type decrease, showing the manner in which the depression of intensity depends upon direction and time. The directions of greatest depression are indicated by dense dotting.
(D) Survey of two great Forbush-type decreases. H_M corresponds to the Hobart meson data; H_N, the Hobart neutron data. Times of sudden storm commencement are indicated.

Two great transient decreases occurred during 1957, namely, those beginning on January 21 and August 29. The nucleon intensity decrease exceeded 10% on these occasions, but the observed onset times at our stations were not very different, and there were no preliminary decreases. Time–direction plots for these two events are shown in Fig. 5D. As the Sulphur Mountain and Mawson neutron monitors were not in operation until after the January event other data have been used. Although there were evidently no strongly developed

TABLE III

The times of occurrence of prominent features of Forbush-type decreases, compared with those predicted from the idealized model

Event \ Feature	Short-lived (preliminary) decrease prior to main decrease				Intensity maximum observed during fluctuations after onset			
Date of commencement	Hobart	Mawson	Ottawa	Sulphur Mt.	Hobart	Mawson	Ottawa	Sulphur Mt.
20 Aug. 1956	17–20	01–06 (Meson)	09–11 (Meson)	N.D.	00–05	07–16 (Meson)	16–20	N.O.
10 Mar. 1957	N.D.	N.D.	N.D.	N.O.	20–01	05–12	14–17	N.O.
3 Aug. 1957	18–22	03–10	08–10	16–20	20–04	11–14	N.D.	05–07
29 Sept. 1957	N.D.	04–06	09–11	N.D.	23–04	08–14	09–15	22–24
8 July 1958	15–18	01–05	10–14	N.D.	N.D.	N.D.	N.D.	N.D.
17 Aug. 1958	16–20	N.D.	09–13	13–17	23–02	N.D.	20–22	20–33
Predicted central values	18–20	04–06	11–13	14–16	23–04	08–13	15–20	19–24

NOTE: Tabulated values are in universal time. Meson telescope data are used where nucleon data are not available. N.D. indicates that the feature was not well defined in the data, and N.O. that the station was not operating at this time.

anisotropies present at the time, these events appear to be consistent with the idealized diagram, since the intensity was depressed in the westerly before the easterly directions.

DISTRIBUTION OF ONSET TIMES OF FORBUSH-TYPE DECREASES

The results given in the previous section indicate that at least on a number of occasions the cosmic rays approaching the earth during the early stages of a Forbush-type event are reduced in intensity in an asymmetrical fashion. The suggestion from these results is that the intensity-depressing agency is located at first in a direction between 0–120° west of the sun–earth line, and that it later extends to influence the cosmic ray flux arriving from all directions. It is obviously desirable to determine whether this form of behavior is common to all events. Evidence strongly in support of this is presented in Fig. 6. In this figure the earliest onset times listed in Table I for each event are

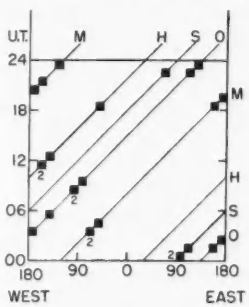

FIG. 6. The earliest time of commencement for the events listed in Table I is indicated by a black square in the time–direction diagram. When the commencement times at two stations were the same both have been shown. The number 2 alongside a square indicates that two events had the same commencement time.

plotted on a time–direction diagram. Only those events for which data were available from the four stations have been used. It is remarkable that although (as would be expected) the onset times are distributed throughout the 24 hours, the directions in which the events were first observed to begin are by no means evenly distributed. Of the 22 onset times included in the figure none corresponds to directions from 45° west to 60° east of the sun–earth line.

We conclude from the above analysis of 22 events that at least during the present cycle of high solar activity the Forbush-type decrease mechanism has associated with it a consistent asymmetrical pattern about the earth–sun line. One may summarize as follows:

(*a*) The onset times are not simultaneous at all points on the earth.

(*b*) The intensity between about 30° and 120° west of the earth–sun line is the first to be depressed.

(*c*) The intensity is depressed last from directions between about 0° and 90° east.

(*d*) The maximum depression occurs about 90° west.

CORRELATION WITH GEOMAGNETIC DISTURBANCE

Considerable attention has been devoted in the past to the connection between geomagnetic activity and cosmic ray intensity variations. Usually the counting statistics have been inadequate to justify the study of individual events; consequently superposed epoch methods have been used. Conflicting results have been reported concerning the correlation between the two phenomena, but most investigators agree that the relationship is not that of cause and effect. Both appear to be effects produced by a common cause, namely, material ejected from the sun, but different properties of this material seem to lead to the magnetic and cosmic ray variations.

From the study of the 22 Forbush-type events listed in Table I the following conclusions may be drawn concerning the relationship between the onset times of the decreases and the storm sudden commencements (S.S.C.) for the period under consideration:

(*a*) The S.S.C. occurred before the intensity was depressed to the east of the sun–earth line.

(*b*) On some occasions the cosmic ray intensity was depressed from the west several hours before the S.S.C. occurred. On other occasions the S.S.C. preceded the cosmic ray effects to the west.

DISCUSSION

The results presented above indicate that many, if not all, Forbush-type decreases conform to a pattern when we take into account the direction of maximum sensitivity of a recorder and the onset time observed by it. This result seems to arise because of a spatial asymmetry which develops in the decrease mechanism at these times.

It is not yet clear why the decrease should be observed first in directions west of the sun–earth line and later to the east. In this connection it should be emphasized that the procedure used to determine the directions of maximum

sensitivity of a neutron monitor involves the assumption that the conventional geomagnetic field configuration is not seriously in error, and that the agency responsible for the decreases lies outside the effective field region. If either of these assumptions should prove unjustified the directions of maximum sensitivity would be different.

It has been noted that the idealized time–direction diagram for Forbush-type decreases predicts characteristic times for intensity maxima that may be observed at different stations during the progress of an event. These characteristic times correspond rather closely with the time of maximum of the daily variation observed at the stations. For example, the characteristic time predicted from Fig. 5 for Hobart is 2300–0400 U.T., which is to be compared with the time of maximum of the average daily variation at Hobart during 1957, namely about 0200 U.T. An enhanced daily variation during Forbush-type decreases and geomagnetically disturbed periods has been reported by others (Elliot 1952). It is possible that the quiet-day daily variation may be due to an asymmetrical mechanism similar to that responsible for the intensity fluctuations during Forbush decreases. The continuous flow of matter from the sun, or solar "wind" (Van de Hulst 1953) may be able to set up an intensity-controlling mechanism similar to that due to matter ejected from active solar regions.

The differences in onset times of Forbush-type decreases observed at different stations provides yet another piece of evidence that there is not a one-to-one correspondence between the decreases and magnetic storm sudden commencements, for the latter are known to coincide to within 1 minute at widely separated observatories. The detection of cosmic ray changes on some occasions for particles arriving from the west of the earth–sun line several hours before the S.S.C. suggests that the agency responsible for the decreases is able to influence the intensity at a considerable distance from the earth. If this is so it means that at least part of the Forbush decrease mechanism is located far from the earth and is not geocentric as suggested by Parker (1956).

Since the cloud of solar material travels at about 5×10^6 km/hour, and since some preliminary decreases lead the S.S.C. by about 10 hours, this distance can apparently be as great as 50×10^6 km (0.33 A.U.). However, conclusions based on the time relations between cosmic ray decreases and S.S.C.'s must be regarded with caution because different features of the ejected solar material may be responsible for these two phenomena (this is suggested by the occurrence of some S.S.C.'s without associated cosmic ray intensity changes and vice versa). It does not seem possible to explain cosmic ray effects originating some distance from the earth in terms of deflection by magnetic fields frozen into clouds of ejected solar matter—in such fields the original isotropy of the radiation is expected to be preserved. If anything, the fact that the clouds are approaching the earth will result in the energy of the albedo from the cloud being increased, hence an increase in intensity would be produced. Electric fields in polarized clouds of ionized matter ejected from the sun offer a possible explanation. However, there appear to be so many inadequately determined parameters in the study of cosmic ray intensity

fluctuations that it seems scarcely worth while at present to attempt a quantitative analysis to test the various mechanisms that have been proposed in recent years.

ACKNOWLEDGMENTS

The authors wish to express appreciation of those operating the various stations from which data were used. Figure 4 includes some data from the Climax neutron monitor operated by the University of Chicago. We wish to thank J. A. Simpson for permission to use this. K. G. McCracken is grateful to the Australian Atomic Energy Commission for the award of a postgraduate scholarship at the University of Tasmania. Analyses of the Hobart data were assisted by the Australian Academy of Science.

REFERENCES

BRUNBERG, E. A. 1953. Tellus, **5**, 135.
BRUNBERG, E. A. and DATTNER, A. 1953. Tellus, **5**, 269.
DORMAN, L. I. 1957. Cosmic ray variations (State Publishing House for Technical and Theoretical Literature, Moscow. Translation by United States Technical Documents Liaison Office).
ELLIOT, H. 1952. Progress in cosmic ray physics, Vol. 1 (Interscience Publishers, Inc., New York).
FENTON, A. G., MCCRACKEN, K. G., ROSE, D. C., and WILSON, B. G. 1959. Can. J. Phys. **37**, 569.
JORY, F. S. 1956. Phys. Rev. **103**, 1068.
MCCRACKEN, K. G. and JOHNS, D. H. 1959. Nuovo cimento (in press).
MCCRACKEN, K. G. and PARSONS, N. R. 1958. Phys. Rev. **112**, 1798.
PARKER, E. N. 1956. Phys. Rev. **103**, 1518.
VAN DE HULST, H. C. 1953. The sun (University of Chicago Press).

APPROXIMATE WAVE FUNCTIONS OF Pb^{+++} BY THE METHOD OF SELF-CONSISTENT FIELD WITHOUT EXCHANGE[1]

J. F. Hart and Beatrice H. Worsley

ABSTRACT

The FERUT program previously described for calculating Hartree–Fock wave functions by the method of the self-consistent field has been adapted to the configuration Pb^{+++}. Although the exchange factors were omitted, the program was extended beyond its original scope in other respects, and an assessment of the difficulties so encountered is made. It might be noted, however, that, except in the case of the $4f$ wave function, it was possible to begin all the integrations at a common point. Initial estimates were made from the Douglas, Hartree, and Runciman results for thallium. The estimates for the core functions were not assumed to be satisfactory. The errors in the final wave functions are considered to be no more than one or two units in the second decimal digit.

1. INTRODUCTION

The FERUT program for the calculation of atomic structures (Worsley 1958) was designed primarily to obtain wave functions with exchange for the atoms up to the end of the second long period. However, with a slight modification, the program could in principle be used to calculate wave functions and energies of any atom in the periodic table, provided the exchange terms were neglected. In this paper we present the self-consistent field calculations for the Pb^{+++} ion as computed by the modified program, and we outline the difficulties encountered.

The neglect of exchange is dictated by the prohibitive amount of machine time which would be required on a medium-speed computer. However, this simplification seems reasonable for heavy atoms when the relatively more important correlation and relativistic effects are being neglected.

The interest in Pb^{+++} arises from a spectroscopic study of the ions of lead being made at the McLennan Laboratory under the direction of Professor M. F. Crawford. Results of this investigation will be published later, but in view of the many uses of atomic wave functions and in view of the value of the tables as an aid to those engaged in computer calculation, it was decided to publish the wave functions separately. Since the functions use the same independent variable as used by Ridley (1957) for uranium, namely, $\rho = \ln 1000r$, they will be particularly useful for interpolation.

2. DISCUSSION

In the case of Pb^{+++} the Hartree equations to be solved may be written in the form

$$P_i''(r)+g_i(r).P_i(r) = 0, \tag{2.1}$$

where $i = 1, 2, 3 \ldots 13$,

[1]Manuscript received April 30, 1959.
Contribution from the Computation Centre, McLennan Laboratory, University of Toronto, Toronto, Ontario.

subject to the boundary conditions

$$P_i(\infty) = 0, \tag{2.2}$$

and the normalization conditions

$$\int_0^\infty P_i^2(r)dr = 1. \tag{2.3}$$

In the exchange calculations there are two energy parameters in each differential equation so that both of the above conditions are required, whereas in the calculations without exchange the condition at infinity is sufficient to determine each wave function to within a multiplicative constant. Leaving this constant arbitrary until the end of a calculation permits it to be used as a scaling factor to prevent overflow during the numerical integration of equation (2.1).

The choice of a suitable numerical method and interval size becomes critically important for heavy atoms. The Numerov method, with an accuracy of five decimal figures and a speed of two steps per second, was considered satisfactory, although the speed could perhaps be improved. On the other hand, the choice of logarithmic independent variable, while it obviates the necessity of jumps in the interval of integration, slows the calculation appreciably by requiring too many points in the region of the core. For example, in the integration of the 6*s* wave function of Pb^{+++}, more than 50% of the points of integration lie within $r \sim 1/10$ atomic units although the function extends to $r \sim 7$ atomic units. If a number of structures were to be calculated with a millisecond computer such as FERUT it might be advisable to start some of the integrations further out, or to make use of the fact that slight changes in the energy parameter only affect the outer portion of the wave function. To simplify the coding, the FERUT program was designed so that, for each wave function, the following procedure was used. The starting values were calculated from the series given by Hartree (1957, p. 81) at $r = 0.001$ and $r = 0.001105$, and integration was continued outward past the last node until a test could be made of the condition (2.2). The use of a common starting point offers no difficulty if the computer has fast floating-point arithmetic. However, since the starting values are of the order of r^{l+1} there may be a complete loss of significant figures when using fixed-point arithmetic. In practice it was found that, if full use was made of the 40 bit word length, all the wave functions of Pb^{+++} could be scaled satisfactorily except the 4*f* function, which was consequently integrated separately using a slower floating-point routine. This work on a heavy atom confirms our opinion that, for a millisecond computer, the automatization must stop short of allowing the entire calculation to continue in the machine without operator interference. It was found convenient to improve a single wave function during one production run. The choice of wave function to be improved and the trial energy value was left to the discretion of the operator. For microsecond computing machines it is un-

doubtedly possible to code a criterion of self-consistency so that production will continue until all wave functions are obtained to a predetermined accuracy.

3. RESULTS

The initial estimates of the wave functions of Pb^{+++} were obtained from the results of Douglas, Hartree, and Runciman (1955) for Au and Tl^{+}. The thallium wave functions had been obtained by "pure scaling" from Au (Hartree 1957, p. 116) for all but the $5d$ and $6s$ groups which were integrated. In the case of Pb^{+++} equation (2.1) was integrated for the wave functions as a check on the estimates, and it was found that improvement was required for a number of inner groups. The procedure adopted was to work outward from the $1s$ group to the $5p$ group, improving only those functions for which the values differed by more than 2% from the estimated values. Where improvement was required, the final wave function was substituted for the estimated wave function. In this way it was found that the $3d$, $4d$, $4f$, $5s$, and $5p$ groups had to be improved, although only the $5p$ group was sufficiently in error to produce a serious change in the total effective field. Finally the $5d$ and $6s$ groups were integrated until self-consistent. The entire calculation required 40 hours' production on FERUT. The penultimate and ultimate wave functions differ by no more than one or two units in the second decimal, or by about 3%. The "ultimate" wave functions are given in Table I (pp. 986–988).

ACKNOWLEDGMENTS

We are grateful to Professors Watson and Gotlieb for making available the facilities of the Computation Centre, and also to the late Professor D. R. Hartree for his suggestions and encouragement in the earlier part of the work.

REFERENCES

Douglas, A. S., Hartree, D. R., and Runciman, W. A. 1955. Proc. Cambridge Phil. Soc. **51**, 486.

Hartree, D. R. 1957. The calculation of atomic structures (John Wiley & Sons, Inc., New York).

Ridley, E. C. 1957. Proc. Roy. Soc. A, **243**, 422.

Worsley, B. H. 1958. Can J. Phys. **36**, 289.

TABLE I

Normalized radial wave functions without exchange for the $(5d)^{10}6s$ configuration of Pb^{+++}
Calculated with independent variable $\rho = \ln 1000r$, $\delta\rho = 0.1$

nl	$1s$	$2s$	$2p$	$3s$	$3p$	$3d$	$4s$	$4p$	$4d$	$4f$	$5s$	$5p$	$5d$	$6s$
$\epsilon_{n,l}$	6029	982	949	236	218	186	52.8	45.2	31.4	12.9	9.80	7.17	3.65	2.48
r	$P(1s)$	$P(2s)$	$P(2p)$	$P(3s)$	$P(3p)$	$P(3d)$	$P(4s)$	$P(4p)$	$P(4d)$	$P(4f)$	$P(5s)$	$P(5p)$	$P(5d)$	$P(6s)$
0.001000	1.37	0.45	0.01	0.22	0.00	0.00	0.11	0.00	0.00	0.00	0.05	0.00	0.00	0.02
0.001105	1.49	0.50	0.01	0.23	0.00	0.00	0.12	0.00	0.00	0.00	0.05	0.00	0.00	0.02
0.001221	1.62	0.55	0.02	0.25	0.01	0.00	0.13	0.00	0.00	0.00	0.06	0.00	0.00	0.02
0.001350	1.77	0.60	0.02	0.28	0.01	0.00	0.14	0.00	0.00	0.00	0.06	0.00	0.00	0.02
0.001492	1.93	0.64	0.02	0.30	0.01	0.00	0.15	0.01	0.00	0.00	0.07	0.00	0.00	0.02
0.001649	2.11	0.70	0.03	0.33	0.01	0.00	0.17	0.01	0.00	0.00	0.08	0.00	0.00	0.03
0.001822	2.31	0.77	0.03	0.36	0.02	0.00	0.18	0.01	0.00	0.00	0.08	0.00	0.00	0.03
0.002014	2.53	0.84	0.04	0.39	0.02	0.00	0.20	0.01	0.00	0.00	0.09	0.00	0.00	0.03
0.002226	2.73	0.91	0.05	0.43	0.03	0.00	0.21	0.01	0.00	0.00	0.10	0.01	0.00	0.03
0.002460	2.95	0.97	0.06	0.46	0.03	0.00	0.23	0.02	0.00	0.00	0.11	0.01	0.00	0.04
0.002718	3.19	1.06	0.07	0.50	0.04	0.00	0.25	0.02	0.00	0.00	0.12	0.01	0.00	0.04
0.003004	3.45	1.15	0.09	0.54	0.04	0.00	0.27	0.02	0.00	0.00	0.12	0.01	0.00	0.04
0.003320	3.71	1.22	0.11	0.58	0.05	0.00	0.29	0.03	0.00	0.00	0.13	0.01	0.00	0.05
0.003669	3.99	1.31	0.13	0.62	0.06	0.00	0.31	0.03	0.00	0.00	0.14	0.01	0.00	0.05
0.004055	4.29	1.41	0.16	0.67	0.08	0.00	0.33	0.04	0.00	0.00	0.15	0.02	0.00	0.05
0.004482	4.57	1.49	0.19	0.70	0.09	0.00	0.35	0.05	0.00	0.00	0.16	0.02	0.00	0.06
0.004953	4.88	1.59	0.22	0.75	0.11	0.01	0.37	0.06	0.00	0.00	0.17	0.02	0.00	0.06
0.005474	5.16	1.67	0.27	0.78	0.13	0.01	0.39	0.07	0.00	0.00	0.18	0.03	0.00	0.06
0.006050	5.45	1.75	0.32	0.82	0.16	0.01	0.41	0.08	0.00	0.00	0.19	0.03	0.00	0.06
0.006686	5.70	1.81	0.38	0.85	0.19	0.01	0.43	0.09	0.00	0.00	0.20	0.04	0.00	0.07
0.007389	5.95	1.87	0.45	0.88	0.23	0.01	0.44	0.11	0.00	0.00	0.20	0.05	0.00	0.07
0.008166	6.18	1.91	0.53	0.90	0.27	0.01	0.45	0.13	0.01	0.00	0.21	0.06	0.00	0.07
0.009025	6.37	1.98	0.63	0.91	0.31	0.02	0.45	0.16	0.01	0.00	0.21	0.07	0.00	0.07
0.009974	6.52	1.99	0.74	0.90	0.37	0.02	0.45	0.18	0.01	0.00	0.21	0.08	0.00	0.07
0.011023	6.52	1.91	0.87	0.86	0.43	0.03	0.44	0.21	0.01	0.00	0.20	0.09	0.00	0.07
0.012182	6.52	1.78	1.01	0.81	0.50	0.03	0.42	0.25	0.02	0.00	0.19	0.11	0.01	0.07
0.013464	6.51	1.71	1.17	0.76	0.58	0.05	0.39	0.29	0.02	0.00	0.18	0.12	0.01	0.06
0.014880	6.51	1.60	1.35	0.71	0.67	0.06	0.35	0.33	0.03	0.00	0.16	0.14	0.01	0.06
0.016445	6.29	1.36	1.55	0.59	0.76	0.08	0.30	0.37	0.04	0.00	0.14	0.16	0.01	0.05
0.018174	6.04	1.11	1.77	0.46	0.86	0.10	0.23	0.42	0.05	0.00	0.11	0.18	0.02	0.04

TABLE I (*Continued*)

Normalized radial wave functions without exchange for the $(5d)^{10}6s$ configuration of Pb^{+++}
Calculated with independent variable $\rho = \ln 1000r$, $\delta\rho = 0.1$

nl	$1s$	$2s$	$2p$	$3s$	$3p$	$3d$	$4s$	$4p$	$4d$	$4f$	$5s$	$5p$	$5d$	$6s$
ϵ_{nl}	6029	982	949	236	218	186	52.8	45.2	31.4	12.9	9.80	7.17	3.65	2.48
r	$P(1s)$	$P(2s)$	$P(2p)$	$P(3s)$	$P(3p)$	$P(3d)$	$P(4s)$	$P(4p)$	$P(4d)$	$P(4f)$	$P(5s)$	$P(5p)$	$P(5d)$	$P(6s)$
0.020086	5.76	0.81	2.01	0.32	0.97	0.13	0.15	0.48	0.07	0.00	0.07	0.21	0.02	0.02
0.022198	5.35	0.45	2.25	0.13	1.08	0.16	0.06	0.53	0.09	0.00	0.03	0.23	0.03	0.01
0.024533	4.89	0.06	2.51	−0.07	1.19	0.21	−0.04	0.58	0.11	0.00	−0.02	0.25	0.04	−0.01
0.027113	4.40	−0.40	2.76	−0.29	1.29	0.26	−0.15	0.63	0.14	0.01	−0.07	0.27	0.05	−0.02
0.029964	3.86	−0.91	3.02	−0.53	1.38	0.33	−0.27	0.67	0.17	0.01	−0.13	0.29	0.06	−0.04
0.033115	3.33	−1.39	3.26	−0.76	1.46	0.41	−0.39	0.70	0.21	0.01	−0.18	0.30	0.07	−0.06
0.036598	2.78	−1.97	3.47	−0.99	1.50	0.51	−0.51	0.72	0.26	0.02	−0.23	0.31	0.09	−0.08
0.040447	2.24	−2.42	3.64	−1.20	1.51	0.62	−0.61	0.72	0.32	0.02	−0.28	0.31	0.11	−0.10
0.044701	1.81	−2.87	3.77	−1.33	1.48	0.76	−0.68	0.69	0.39	0.03	−0.31	0.29	0.13	−0.10
0.049402	1.33	−3.26	3.84	−1.47	1.39	0.91	−0.73	0.64	0.46	0.04	−0.33	0.27	0.16	−0.11
0.054598	1.00	−3.54	3.83	−1.48	1.24	1.08	−0.73	0.55	0.55	0.06	−0.33	0.23	0.19	−0.11
0.060340	0.67	−3.76	3.75	−1.45	1.02	1.27	−0.69	0.42	0.64	0.08	−0.31	0.18	0.22	−0.11
0.066686	0.46	−3.79	3.59	−1.28	0.73	1.48	−0.59	0.26	0.73	0.10	−0.26	0.11	0.25	−0.09
0.073700	0.30	−3.73	3.36	−1.01	0.37	1.69	−0.43	0.07	0.81	0.14	−0.19	0.02	0.28	−0.06
0.081451	0.19	−3.55	3.05	−0.70	−0.40	1.90	−0.22	−0.14	0.89	0.18	−0.09	−0.07	0.30	−0.03
0.090017	0.10	−3.25	2.70	−0.32	−0.49	2.10	0.03	−0.37	0.96	0.23	0.02	−0.17	0.32	0.01
0.099484	0.07	−2.87	2.31	0.15	−0.97	2.28	0.30	−0.59	0.99	0.29	0.15	−0.26	0.33	0.05
0.109947	0.04	−2.42	1.91	0.73	−1.43	2.43	0.57	−0.79	1.00	0.37	0.27	−0.35	0.33	0.10
0.121510	0.02	−1.96	1.52	1.33	−1.85	2.52	0.81	−0.95	0.95	0.46	0.38	−0.41	0.31	0.13
0.134290	0.00	−1.53	1.16	1.87	−2.20	2.56	0.99	−1.03	0.86	0.56	0.46	−0.43	0.27	0.16
0.148413		−1.14	0.85	2.24	−2.44	2.53	1.07	−1.03	0.71	0.68	0.48	−0.43	0.21	0.16
0.164022		−0.79	0.60	2.50	−2.56	2.43	1.04	−0.93	0.50	0.81	0.45	−0.37	0.13	0.15
0.181272		−0.52	0.39	2.61	−2.56	2.26	0.88	−0.72	0.24	0.94	0.36	−0.26	0.04	0.12
0.200337		−0.32	0.25	2.55	−2.42	2.04	0.59	−0.41	−0.07	1.07	0.20	−0.11	−0.07	0.07
0.221406		−0.18	0.14	2.35	−2.19	1.78	0.19	−0.02	−0.41	1.20	0.00	0.06	−0.19	0.00
0.24469		−0.09	0.08	2.04	−1.88	1.49	−0.26	0.40	−0.75	1.32	−0.22	0.25	−0.30	−0.08
0.27043		−0.04	0.05	1.68	−1.53	1.20	−0.74	0.83	−1.06	1.42	−0.43	0.43	−0.39	−0.15
0.29887		−0.01	0.02	1.30	−1.18	0.93	−1.17	1.22	−1.34	1.49	−0.59	0.56	−0.46	−0.21
0.33030		0.00	0.01	0.95	−0.85	0.69	−1.52	1.52	−1.54	1.52	−0.69	0.64	−0.49	−0.23
0.36504			0.00	0.65	−0.58	0.48	−1.74	1.71	−1.66	1.52	−0.69	0.63	−0.47	−0.23

TABLE I (*Concluded*)

Normalized radial wave functions without exchange for the $(5d)^{10}6s$ configuration of Pb^{+++}
Calculated with independent variable $\rho = \ln 1000r$, $\delta\rho = 0.1$

nl	1s	2s	2p	3s	3p	3d	4s	4p	4d	4f	5s	5p	5d	6s
$\epsilon_{n,l}$	6029	982	949	236	218	186	52.8	45.2	31.4	12.9	9.80	7.17	3.65	2.48
r	$P(1s)$	$P(2s)$	$P(2p)$	$P(3s)$	$P(3p)$	$P(3d)$	$P(4s)$	$P(4p)$	$P(4d)$	$P(4f)$	$P(5s)$	$P(5p)$	$P(5d)$	$P(6s)$
0.40343				0.41	−0.37	0.31	−1.82	1.78	−1.69	1.49	−0.58	0.55	−0.41	−0.19
0.44586				0.24	−0.22	0.19	−1.77	1.73	−1.64	1.42	−0.38	0.38	−0.31	−0.11
0.49275				0.13	−0.12	0.11	−1.60	1.58	−1.51	1.31	−0.11	0.14	−0.16	−0.01
0.54457				0.06	−0.06	0.06	−1.36	1.35	−1.32	1.19	0.22	−0.14	0.02	0.11
0.60185				0.03	−0.03	0.03	−1.08	1.10	−1.11	1.05	0.54	−0.43	0.21	0.22
0.66514				0.01	−0.01	0.01	−0.81	0.84	−0.88	0.90	0.84	−0.70	0.41	0.30
0.73510				0.00	0.00	0.00	−0.56	0.60	−0.67	0.75	1.06	−0.92	0.59	0.36
0.81241							−0.36	0.40	−0.48	0.60	1.20	−1.08	0.75	0.36
0.89785							−0.22	0.25	−0.33	0.47	1.23	−1.16	0.86	0.32
0.99227							−0.12	0.15	−0.21	0.35	1.18	−1.15	0.94	0.23
1.09663							−0.06	0.08	−0.13	0.25	1.06	−1.08	0.96	0.10
1.21197							−0.03	0.04	−0.08	0.18	0.89	−0.96	0.95	−0.05
1.33943							−0.01	0.02	−0.04	0.13	0.71	−0.80	0.90	−0.21
1.48030							0.00	0.01	−0.02	0.08	0.53	−0.64	0.82	−0.37
1.63598								0.00	−0.01	0.05	0.37	−0.49	0.72	−0.52
1.80804									0.00	0.03	0.25	−0.35	0.62	−0.63
1.99820										0.02	0.15	−0.24	0.51	−0.71
2.20835										0.01	0.09	−0.15	0.40	−0.74
2.44060										0.00	0.05	−0.09	0.31	−0.74
2.69728											0.02	−0.05	0.22	−0.69
2.98096											0.01	−0.03	0.16	−0.61
3.29447											0.00	−0.01	0.10	−0.51
3.64095												0.00	0.06	−0.40
4.02387													0.04	−0.29
4.44707													0.02	−0.20
4.91477													0.01	−0.13
5.43166													0.01	−0.08
6.00291													0.00	−0.04
6.63424														−0.02
7.33197														−0.01

NOTE: Hartree atomic units are used in this table.

A CRYOSTAT FOR MEASURING SPECIFIC HEATS BETWEEN 1 AND 4.2° K USING A MECHANICAL THERMAL SWITCH[1]

F. D. MANCHESTER[2]

ABSTRACT

A design for a low temperature cryostat using a mechanical thermal switch is described and its performance and some general features of interest in its operation, such as the importance of vibration, are discussed. Sample measurements on pure copper and a cupro–nickel alloy are presented.

In recent years interest has been revived in a design of cryostat for specific heat measurements which makes use of a mechanical thermal switch instead of helium exchange gas for cooling the specimen to the working temperature. This method, first tried out by Keesom and Kok (1933), has been used in cryostats designed by Ruehrwein *et al.* (1943), Westrum *et al.* (1953), Kostryokova and Strelkov (1953), Dolecek and Madden (1953), Ramanathan and Srinivasan (1955), Webb and Wilks (1955), and Rayne (1956). A discussion of the undesirable effects produced by exchange gas has been given by Webb and Wilks (1955) and Corak *et al.* (1955) and their occurrence in experiments has been described by Keesom and Kok (1933) and Horowitz *et al.* (1952). The present paper describes a cryostat using a mechanical thermal switch patterned after the design of Webb and Wilks and presents some information and experience gained from its use in specific heat measurements. This design was chosen because it seemed to offer the best scope for extension of its application to other experimental situations, after some experience had been gained in using it for calorimetry.

DESCRIPTION OF THE APPARATUS

The general layout of the mechanical thermal switch cryostat is shown in Fig. 1 and the details of the thermal switch in Fig. 2.

The calorimeter C was suspended by nylon threads from the frame F and the space surrounding the calorimeter was maintained at a pressure of about 10^{-5} mm Hg by continuous pumping through one of the lines P. Temperatures between 1.1 and 4.2° K were obtained by pumping on the liquid in the inner liquid helium chamber H and the thermal switch was used to make contact between the chamber bottom and the sample. The mechanism M of the thermal switch was controlled by the actuating rod R, which passed through a tube to the room temperature end of the apparatus, where it left the vacuum system through a flexible bellows S and connected with a screw arrangement used for raising or lowering the rod. The switching action was such that the rod was

[1]Manuscript received April 21, 1959.
Contribution from the Division of Pure Physics, National Research Council, Ottawa, Canada.
Issued as N.R.C. No. 5319.
[2]National Research Council Postdoctorate Fellow. Present address: Physics Department, University of Alberta, Edmonton, Alberta.

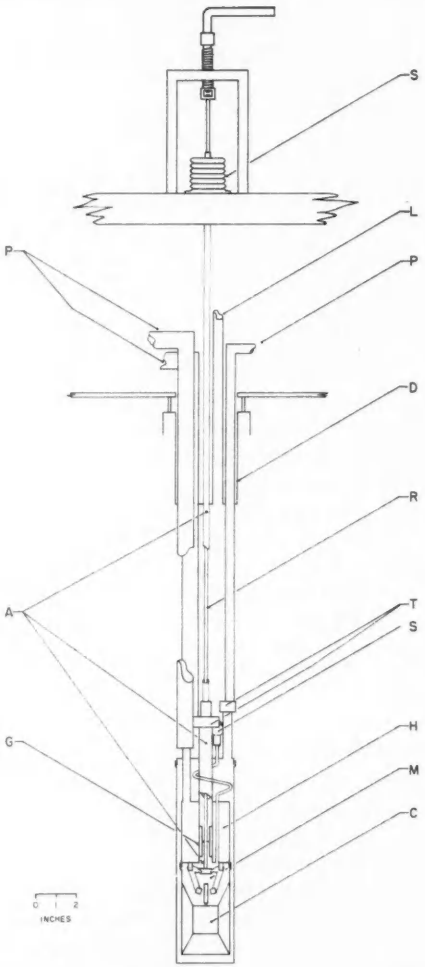

FIG. 1. General arrangement of mechanical thermal switch cryostat.

under tension when the switch was closing, i.e. when the maximum force was required. A total force of up to 6 kilograms could be applied between the jaws of the switch. The rod was thermally anchored at three points A, along its length. One, just under the Dewar cap D, was just below the temperature of liquid nitrogen; another, just above the main part of the cryostat, was at a temperature of 4.2° K; and the third was at the bottom of the rod at a temperature corresponding to that of the pumped inner helium chamber. The switch mechanism consisted of the copper jaws J, faced with a layer of indium metal

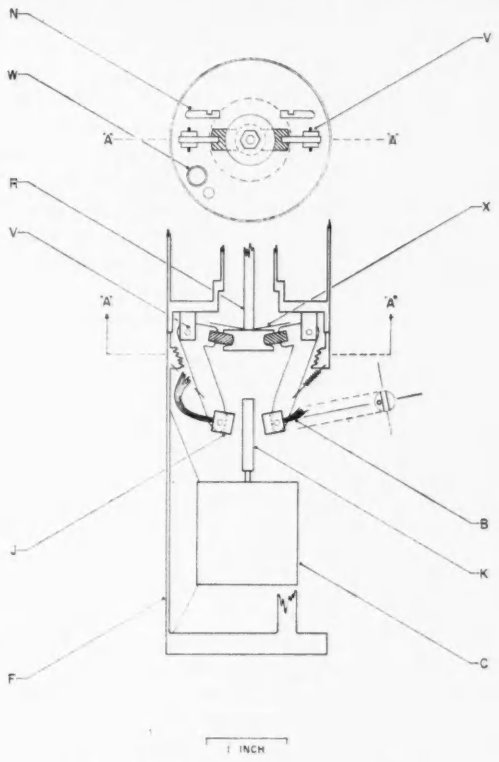

FIG. 2. Detail of mechanical thermal switch.

approximately 1 mm thick, which could be made to grip the cylindrical clamping post K. Motion was imparted to the jaws through the switch arms moving about the pivots V and coupled to the Teflon head on the end of the actuating rod. A combined extra radiation shield and guide for the actuating rod was provided at G and a copper disk X was used as a further radiation shield and a thermal anchoring point. Teflon was used for the head and for bushes in the pivots V, to minimize any heat produced by friction between the moving parts of the switch. Copper braid B was used to connect the jaws of the thermal switch to the copper posts N on the bottom of the inner helium chamber. This provided a direct connection which did not depend on the components of the switch mechanism. The clamping post K was a small copper cylinder drilled out to reduce its mass and was well polished on its outside surface. Initially the jaws which engaged with the post were also of polished copper but were later faced with indium metal. The difference in performance which resulted can be seen in Fig. 3. These indium-coated jaws proved quite serviceable in use, no trouble was experienced with the indium sticking to the

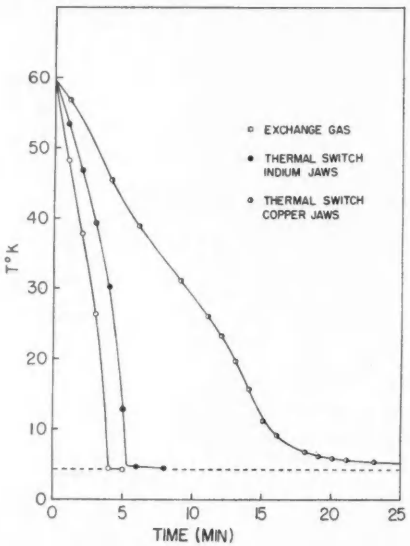

FIG. 3. Comparison of cooling rates obtained with helium exchange gas, indium-clad switch jaws, and copper jaws.

clamping post, and the jaws remained usable with no special treatment, other than working the switch a few times to improve the matching of the surfaces, after repositioning the calorimeter. Following Webb and Wilks an insulated wire was connected to the calorimeter and a simple indicator circuit arranged to tell when the thermal switch had made contact with the calorimeter. The electrical leads to the calorimeter were brought through the tubing shown in Fig. 1 to the seal S, then into the helium bath at 4.2° K, and from there to room temperature.

OPERATION OF THE MECHANICAL THERMAL SWITCH

The calorimeter was suspended in the frame by its nylon threads and carefully adjusted to be centrally placed with respect to the jaws of the switch, so that no discernible movement of the calorimeter occurred when the switch was worked.

Cooling with the switch was normally done in three stages: room temperature to liquid nitrogen temperatures, then to 4.2° K, and then down to as low as 1.1° K. In many cases the specific heat of the sample was large enough that the switch had to be connected only lightly when cooling from liquid nitrogen to liquid helium temperatures to prevent excessive boil-off of liquid helium. In cases where this was not a limitation (for example, for 75 g of copper) a sample could be cooled from room temperature to below 2° K in less than 4 hours. The force applied to the switch was also determined by the temperature at which it was intended to be opened and the thermal capacity of the body

being cooled. The larger the force applied, the larger the heating produced at the parting surfaces when the switch was disconnected, and the resultant temperature rise of the cooled sample would depend on its thermal capacity. At 4° K the specific heat of the sample was in most cases sufficiently high that the amount of heat developed at the break was not important. Thus down to 4° K the force on the jaws could be large, and particularly from room temperature to liquid nitrogen temperatures it could be a maximum. In cooling from 4° K down, however, a balance had to be struck between a loading sufficient to cool the sample at a reasonable rate and one not so great that the heat developed at the break was inconveniently large. This could mean that one had to wait up to 1 hour to cool down to about 1.1° K but if one did this, the switch could be disconnected with almost no warming up at all (see Table I).

TABLE I

Thermal data on performance of mechanical switch

Sample run No.	T,° K	ΔT,° K	Q, joule
1	1.124	0.004	1.22×10^{-5}
2	1.163	0.002	0.85×10^{-5}
2	1.145	0.005	2.09×10^{-5}
3	1.143	0.001	0.64×10^{-5}
6	1.187	0.002	1.29×10^{-5}
Webb and Wilks (1955)	—	—	10^{-4}
Dolecek and Madden (1953)	—	—	$0.75\text{–}2.25\times10^{-4}$

Apart from the force applied to the jaws of the switch the other most important consideration was vibration, that is, the mechanical vibration transmitted through the framework of the apparatus to the switch mechanism and the sample. The role of vibration as a source of extraneous heating in low temperature experiments employing thermally isolated samples, such as in calorimetry and adiabatic demagnetization work, is already widely appreciated (Hull, Wilkinson, and Wilks 1951; Darby *et al.* 1951; Wheatley, Griffing, and Estle 1956). However, in the case of the mechanical thermal switch the vibration also affects the action of the switch itself. Firstly, the amount of extraneous heat received by the sample and the thermal conductance of the switch determine how nearly the sample can be cooled to the temperature of the pumped helium bath, and vibration is a very important source of extraneous heating. Secondly, the amount of heat produced at the disconnecting of the switch is affected, because the relative vibration of the jaws and the clamping post produce a heating additional to that which results just from the friction of the surfaces parting simply. For these reasons it is essential to have vibration in the apparatus reduced as far as possible; indeed, the extent to which this can be done essentially determines the useful limiting temperature to which the switch can cool the sample. In the case of the present apparatus the site on which it was placed initially was such that the extraneous heating of the sample produced by vibration was more than 200 ergs/minute. Similar figures have been quoted by Hull, Wilkinson, and Wilks (1951) and Darby *et al.* (1951). Vibration of this magnitude made calorimetric measurements with metals virtually im-

possible and the performance of the thermal switch quite misleading. Collins and Zimmerman (1953) refer to the importance of heat generated by vibration in their description of a mechanical thermal switch used in a two-stage adiabatic demagnetization apparatus, although not specifically to its effect on the switching action. Once the apparatus had been placed on a relatively vibration-free support the extraneous heat input to the sample was reduced to a tolerable level and the performance of the switch was much improved. Even so, vibration in the apparatus varied from day to day and with the time of day, so that in general, except for quiet days in week ends, it was not possible to operate the thermal switch, during the day, to cool a sample to the lowest parts of the 1 to 4° K temperature region and disconnect it satisfactorily. All work in this region had to be left until late evening.

THE PERFORMANCE OF THE MECHANICAL THERMAL SWITCH

In Fig. 3 comparative cooling rate curves are given for a sample of 75 g of copper being cooled from about liquid nitrogen temperatures to the boiling point of helium. It can be seen from this that the cooling rate with the thermal switch is sufficiently close to that obtained with exchange gas that there is no loss in experimental convenience. In Fig. 4 the temperature dependence of the

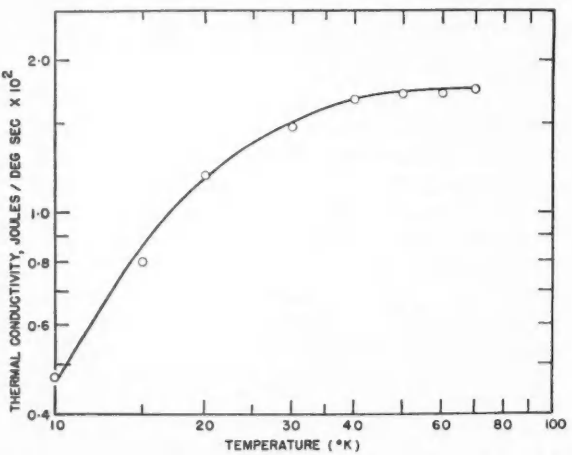

FIG. 4. Temperature dependence of the thermal conductivity of the switch in the region below liquid nitrogen temperatures.

thermal conductance of the thermal switch (using indium-clad jaws) is shown for the region between liquid nitrogen and liquid helium temperatures and in Fig. 5 it is shown for temperatures between 4 and 1° K. The temperature dependence of the conductance is similar to that found by Berman (1956), close to T^2 in the 2–4° K region and gradually decreasing to become essentially temperature independent at liquid nitrogen temperatures. These results are not presented as a continuous curve as they were taken while routine cooling

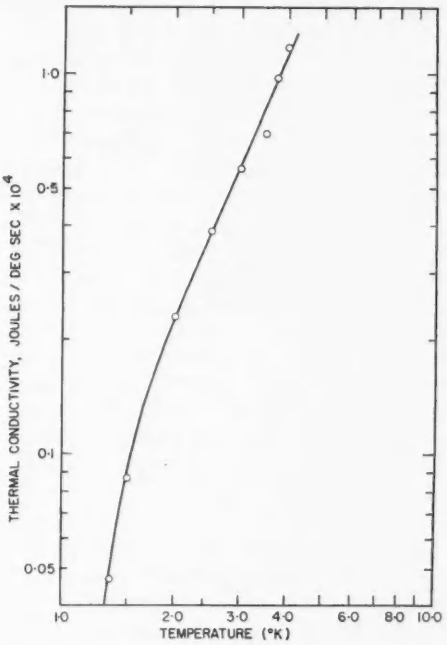

FIG. 5. Temperature dependence of the thermal conductivity of the switch in the liquid helium temperature region.

was being performed, with different forces on the jaws in the two temperature regions. Nevertheless, the curves in Figs. 4 and 5 represent the typical temperature dependence and magnitude of the thermal conductance. The figure quoted by Webb and Wilks (1955) for the thermal conductance of their switch is "of the order of " 1.5×10^{-4} joule/deg sec, presumably in the liquid helium temperature range. Dolecek and Madden (1953) found a temperature dependence of $T^{1.4}\times10^{-5}$ joule/sec deg for their switch in the liquid helium temperature range. This gives a value of 7×10^{-5} joule/sec deg at 4° K, which is 30% less than the value obtained from Fig. 4. Greater conductances could be obtained in the liquid helium region by applying more force to the switch but the values given in Fig. 5 are those obtained from experiments in which the switch was successfully disconnected with very little thermal disturbance. This would not be the case if the switch was clamped tightly as was discussed earlier.

Table I gives typical data on the warming up, Q, produced in the sample by the opening of the switch. The data are taken from observations made when vibration in the sample was very small and represent the warming produced essentially by the parting surfaces. No discernible warming was produced when the switch was closed, which is in contrast to the findings of Dolecek and

Madden (1953). When vibration conditions were bad the warming would be a good deal greater and the temperature drift of the specimen after disconnecting the switch made it difficult to tell how much warming had been produced just by the switching action. The table also shows typical temperatures to which the sample was cooled and the useful temperature at which measurements could be started, i.e. $T+\Delta T$. That measurements can be started at such temperatures is one advantage of a thermal switch; as in cases where the heat input due to vibration is reasonable, specific heat measurements can be started immediately the switch is disconnected. When exchange gas is used there is a delay while the exchange gas is pumped out to a sufficient extent for measurements to begin and in this period the sample will generally warm up, as the temperature drift is usually in the direction of warming at the lowest temperatures. Also, if it is desired to repeat measurements at the low temperature end, this can be done very conveniently using the switch.

The thermal isolation of the specimen was very good and for most of the temperature range, the drift of the sample temperature was compatible with the conduction of heat, along the nylon suspension threads, to the helium being pumped in the chamber H. It was usually only necessary to raise the temperature of the pumped helium once in the course of taking measurements between 1 and 4° K and for some substances with large specific heats there was no need at all. If vibration had been less of a problem, then finer suspension threads could have been used and the heat leak further reduced.

The foregoing represents the essential data on the performance of the mechanical thermal switch. These observations were made in the course of using the apparatus for measurements of specific heat and were to some extent incidental to the main purpose of the experiment. Thus no measurements were made of the force applied to the jaws during the cooling down and of the corresponding thermal conductivity. Some low temperature measurements of thermal conduction across metallic surfaces in contact and under varying loads have been made by Jacobs and Starr (1939) and more recently by Berman (1956). These studies are of help in understanding the processes involved and in designing a mechanical contact, although more work remains to be done in this field.

SPECIFIC HEAT MEASUREMENT

Experimental Details

Temperatures were measured with a 10-ohm, 1/2-watt, Allen Bradley resistor calibrated against the vapor pressure of liquid helium. The two-constant interpolation formula (Clement *et al.* 1955*a*)

$$\sqrt{(\log R/T)} = a \log R + b$$

was used in the manner suggested by Keesom and Pearlman (1956). The thermometer was calibrated by admitting exchange gas to the calorimeter space at the conclusion of a set of specific heat measurements on a sample and a total of about 24 calibration points taken over the range 1.1 to 4.2° K. This calibration procedure had to be repeated for each run made at liquid helium

temperatures, after the cryostat had been allowed to return to room temperature, as under these circumstances the calibration curve was displaced in an unpredictable fashion from run to run. As an example of the magnitude of this displacement, the two most extreme cases out of seven runs with one particular thermometer showed a change of 0.050° K for the temperature corresponding to a resistance of 100 ohms. Vapor pressure readings were corrected where necessary for thermomolecular pressure difference using the tables of Roberts and Sydoriak (1956) and converted to absolute temperatures using the 1955 E scale (Clement *et al.* 1955*b*). The resistance of the carbon resistor was measured using a method developed by Dauphinee and described by Dauphinee and Mooser (1955). This method has the advantage that thermoelectric e.m.f.'s had no effect on the measurement and that the thermometer resistance was compared directly with a reference resistance decade and the comparison presented continuously on a chart recorder. The temperature drift before and after the heating period was measured from the chart and then extrapolated to the middle of the heating period, as described by Keesom and Kok (1932). The temperature drift varied from zero to 10^{-5}° K/sec. Thermometer currents varying from 2 μa to 15 μa were used over the temperature range, and within the required precision of the thermometry, this variation of the current had no effect on the measured resistance. The size of the temperature increment used, ΔT, was kept such that the resultant error in the measured specific heat $\{\frac{1}{4}(\Delta T/T)^2$ for $C \propto T^3\}$ was less than 0.1% for all parts of the temperature range. Errors arising from the calibration of the thermometers and from the vapor pressure – temperature relations themselves have been discussed by Corak *et al.* (1955) and by Rayne (1956). The calibration procedure in the present work has been carried out in such a way that the errors involved are well within the limits discussed by these authors. On some occasions when a specific heat measurement was being made, there were small amounts of energy fed into the heater circuit from induction effects produced by the shutting off of the neighboring electric clock circuit. These stray energy inputs were largely eliminated but could be noticed now and again near 1° K. As, however, they showed up plainly on the chart record, suitable correction could easily be made.

The calorimeter heater was wound from manganin wire and had a resistance of about 2000 ohms. The electrical leads connecting the heater on the calorimeter with the rest of the circuit on the body of the cryostat were made from manganin wire with an outer coating of soft solder. The soft solder became superconducting at liquid helium temperatures, providing leads which combined zero electrical resistance with high thermal resistance. The power dissipated in the heater was measured using a potentiometer to measure the current through, and the potential drop across, the heater, in conjunction with an electric clock, driven by a standard 60-cycle supply, which was used to measure the duration of the heating period.

The calorimeter arrangement depended on the substance being measured. For most of the measurements, which were on copper alloys, a "jacket" type of calorimeter was used. This consisted of a copper cylinder $1\frac{1}{4}$ in. long provided with a slightly off-center hole of 1.000-in. diameter along its length. Into this

hole the carefully machined sample could be slid and clamping screws used to tighten the jacket around the sample. Clamping post, thermometer, and heater were permanently attached to the jacket and thus once the specific heat of the jacket had been measured, successive samples could be measured with a minimum of trouble. The heater was wound on a small copper bobbin placed in a hole running through the length of the jacket wall and the bobbin was soldered to the jacket at one end of the hole. The carbon resistor had its outer plastic covering ground off and after being covered with an insulating layer of baking varnish it was slipped into another hole in the jacket wall and held in place with more varnish. The thermal contact between the jacket and the sample was good and for all of the samples measured, there was never any indication of a lack of thermal equilibrium in the calorimeter. For the measurement of the specific heat of rubidium (Manchester 1959) the calorimeter was a cylindrical copper shell provided with similar fittings.

Results

As a check on the performance of the apparatus the specific heat of pure copper was measured. The copper, of nominal purity 99.999%, obtained from the American Smelting and Refining Company, was melted under vacuum using an induction furnace and a graphite crucible. For this sample the values

$$\gamma = 0.696 \mp 0.021 \text{ millijoules/mole deg}^2$$

$$\theta_0 = 344 \mp 7^\circ \text{ K}$$

were obtained by using the method of least squares to fit a straight line to the data plotted in the form of C/T vs. T^2. The error in γ and θ_0, assumed to be random, was estimated from this fit at the 95% confidence level. The scatter of the measurements is greater in this particular case than in later experiments, because this was the first experience with this apparatus. However, the mean values for γ and θ_0 compare reasonably well with those quoted by Corak *et al.* (1955), Rayne (1956), Griffel *et al.* (1957), as shown in Table II. It is possible

TABLE II

Comparison of values for specific heat of copper

θ_0, °K	γ millijoules/mole deg^2	References
344.5±3	0.687±0.012	Rayne (1958)
342±2	0.691±0.006	Griffel *et al.* (1957)
344±7	0.696±0.021	This work

that the fact that the copper was melted in a graphite crucible enabled some of the metallic impurities to enter into solid solution and thus contribute to a higher electronic specific heat. Following this check with copper, measurements were made of the specific heat of some dilute iron-in-copper alloys. These will be discussed in a separate publication. Also a measurement was made on a cupro–nickel alloy. This last measurement was in the nature of an exploratory one, undertaken for the following reason. Some measurements on cupro–nickel alloys had been made by Keesom and Kurrelmeyer (1940) and from

these they obtained a curve giving the dependence of the electronic specific heat on the composition of the alloy, a curve that has not been very amenable to theoretical interpretation. Because of this and because of the behavior of some of the C/T vs. T^2 plots shown in Keesom and Kurrelmeyer's paper (a pronounced upward displacement of the curve at the low temperature end, see also Keesom and Pearlman 1956), it was decided to re-examine the specific heat of a cupro–nickel alloy. It seemed most likely that the unusual behavior of the C/T vs. T^2 curves could be due to the helium exchange gas which Keesom and Kurrelmeyer had to use, in order to reduce the thermal equilibrium time of their calorimeter to a reasonable value. In their estimate of the contribution to the measured specific heat made by the helium gas contained in their sample, Keesom and Kurrelmeyer only took into account the specific heat of the gas and not the heat of its desorption. Actually, the heat of desorption for helium gas was not known until it was measured, later on, by Keesom and Schweers (1941). The heat of desorption is considerable, however, and would be quite capable of accounting for the observed behavior of the measured specific heat.

To investigate this point and to see if measurements could be made without using any exchange gas in the sample, a cupro–nickel alloy (30% nickel) was prepared and its specific heat measured. The alloy was prepared from spectroscopically pure nickel and copper, melted by induction and chill-cast under vacuum in a split copper mold. After casting, the ingot was annealed for 72 hours at a temperature of 1000° C to remove coring, and was then machined to size. Even with the sample prepared in this way, there were variations in composition of as much as 3% between ends, as determined by chemical analysis. However, for the exploratory measurement undertaken in the present instance this is not a serious matter. In the measurement of the specific heat no trouble at all was experienced with lack of thermal equilibrium in the sample and the measurements were straightforward. This was presumably because of the good thermal contact afforded by the jacket design of calorimeter. Thus even though the thermal conductivity of samples of 50 to 60% nickel would be still less, the experience with the 30% sample is good indication that a full range of alloys could be measured without any real difficulty being encountered from lack of thermal equilibrium, especially as the thermal isolation of the sample was sufficiently good that some lack of thermal equilibrium could be tolerated anyway.

Figure 6 shows C/T vs. T^2 plotted for the 30% nickel alloy (curve (*b*)) and compared on the same scale with data for two of the alloys ((*a*) 40% nickel, (*c*) 20% nickel) measured by Keesom and Kurrelmeyer. The ordinates have been displaced in order to show the plots more clearly. It can be seen that for the 30% alloy the experimental points lie fairly close to a straight line and do not show the systematic deviation from it which was found by Keesom and Kurrelmeyer for the 20% and particularly for the 40% alloy. Thus probably, although not conclusively, this effect was due to the desorption of exchange gas inside the sample. Certainly, the measurements on the 30% alloy indicate that more reliable measurements of γ and θ_0 could be obtained with apparatus of the

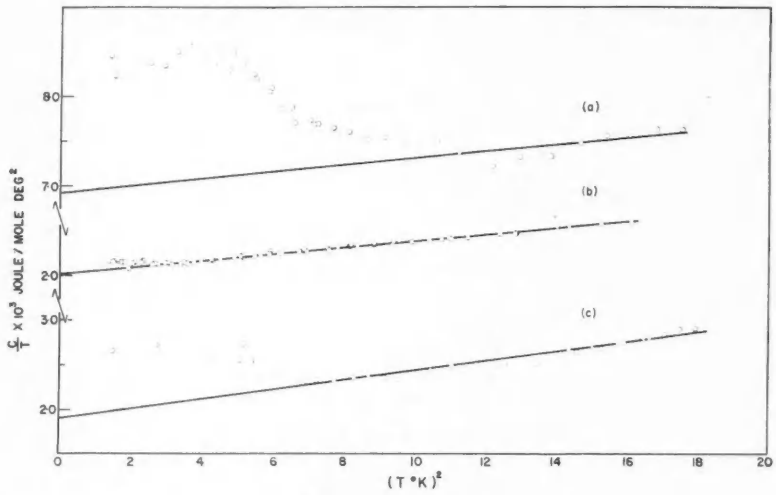

FIG. 6. C/T vs. T^2 for cupro–nickel alloys:
(*a*) $Cu_{60}\,Ni_{40}$ (Keesom and Kurrelmeyer 1940),
(*b*) $Cu_{70}\,Ni_{30}$ (this work),
(*c*) $Cu_{80}\,Ni_{20}$ (Keesom and Kurrelmeyer 1940).
All the data have been plotted on the same scale but the ordinates have been displaced for clarity.

type used in the present work. The measured specific heat of the cupro–nickel alloy (31.3 at.% Ni, effective atomic weight = 62.04 g) is represented by

$$\gamma = 2.027 \pm 0.013 \text{ millijoules/mole deg}^2,$$

$$\theta_0 = 375 \pm 5^\circ \text{ K}.$$

The errors in γ and θ_0 were estimated from straight-line fits to plots of C/T vs. T^2, evaluated at the 95% level of confidence.

In a publication which appeared since the completion of the present work (Guthrie *et al.* 1959) further measurements of the specific heat of some cupro–nickel alloys have been reported. For copper concentrations of less than about 75% these authors find a negative slope for C/T vs. T^2, which, however, is not as discontinuous as that found by Keesom and Kurrelmeyer, and Guthrie *et al.* attribute this rise in specific heat to a magnetic contribution. However, some of these measurements were carried out with helium exchange gas inside the calorimeter, performing a similar function to that used in Keesom and Kurrelmeyer's experiments, so that some of the results could still be misleading, because of the contribution from helium gas desorption. If the measurements on solid bars were made without any internal exchange gas, as seems likely, then there would appear to be a genuine effect associated with the specific heat of the alloy; but to make interpretation more certain, measurements should be made with an apparatus such as is described in the present paper, where exchange gas is not necessary.

CONCLUSION

A mechanical thermal switch cryostat has been developed along the lines of the design by Webb and Wilks. Its performance and some features of interest in its operation have been described; for instance, vibration is a very important consideration in determining the performance of the switch. Reasonable and practical cooling rates can be achieved without applying a large force to the switch and, in fact, a large force is undesirable if warming at the breaking of the switch is to be minimized. The switch has been successfully used for cooling metal samples in specific heat measurements in an arrangement which should be readily applicable to other experimental situations.

ACKNOWLEDGMENTS

I am grateful to Mr. F. W. Richardson and Mr. J. Broome for supplying the liquid helium and for a great deal of help during the course of this work, to Mr. B. Evans for performing the necessary glass blowing, to Mr. W. Stockdale for making chemical analyses, and to Mr. R. L. Snowdon for some help with the construction of the apparatus. I am also indebted to Dr. D. L. Martin for helpful discussions on various matters and for the design of the jacket calorimeter. Again, I wish to thank Miss Lorraine Peters for help with the calculation of the specific heat results.

REFERENCES

BERMAN, R. 1956. J. Appl. Phys. **27**, 318.
CLEMENT, J. R., LOGAN, J. K., and GAFFNEY, J. 1955*a*. U.S. Naval Research Laboratory Report, 4542.
——— 1955*b*. Phys. Rev. **100**, 743.
COLLINS, S. C. and ZIMMERMAN, J. E. 1953. Phys. Rev. **90**, 991.
CORAK, W. S., GARFUNKEL, M.P., SATTERTHWAITE, C. B., and WEXLER, A. 1955. Phys. Rev. **98**, 1699.
DARBY, J., HATTON, J., ROLLIN, B. V., SEYMOUR, E. F. W., and SILSBEE, H. B. 1951. Proc. Phys. Soc. (London), A, **64**, 861.
DAUPHINEE, T. M. and MOOSER, E. 1955. Rev. Sci. Instr. **26**, 660.
DOLECEK, R. L. and MADDEN, J. J. 1953. Rev. Sci. Instr. **24**, 1063.
GRIFFEL, M., VEST, R. W., and SMITH, J. F. 1957. J. Chem. Phys. **27**, 1267.
GUTHRIE, G. L., FRIEDBERG, S. A., and GOLDMAN, J. E. 1959. Phys. Rev. **113**, 45.
HULL, R. A., WILKINSON, K. R., and WILKS, J. 1951. Proc. Phys. Soc. (London), A, **64**, 379.
HOROWITZ, M., SILVIDI, A. A., MALAKER, S. F., and DAUNT, J. G. 1952. Phys. Rev, **88**, 1182.
JACOBS, R. B. and STARR, C. 1939. Rev. Sci. Instr. **10**, 140.
KEESOM, P. H. and PEARLMAN, N. 1956. Handbuch der Physik, **14**, 325.
KEESOM, W. H. and KOK, J. A. 1933. Physica, **1**, 770.
——— 1932. Leiden. Comm. 219*c*.
KEESOM, W. H. and KURRELMEYER, B. 1940. Physica, **7**, 1003.
KEESOM, W. H. and SCHWEERS, J. 1941. Physica, **8**, 1020, 1032.
KOSTRYUKOVA, M. O. and STRELKOV, P. G. 1953. Compt. rend. acad. sci. U.R.S.S. **90**, 525.
MANCHESTER, F. D. 1959. Can J. Phys. **37**, 525.
RAMANATHAN, K. G. and SRINIVASAN, T. M. 1955. Phil. Mag. **46**, 338.
RAYNE, J. A. 1956. Australian J. Phys. **9**, 189.
——— 1958. Phys. Rev. **110**, 606.
ROBERTS, T. R. and SYDORIAK, G. 1956. Phys. Rev. **102**, 304.
RUEHRWEIN, R. A. and HUFFMAN, H. M. 1943. J. Am. Chem. Soc. **65**, 1620.
WEBB, F. J. and WILKS, J. 1955. Proc. Roy. Soc. (London), A, **230**, 549.
WESTRUM, E. F., HATCHER, J. B., and OSBORNE, D. W. 1953. J. Chem. Phys. **21**, 419.
WHEATLEY, J. C., GRIFFING, D. B., and ESTLE, T. R. 1956. Rev. Sci. Instr. **27**, 1070.

ORBITAL FOLLOWING IN TETRAHEDRAL MOLECULES[1]

LESSER BLUM AND NORAH V. COHAN

ABSTRACT

On the basis of Heath and Linnett's formulas, the "orbital following" force constants of NH_3- and NH_4^+-like molecules are calculated. The anomalous results are interpreted as a consequence of orbital deformation during the vibratory movement.

For the study of molecular phenomena it is of interest to know what happens to the electronic charge distribution during vibration. According to the Born–Oppenheimer (1927) approximation the charge is disposed in such a way as to minimize the electronic energy. On the basis of similar considerations Heath and Linnett (1948*a*, *b*) introduced the concept of "orbital valence force field": they supposed that the function can be taken as resulting from the contributions of (*a*) the interaction of the nuclei with the electronic clouds and (*b*) the interaction between the electronic clouds; and, as the electronic clouds are disposed so as to minimize the electronic energy for each nuclear configuration, the electronic clouds do not follow this movement of the nuclei.

In this paper it is supposed (as was supposed by Heath and Linnett 1948*b*, 1950) that the orbitals correspond to the hybrids of the central atom, and that they are rigid and free to rotate during molecular vibration (Heath 1948*b*; Cohan 1956). The different modes of vibration are not treated separately, however, so that the formulas obtained are invariant under the transformations of the molecular symmetry group and are also valid for the combination modes.

THEORY C_{3v} MOLECULES

The function proposed by Heath and Linnett may be taken as follows:

$$V = V_l + V_{(\mathrm{ang})}$$

where

$$V_l = \tfrac{1}{2}k\sum \Delta l^2 \qquad \text{(see Fig. 1)},$$

$$(1)\quad 2V_{(\mathrm{ang})} = k_f[(A'\hat{N}A'')^2+(B'\hat{N}B'')^2+(C'\hat{N}C'')^2] + k_h[(A''\hat{N}B''-A\hat{N}B)^2+(B''\hat{N}C''-B\hat{N}C)^2+(C''\hat{N}A''-C\hat{N}A)^2].$$

Following a series expansion (with ω as the dihedral angle between two faces of the tetrahedron, see figure) it can be shown that

$$(A'\hat{N}A'')^2 = \frac{1}{l^2}[\overline{AA'}^2+\overline{AA''}^2-2\overline{AA'}\cdot\overline{AA''}\cos(\alpha'-\alpha'')],$$

$$(A''\hat{N}B''-A\hat{N}B)^2 = \frac{1}{l^2}[\overline{AA''}\cos\alpha''+\overline{BB''}\cos(\beta+\omega)]^2, \text{ etc.}$$

[1]Manuscript received April 10, 1959.
Contribution from the Facultad de Ciencias, Exactas y Naturales, Buenos Aires, Argentina.

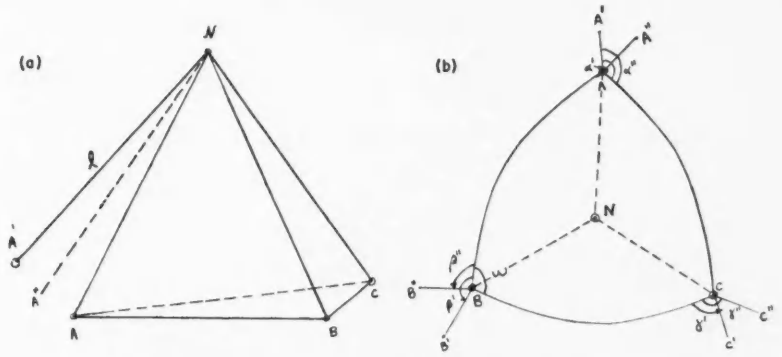

FIG. 1. (*a*) *A*, *B*, *C* represents the position of H in equilibrium; *A'*, *B'*, *C'* represents the position of H during vibration; *NA''*, *NB''*, *NC''* represents the position of "valence line" direction; *N* represents the position of *N* (or similar atom).
(*b*) Top view of the figure on the left, inscribed in a sphere of radius *l* and center *N*

are exact to the first degree of approximation. If the variab les are changed:

$$A \equiv \overline{AA}' \cos \alpha' \qquad a \equiv \overline{AA}'' \cos \alpha''$$
$$A' \equiv \overline{AA}' \sin \alpha' \qquad a' \equiv \overline{AA}'' \sin \alpha'', \text{ etc.}$$

The formula (1) will be

$$(2)\quad 2l^2 V_{(\text{ang})} = k_f[A^2+A'^2+B^2+B'^2+C^2+C'^2+a^2+a'^2+b^2+b'^2+c^2+c'^2 - 2[Aa+A'a'+Bb+B'b'+Cc+C'c']+k_h[(a+b\cos\omega-b'\sin\omega)^2 + (b+c\cos\omega-c'\sin\omega)^2+(c+a\cos\omega-a'\sin\omega)^2]$$

and if this formula is differentiated with respect to a,a', b,b', c, and c', the necessary condition for a minimum is obtained. Resolving these equations leads to:

$$(3)\quad 2l^2 V_{(\text{ang})} = (A^2+B^2+C^2)K_1+(A'^2+B'^2+C'^2)K_2+(AB+BC+CA)K_3 + (A'B'+B'C'+C'A')K_4+(AA'+BB'+CC')K_5 + (A'B+B'C+C'A)K_6+(AB'+BC'+CA')K_7$$

where

$$K_1 = [(r_1^2+2r_2^2+r_4^2+r_5^2+r_3^2-2r_1+1)\,k_f+(h_1^2+h_2^2+h_3^2)k_h]$$
$$K_2 = [(1+r_4^2+g_4^2+2g_5^2+r_5^2+r_3^2-2g_4)\,k_f+(h_4^2+h_5^2+h_6^2)k_h]$$
$$K_3 = 2[(r_2^2-r_3r_5+r_4r_3-r_4r_5+2r_2-2r_1r_2)k_f+(h_1h_2+h_2h_3+h_3h_1)k_h]$$
$$K_4 = 2[(r_3r_4-r_3r_5-2g_5+g_5^2+2g_4g_5-r_4r_5)k_f+(h_4h_5+h_5h_6+h_6h_4)k_h]$$
$$K_5 = 2[(r_1r_3+r_2r_5-2r_3-r_5g_5+r_4g_5+r_3g_4-r_2r_4)k_f+(h_1h_4+h_3h_6+h_2h_5)k_h]$$
$$K_6 = 2[(-r_2r_3-r_1r_5+2r_5+r_4g_5+r_3g_5-r_5g_4-r_2r_4)k_f+(h_2h_4+h_1h_6+h_3h_5)k_h]$$
$$K_7 = 2[(r_1r_4-2r_4-r_2r_3-r_5g_5+r_4g_4+r_3g_5+r_2r_5)k_f+(h_2h_6+h_1h_5+h_3h_4)k_h]$$

$$r_1 = \frac{1}{D}(N+2+x)(N+y^2); \quad r_2 = \frac{x}{D}(N+y^2); \quad r_3 = \frac{xy}{D}(N+1+x);$$

$$r_4 = \frac{y}{D}(N+2+x-x^2);$$

$$r_5 = \frac{xy}{D}(1+x); \quad g_4 = \frac{1}{D(N+y^2)}[N^3+N^2(2+x)+N(5+2x-2x^2-x^4)$$

$$+y^2(2+2x-y^2x)];$$

$$g_5 = \frac{xy}{D}; \quad h_1 = \frac{N}{D}(N+2+x-x^2); \quad h_2 = \frac{Nx}{D}(N+1+x); \quad h_3 = -\frac{N}{D}(x^2+x);$$

$$h_4 = h_6 = \frac{Nxy}{D}; \quad h_5 = -\frac{Ny}{D(N+y^2)}[N^2+N(3+x-x^2)+(2+x-2x^2-x^3)]$$

where

$$x \equiv \cos\omega; \qquad y \equiv \sin\omega; \qquad N \equiv \frac{k_f}{k_h};$$

$$D \equiv N^2+N(2+X)+4+2x-2x^2.$$

To obtain the expression in terms of bending angles of hydrogen atoms, their rotation around the central nitrogen atom must be suppressed. Then:

$$F_{\alpha^2} = \left[\frac{11}{36}K_1+(s_1^2+s_2^2+s_3^2)K_2-\frac{1}{36}K_3+(s_1s_2+s_2s_3+s_3s_1)K_4+\frac{1}{6}(s_1+3s_2-s_3)\right.$$

$$\left.\times K_5+\frac{1}{6}(-s_1+s_2-3s_3)K_6+\frac{1}{6}(3s_1-s_2+s_3)K_7\right],$$

$$F_{\alpha\beta} = \left[-\frac{2}{36}K_1+2(s_1s_2+s_2s_3+s_3s_1)K_2+\frac{10}{36}K_3+(s_1^2+s_2^2+s_3^2+s_1s_2+s_2s_3+s_3s_1)\right.$$

$$\left.\times K_4+\frac{1}{3}(s_1+2s_3)K_5+\frac{1}{3}(2s_1+s_2)K_6+\frac{1}{3}(2s_2+s_3)K_7\right]$$

$$s_1 = \frac{1}{6y}(x-3); \qquad s_2 = \frac{1}{6y}(3x-1); \qquad s_3 = \frac{1}{6y}(1-x).$$

TETRAHEDRAL T_d MOLECULES

The matrix of the potential energy, completely factored, is composed of two matrices of 1×1 (corresponding to the modes A_1 and E) and one of 2×2 (corresponding to F_2). The angular part of the potential function has three force constants to be determined, but from the secular determinants it is possible to obtain only two constants, even with the data of ND_4^+. This is in accordance with the fact that there are only two really independent constants, which can be initially selected according to the condition of redundance

$$\sum_{\text{all angles}} (R'\hat{N}S')-(R\hat{N}S) = 0.$$

Using a treatment completely similar to the one utilized on the NH_3-like molecules, the following results are obtained:

$$F_{\alpha^2} = k_h \frac{N^4+8N^3+21N^2+18N}{N^4+10N^3+37N^2+60N+36},$$

$$F_{\alpha\beta} = k_h \frac{N^4+10N^3+34N^2+36N}{24(N^4+10N^3+37N^2+60N+36)}.$$

($F_{\alpha\beta}$ denotes the interaction constant between adjacent angles.)

RESULTS

Infrared frequencies, suitably corrected for anharmonicity, were used in the calculation of force constants. The data used are those of Dennison (1940) (NH_3, ND_3), McConaghie and Nielsen (1949, 1953) (PH_3, PD_3, AsH_3, AsD_3), Haynie and Nielsen (1953) (SbH_3, SbD_3), and Gamo (1953) (NH_4^+, ND_4^+). The geometric constants were taken from the same papers. The calculations were performed following Wilson (1955).

TABLE I

Force constants

	NH_3	ND_3	PH_3	PD_3	AsH_3	AsD_3	SbH_3	SbD_3	NH_4^+
$10'' \times F_{\alpha^2}$, dynes/cm	0.61	0.47	0.72	0.72	0.67	0.67	0.59	0.59	0.2
$10'' \times F_{\alpha\beta}$	−0.129	−0.42	−0.067	−0.068	−0.045	−0.046	−0.035	−0.035	−0.2, −0.3

If the values of Table I were put in formula (3), the following expressions are obtained:

For NH_3:

$$F_{\alpha^2} = \frac{k_h(N^6+6.351N^5+12.586N^4+15.149N^3+6.972N^2+3.178N)}{N^6+4.858N^5+14.280N^4+25.130N^3+29.152N^2+17.635N+5.699},$$

$$F_{\alpha\beta} = \frac{k_h(1.131N^5+3.760N^4+4.234N^3+3.834N^2+1.619N)}{N^6+4.858N^5+14.280N^4+25.130N^3+29.152N^2+17.635N+5.699}.$$

For PH_3:

$$F_{\alpha^2} = \frac{k_h(N^6+7.116N^5+16.817N^4+23.294N^3+13.889N^2+7.354N)}{N^6+5.846N^5+20.075N^4+41.358N^3+55.607N^2+37.053N+14.644},$$

$$F_{\alpha\beta} = \frac{k_h(0.01656N^5+0.412N^4+0.710N^3+1.817N^2+0.543N)}{N^6+5.846N^5+20.075N^4+41.358N^3+55.607N^2+37.053N+14.644}.$$

For AsH_3:

$$F_{\alpha^2} = \frac{k_h(N^6+7.226N^5+17.467N^4+25.105N^3+15.157N^2+8.023N)}{N^6+6.006N^5+21.035N^4+44.098N^3+60.162N^2+40.104N+16.046},$$

$$F_{\alpha\beta} = \frac{k_h(-0.231N^5-0.478N^4-0.604N^3+0.850N^2-0.023N)}{N^6+6.006N^5+21.035N^4+44.098N^3+60.162N^2+40.104N+16.046}.$$

For SbH_3:

$$F_{\alpha^2} = \frac{k_h(N^6+7.176N^5+17.168N^4+23.855N^3+14.569N^2+7.715N)}{N^6+5.932N^5+20.589N^4+42.831N^3+58.065N^2+38.729N+15.424},$$

$$F_{\alpha\beta} = \frac{k_h(-0.1198N^5+0.048N^4+0.1137N^3+1.333N^2+0.159N)}{N^6+5.932N^5+20.589N^4+42.831N^3+58.065N^2+38.729N+15.424}.$$

Upon solution of these equations the values of k_f and k_h are obtained (see Table II).

TABLE II

Orbital following force constants

	NH_3	PH_3	AsH_3	SbH_3
N	−8.64	−0.85	−0.32	−0.42
$10'' \times k_h$, dynes/cm	0.89	−1.23	−3.19	−2.01
$10'' \times k_f$	−7.68	1.041	1.037	0.847

For the tetrahedral molecules there is only one real solution $N = -2$ if $F_{\alpha}^2/F_{\alpha\beta}$ is negative, and the problem remains, in this case, undetermined for k_f and k_h.

DISCUSSION OF RESULTS

It is clear that a negative value of N is anomalous as it means that not a minimum, but a maximum of the potential function is obtained; otherwise, the type of equation obtained for N allows only negative (real) solutions, unless in the case of the ammonia-like molecules, relations between the angular force constants are very different from those obtained experimentally.

The exclusion of a term corresponding to the lone pair of electrons could be criticized (Duncan 1953; Coulson 1951), but there are no reliable criteria to remove the indetermination of the problem with such a term present. Also calculations made by Cohan and Coulson (1956) in which the influence of the lone pair was taken into account led to negative force constants.

On the other hand, in the case of molecules of the ammonium ion type, in which these problems do not exist, a single solution for the maximum is obtained.

It is thought that the discrepancy is due to the deformation of the valence hybrids during the vibrations. It is possible also, that the valence line approximation may have affected the final result.

LIST OF NON-EVIDENT SYMBOLS

C_{3v}, T_d symmetry group (notation of Mulliken),

V = potential function,

V_l = part of the p.f. which corresponds to bond stretching,

$V_{(ang)}$ = angular part of the p.f.,

Δl = bond stretching,

A_1, E, F_2 correspond to the vibration modes; the notation is the same as the one used by Wilson (1955),

$\overset{\wedge}{A''NA'}$ = angle $A''NA'$, etc.,

$\overline{AA'}$ = segment $\overline{AA'}$, etc.,

l = bond length (see Fig. 1).

REFERENCES

BORN, M. and OPPENHEIMER, R. 1927. Ann. Physik, **84**, 457.
COHAN, N. V. and COULSON, C. A. 1956. Trans. Faraday Soc. **52**, 1163.
COULSON, C. A. 1951. Proc. Roy. Soc. **207**, 63.
DENNISON, D. M. 1940. Revs. Modern Phys. **12**, 175.
DUNCAN, F. and POPLE, J. 1953. Trans. Faraday Soc. **49**, 217.
GAMO, I. 1953. Compt. rend. **236**, 911.
HAYNIE, W. H. and NIELSEN, H. H. 1953. J. Chem. Phys. **21**, 1839.
HEATH, D. F. and LINNETT, J. W. 1948*a*. Trans. Faraday Soc. **44**, 556.
——— 1948*b*. Trans. Faraday Soc. **44**, 873.
——— 1950. Trans. Faraday Soc. **46**, 147.
MCCONAGHIE, V. M. and NIELSEN, H. H. 1949. Phys. Rev. **75**, 633.
——— 1953. J. Chem. Phys. **21**, 1836.
WILSON, E. B., DECIUS, J. C., and CROSS, P. C. 1955. Molecular vibrations (McGraw-Hill Book Co., Inc.).

THE HUND GRAVITATIONAL EQUATIONS AND GEONS[1]

LL. G. CHAMBERS

ABSTRACT

Certain solutions of the Hund gravitational equations which represent geons are derived, and the stability of steady solutions is discussed.

1. INTRODUCTION

In the absence of matter, Hund's gravitational field equations take the form

$$\nabla . \mathbf{g} = 0, \tag{1}$$

$$\nabla \times \mathbf{f} = -\frac{1}{c}\frac{\partial \mathbf{g}}{\partial t}, \tag{2}$$

$$\nabla . \mathbf{f} = \frac{1}{2c^2}(f^2+g^2), \tag{3}$$

$$\nabla \times \mathbf{g} = \frac{1}{c}\frac{\partial \mathbf{f}}{\partial t}+\frac{1}{c^2}\mathbf{f}\times\mathbf{g}. \tag{4}$$

By virtue of their non-linearity, these equations admit non-zero solutions which are not merely combinations of plane waves, and it has been pointed out to me by a referee of a previous paper (Chambers 1959) on this subject that such solutions in fact represent geons. It may be shown fairly easily that certain conditions on $\mathbf{f}$ must apply for a non-trivial solution of equations (1), (2), (3), (4) to be possible.

(*a*) No solution is possible for which $\mathbf{f}$ is zero everywhere or for which $\mathbf{f}$ is the curl of a vector. For were either of these true, the right-hand side of equation (3) would be zero, and as it is positive definite, it would follow that both $\mathbf{f}$ and $\mathbf{g}$ would have to vanish.

(*b*) Certain conditions on $\mathbf{f}$ stronger than those given in the last paragraph must be satisfied. For, if equation (3) be integrated over a volume inside a bounding surface

$$\int_v (f^2+g^2)\, d\tau = 2c^2 \int_v \nabla . \mathbf{f}\, d\tau = 2c^2 \int_s \mathbf{f} . d\mathbf{S} \tag{5}$$

and if the last integral vanishes then $\mathbf{f}$ and $\mathbf{g}$ must be intrinsically zero. This will be true for example if S is a large sphere of radius R and the radial component of $\mathbf{f}$ is $o(R^{-2})$. It may be remarked, however, that equation (5) does not preclude the possibility of a geon with a hollow core as for it to apply S must enclose v.

[1]Manuscript received April 14, 1959.
Contribution from the Department of Mathematics, University College of North Wales, Bangor, Caernarvonshire, Wales.

2. STATIC GEONS

Static solutions of equations (1) to (4) are given by $\mathbf{f}_S$, $\mathbf{g}_S$, which satisfy

$$\nabla . \mathbf{g}_S = 0, \tag{6}$$

$$\nabla \times \mathbf{f}_S = 0, \tag{7}$$

$$\nabla . \mathbf{f}_S = \frac{1}{2c^2}(f_S^2 + g_S^2), \tag{8}$$

$$\nabla \times \mathbf{g}_S = \frac{1}{c^2}\mathbf{f}_S \times \mathbf{g}_S. \tag{9}$$

In general, it is not possible to solve these equations. If, however, either (α) $\mathbf{f}_S$ and $\mathbf{g}_S$ are parallel or (β) $\mathbf{g}_S$ vanishes, a solution is possible. In both these cases equation (9) becomes

$$\nabla \times \mathbf{g}_S = 0. \tag{10}$$

Thus from equation (7)

$$\mathbf{f}_S = 2c^2 \nabla u \tag{11}$$

and from equations (6) and (10)

$$\mathbf{g}_S = 2c^2 \nabla v \tag{12}$$

where

$$\nabla^2 v = 0, \qquad u \text{ and } v \text{ are dimensionless.} \tag{13}$$

Now, in case (α), $\mathbf{f}_S$ and $\mathbf{g}_S$ are parallel and this implies that ∇u and ∇v are parallel. That is u and v form the same equipotential surfaces. In other words

$$u = F(v), \tag{14}$$

$$\mathbf{f}_S = 2c^2 F'(v) \nabla v, \tag{15}$$

$$\nabla . \mathbf{f}_S = 2c^2 F''(v)(\nabla v)^2, \tag{16}$$

using equation (13). Substituting in equation (8),

$$2c^2 F''(v)(\nabla v)^2 = 2c^2\{(F'(v))^2 + 1\}(\nabla v)^2$$

whence

$$F'(v) = \tan(v - v_0)$$

where v_0 is a constant,

whence

$$\mathbf{f}_S = 2c^2 \tan(v - v_0) \nabla v \tag{17a}$$

$$\mathbf{g}_S = 2c^2 \nabla v \tag{17b}$$

where v is subject to equation (13). On differentiation v_0 drops out and $v - v_0$ is also a solution of equation (13), and so the solutions may be written

$$\mathbf{f}_S = 2c^2 \tan v \nabla v = 2c^2 \nabla (\log \sec v) \tag{18a}$$

$$\mathbf{g}_S = 2c^2 \nabla v. \tag{18b}$$

This method indicates how the case (β) may be dealt with. Putting

$$\mathbf{f}_S = 2c^2 F'(v) \nabla v = 2c^2 \nabla \{F(v)\},$$

where v again satisfies equation (13), equation (8) becomes

$$2c^2 F''(v)(\nabla v)^2 = 2c^2 \{(F'(v))^2\}(\nabla v)^2$$

whence

$$F'(v) = \frac{1}{v_0 - v}.$$

Here again the constant v_0 may be dropped, and

$$\mathbf{f}_S = -\frac{2c^2}{v} \nabla v = -2c^2 \nabla (\log v). \tag{19}$$

As the range of solutions of equation (13) is large a correspondingly large set of solutions is possible for $\mathbf{f}_S$ and $\mathbf{g}_S$, subject always to the conditions of Section 1 being satisfied.

The equivalent mass distributions are given by

$$-\frac{1}{8\pi\gamma c^2}(f_S^2 + g_S^2) = -\frac{1}{4\pi\gamma} \nabla . \mathbf{f}_S. \tag{20}$$

In case (α) the equivalent distribution is

$$-\frac{1}{4\pi\gamma} \nabla . \{2c^2 \tan v \nabla v\} = -\frac{c^2}{2\pi\gamma} \sec^2 v (\nabla v)^2 \tag{21}$$

and in case (β) the equivalent distribution is

$$-\frac{1}{4\pi\gamma} \nabla . \left\{-\frac{2c^2}{v} \nabla v\right\} = -\frac{c^2}{2\pi\gamma} \frac{(\nabla v)^2}{v^2}. \tag{22}$$

Using Green's theorem the total equivalent mass is

$$-\frac{1}{4\pi\gamma} \int_v (\nabla . \mathbf{f}_S)\, d\tau = -\frac{1}{4\pi\gamma} \int \mathbf{f}_S . d\mathbf{S} \tag{23}$$

where S is the bounding surface.

3. PERTURBATION OF HUND'S EQUATIONS

Hund's equations are

$$\nabla . \mathbf{g} = 0, \tag{24}$$

$$\nabla \times \mathbf{f} = -\frac{1}{c} \frac{\partial \mathbf{g}}{\partial t}, \tag{25}$$

$$\nabla . \mathbf{f} = -4\pi\gamma\rho + \frac{1}{2c^2}(f^2 + g^2), \tag{26}$$

$$\nabla\times\mathbf{g} = \frac{1}{c}\frac{\partial \mathbf{f}}{\partial t} - \frac{4\pi\gamma\rho\mathbf{v}}{c} + \frac{1}{c^2}(\mathbf{f}\times\mathbf{g}). \tag{27}$$

For a steady universe, equations (25) and (27) become

$$\nabla\times\mathbf{f}_S = 0, \tag{28}$$

$$\nabla\times\mathbf{g}_S = -\frac{4\pi\gamma\rho\mathbf{v}}{c} + \frac{1}{c^2}(\mathbf{f}_S\times\mathbf{g}_S). \tag{29}$$

ρ and $\mathbf{v}$ are independent of time.

If $\mathbf{f}$ and $\mathbf{g}$ be disturbed, ρ and $\mathbf{v}$ remaining the same, the disturbance may be discussed in terms of $\mathbf{F}$ and $\mathbf{G}$ where

$$\mathbf{f} = \mathbf{f}_S + \mathbf{F}, \qquad \mathbf{g} = \mathbf{g}_S + \mathbf{G}.$$

Substituting these in equations (24) to (27) it follows that

$$\nabla\cdot\mathbf{g}_S + \nabla\cdot\mathbf{G} = 0, \tag{30}$$

$$\nabla\times\mathbf{f}_S + \nabla\times\mathbf{F} = -\frac{1}{c}\frac{\partial \mathbf{G}}{\partial t}, \tag{31}$$

$$\nabla\cdot\mathbf{f}_S + \nabla\cdot\mathbf{F} = -4\pi\gamma\rho + \frac{1}{2c^2}\{(\mathbf{f}_S+\mathbf{F})^2 + (\mathbf{g}_S+\mathbf{G})^2\}, \tag{32}$$

$$\nabla\times\mathbf{g}_S + \nabla\times\mathbf{G} = \frac{1}{c}\frac{\partial \mathbf{F}}{\partial t} - \frac{4\pi\gamma\rho\mathbf{v}}{c} + \frac{1}{c^2}\{(\mathbf{f}_S+\mathbf{F})\times(\mathbf{g}_S+\mathbf{G})\}. \tag{33}$$

Subtracting out the stationary parts from equations (30) to (33) it follows that

$$\nabla\cdot\mathbf{G} = 0, \tag{34}$$

$$\nabla\times\mathbf{F} = -\frac{1}{c}\frac{\partial \mathbf{G}}{\partial t}, \tag{35}$$

$$\nabla\cdot\mathbf{F} = \frac{1}{c^2}\{\mathbf{f}_S\cdot\mathbf{F} + \mathbf{g}_S\cdot\mathbf{G}\} + \frac{1}{2c^2}(F^2+G^2), \tag{36}$$

$$\nabla\times\mathbf{G} = \frac{1}{c}\frac{\partial \mathbf{F}}{\partial t} + \frac{1}{c^2}(\mathbf{F}\times\mathbf{g}_S + \mathbf{f}_S\times\mathbf{G} + \mathbf{F}\times\mathbf{G}). \tag{37}$$

It will be observed that equations (34) to (37) do not depend explicitly on ρ and $\mathbf{v}$, but only implicitly through $\mathbf{f}_S$ and $\mathbf{g}_S$. Thus the discussion which follows will be true both for geons and for mass distributions.

In order to discuss the stability of $\mathbf{f}$ and $\mathbf{g}$, it is necessary to linearize equations (36) and (37). These then become

$$\nabla\cdot\mathbf{F} = \frac{1}{c^2}(\mathbf{f}_S\cdot\mathbf{F} + \mathbf{g}_S\cdot\mathbf{G}) \tag{38}$$

and

$$\nabla\times\mathbf{G} = \frac{1}{c}\frac{\partial \mathbf{F}}{\partial t} + \frac{1}{c^2}(\mathbf{F}\times\mathbf{g}_S + \mathbf{f}_S\times\mathbf{G}). \tag{39}$$

Equations (34) and (35) are solved immediately by putting

$$\mathbf{G} = \nabla \times \mathbf{A}, \tag{40}$$

$$\mathbf{F} = -\frac{\partial \mathbf{A}}{\partial \tau}, \tag{41}$$

where

$$ct = \tau. \tag{42}$$

(It is not necessary to introduce a scalar potential (Stratton 1941*a*).) Writing

$$\alpha_S c^2 = \mathbf{f}_S, \qquad \beta_S c^2 = \mathbf{g}_S$$

equations (38) and (39) become

$$-\frac{\partial}{\partial \tau}(\nabla . \mathbf{A}) = -\alpha_S . \frac{\partial \mathbf{A}}{\partial \tau} + \beta_S . (\nabla \times \mathbf{A}), \tag{43}$$

$$\nabla \times (\nabla \times \mathbf{A}) = -\frac{\partial^2 \mathbf{A}}{\partial \tau^2} + \beta_S \times \frac{\partial \mathbf{A}}{\partial \tau} + \alpha_S \times (\nabla \times \mathbf{A}). \tag{44}$$

Equation (44) may be simplified slightly. From equation (28)

$$\mathbf{f}_S = c^2 \nabla u \tag{45}$$

and it follows that if

$$W = e^{-u} \tag{46}$$

equation (44) may be rewritten as

$$\nabla \times \{W(\nabla \times \mathbf{A})\} = -W \frac{\partial^2 \mathbf{A}}{\partial \tau^2} + W \beta_S \times \frac{\partial \mathbf{A}}{\partial \tau}. \tag{47}$$

Extending the ideas of non-linear mechanics (Minorsky 1947) it is possible to consider each stationary configuration of $\mathbf{f}$ and $\mathbf{g}$ as a point in an abstract phase space. When there is a disturbance, a path is traced out in phase space according as to the type of stability of the system at that point, and the temporal variation in the linearized problem.

The possible types of steady fields will be considered and the conditions found which $\mathbf{A}$ must satisfy.

4. NATURE OF STABILITY OF STEADY SOLUTIONS

(*a*) *Stable Vortex Point*

In this $\mathbf{A} = \mathbf{A}_0 \exp(i\omega\tau)$ ($\mathbf{A}_0$ real). Equation (43) becomes

$$i\omega\{\nabla . \mathbf{A}_0 - \alpha_S . \mathbf{A}_0\} = \beta_S . (\nabla \times \mathbf{A}_0), \tag{48}$$

$$\nabla \times \{W(\nabla \times \mathbf{A}_0)\} = \omega^2 W \mathbf{A}_0 + i\omega W \beta_S \times \mathbf{A}_0. \tag{49}$$

Splitting into real and imaginary parts

$$\nabla . \mathbf{A}_0 - \alpha_S . \mathbf{A}_0 = 0, \tag{50a}$$

$$\beta_S.(\nabla\times\mathbf{A}_0) = 0, \tag{50b}$$

$$\beta_S\times\mathbf{A}_0 = 0, \tag{50c}$$

$$\nabla\times\{W(\nabla\times\mathbf{A}_0)\} = \omega^2 W\mathbf{A}_0. \tag{50d}$$

It is also necessary that ω^2 is positive. Multiplying equation (50*d*) scalarly by $\mathbf{A}_0$ and integrating over the whole of space it follows that

$$\omega^2\int A_0^2\,d\tau = \int\mathbf{A}_0.[\nabla\times\{W(\nabla\times\mathbf{A}_0)\}]\,d\tau \tag{51}$$

$$= \int W(\nabla\times\mathbf{A}_0)^2\,d\tau - \int W[\mathbf{A}_0\times(\nabla\times\mathbf{A}_0)].d\mathbf{S}$$

and if this last integral vanishes, ω^2 is always positive. If this is not the case, then the splitting up into real and imaginary parts is not admissible. It will be noted that ω vanishes with $\nabla\times\mathbf{A}_0$ and if this be the case all the equations (50) are satisfied identically. This case is not stable, however, as it corresponds to a time variation $Ct+D$.

It may be remarked that (50*c*) sometimes implies (50*b*) for

$$0 = \nabla.\{\beta_S\times\mathbf{A}_0\} = \mathbf{A}_0.(\nabla\times\beta_S) - \beta_S.(\nabla\times\mathbf{A}_0) = -\beta_S.(\nabla\times\mathbf{A}_0)$$

by virtue of equation (9) if $\mathbf{f}_S$ and $\mathbf{g}_S$ are parallel.

(*b*) *Focus*

In this $\mathbf{A} = \mathbf{A}_0 e^{p\tau}e^{it\omega\tau}$ ($\mathbf{A}_0$ real) where p is positive for instability and negative for stability.

Equation (47) becomes

$$\nabla\times\{W(\nabla\times\mathbf{A}_0)\} = (p+i\omega)^2 W\mathbf{A}_0 + (p+i\omega)W\beta_S\times\mathbf{A}_0. \tag{52}$$

Taking the imaginary part of equation (52), it follows that

$$2p\omega\mathbf{A}_0 + i\omega\beta_S\times\mathbf{A}_0 = 0. \tag{53}$$

This is a vector equation the only possible solution of which is $\mathbf{A}_0 = 0$. Thus there is no steady state which corresponds to a focus.

(*c*) *Saddle Point*

In this case the time variation is either $e^{\pm p\tau}$ depending on the nature of the small disturbance.

(*d*) *Stable Node*

In this case the time variation is $e^{-p_1\tau}$ or $e^{-p_2\tau}$ where p_1 and p_2 are positive, depending on the nature of the small disturbance.

(*e*) *Unstable Node*

In this case the time variation is $e^{p_1\tau}$ or $e^{p_2\tau}$ where p_1 and p_2 are positive, depending on the nature of the small disturbance.

These three cases, (*c*), (*d*), (*e*), may be dealt with by assuming a time variation $e^{k\tau}$ in equations (43) and (47).

Equation (43) becomes

$$k(\nabla.\mathbf{A}_0-\boldsymbol{\alpha}_S.\mathbf{A}_0)+\boldsymbol{\beta}_S.(\nabla\times\mathbf{A}_0) = 0 \tag{54}$$

and equation (47) becomes

$$\nabla\times\{W(\nabla\times\mathbf{A}_0)\} = -k^2W\mathbf{A}_0+kW\boldsymbol{\beta}_S\times\mathbf{A}_0. \tag{55}$$

Multiplying scalarly by $\mathbf{A}_0$

$$\mathbf{A}_0.[\nabla\times\{W(\nabla\times\mathbf{A}_0)\}] = -k^2WA_0^2. \tag{56}$$

It follows therefore that there cannot be nodes, because the two roots of (56) are equal and opposite in sign, and therefore there must be a saddle point. Thus the stability of a steady-state solution depends on the quantity

$$\mathbf{A}_0.[\nabla\times\{W(\nabla\times\mathbf{A}_0)\}] = W(\nabla\times\mathbf{A}_0)^2-\nabla.\{W\mathbf{A}_0\times(\nabla\times\mathbf{A}_0)\}. \tag{57}$$

If this is positive there is stability and a vortex point. If it is negative, there is a saddle point and instability.

It follows therefore that a condition for stability is

$$\int W(\nabla\times\mathbf{A}_0)^2d\tau > \int W[\mathbf{A}_0\times(\nabla\times\mathbf{A}_0)].d\mathbf{S} \tag{58}$$

and in particular this is true when the integral on the right-hand side vanishes. This may be done by any of W, $\mathbf{A}_0$, $\nabla\times\mathbf{A}_0$ vanishing on the surface, by the surface being parallel to either $\mathbf{A}_0$ or $\nabla\times\mathbf{A}_0$, by the product $W\mathbf{A}_0\times(\nabla\times\mathbf{A}_0)$ being sufficiently small at infinity if the whole of space is under consideration, or of course by some orthogonality property.

Further conditions for stability which must hold are equations (50*a*) to (50*c*) in the general case, equations (50*a*) and (50*c*) when $\mathbf{f}_S$ is parallel to $\mathbf{g}_S$ and equation (50*a*) when $\mathbf{g}_S$ vanishes.

5. AN EXAMPLE OF A GEON AND ITS STABILITY

For simplicity consider a static geon in which $\mathbf{g}_S$ vanishes, and there is spherical symmetry. Consider the potential

$$v = \frac{a}{r}. \tag{59}$$

This function is harmonic and

$$\mathbf{f}_S = -2c^2\frac{\nabla v}{v} = \frac{2c^2}{r}\hat{\mathbf{r}}. \tag{60}$$

The value of W corresponding to this is given by

$$W = e^{-u}, \qquad \mathbf{f}_S = c^2\nabla u. \tag{61}$$

Clearly

$$u = -\log v^2$$

and so

$$W = r^2/a^2. \tag{62}$$

The equations governing a perturbation **A** are given by

$$\nabla.\mathbf{A}-\frac{2}{r}A_r = 0, \tag{63}$$

$$\nabla\times(\nabla\times\mathbf{A})-\frac{2}{r}\mathbf{r}\times(\nabla\times\mathbf{A})-\omega^2\mathbf{A} = 0. \tag{64}$$

These equations can be solved by the following method (Stratton 1941*b*).

Let

$$\mathbf{A} = \nabla\times(L\hat{\mathbf{r}}) \tag{65}$$

where L is a scalar. It is clear that this equation satisfies equation (65) identically as

$$A_r = 0, \qquad A_\theta = \frac{1}{r\sin\theta}\frac{\partial L}{\partial\phi}, \qquad A_\phi = -\frac{1}{r}\frac{\partial L}{\partial\theta}. \tag{66}$$

Expanding equation (64) into its components it is found that the r component vanishes, and that the θ and ϕ components are respectively given by

$$\frac{1}{r\sin\theta}\left\{-\frac{\partial}{\partial\phi}\left[\frac{1}{r^2\sin\theta}\left(\frac{\partial}{\partial\theta}(\sin\theta\frac{\partial L}{\partial\theta})+\frac{1}{\sin\theta}\frac{\partial^2 L}{\partial\phi^2}\right)\right]-\frac{\partial^3 L}{\partial r^2\partial\phi}\right\} \tag{67}$$
$$-\frac{2}{r}\cdot\frac{1}{r}\frac{\partial}{\partial r}\left(\frac{1}{\sin\theta}\frac{\partial L}{\partial\phi}\right)-\frac{\omega^2}{r\sin\theta}\frac{\partial L}{\partial\phi} = 0$$

and

$$-\frac{1}{r}\left\{\frac{\partial^3 L}{\partial r^2\partial\theta}-\frac{\partial}{\partial\theta}\left[\frac{1}{r^2\sin\theta}\left(\frac{\partial}{\partial\theta}(\sin\theta\frac{\partial L}{\partial\theta})+\frac{1}{\sin\theta}\frac{\partial^2 L}{\partial\phi^2}\right)\right]\right\} \tag{68}$$
$$-\frac{2}{r}\cdot\frac{1}{r}\frac{\partial}{\partial r}\left(-\frac{\partial L}{\partial\theta}\right)+\frac{\omega^2}{r}\frac{\partial L}{\partial\theta} = 0.$$

It will be seen that equations (67) and (68) are satisfied provided that

$$\frac{\partial^2 L}{\partial r^2}+\frac{2}{r}\frac{\partial L}{\partial r}+\frac{1}{r^2\sin\theta}\frac{\partial}{\partial\theta}(\sin\theta\frac{\partial L}{\partial\theta})+\frac{1}{r^2\sin\theta}\frac{\partial^2 L}{\partial\phi^2}+\omega^2 L = 0, \tag{69}$$

i.e.

$$\nabla^2 L+\omega^2 L = 0;$$

a solution of this equation is given by

$$L = \{A_1 h_n^{(1)}(\omega r)+A_2 h_n^{(2)}(\omega r)\}\, S_{mn}(\theta,\phi) \tag{70}$$

where $h_n^{(1)}$ and $h_n^{(2)}$ are spherical Bessel functions (Stratton 1941*c*) and $S_{mn}(\theta,\phi)$ is a surface harmonic.

The stability depends upon the value of the surface integral in equation (51). If the surface is a sphere of radius R,

$$\int W\{\mathbf{A}\times(\nabla\times\mathbf{A})\}.d\mathbf{S} = \frac{R^4}{a^2}\int[\mathbf{A}\times(\nabla\times\mathbf{A})]_r\, d\Omega \tag{71}$$

where $d\Omega$ is an elementary solid angle. This becomes, on substituting the appropriate values for $\mathbf{A}$ and $\nabla\times\mathbf{A}$

$$\frac{R^3}{a^2}\int d\Omega\left[\frac{\partial}{dr}\left\{\left(\frac{\partial L}{\partial\theta}\right)^2+\left(\frac{1}{\sin\theta}\frac{\partial L}{\partial\phi}\right)^2\right\}\right]_{r=R}. \tag{72}$$

It is clear that in general this does not vanish.

However, if $L = L_0 j_n(\omega r) P_n(\cos\theta)$ where L_0 is a suitable dimensional factor, expression (72) becomes

$$2\frac{R^3}{a^2}L_0^2\omega j_n'(\omega R) j_n(\omega R)\int d\Omega\{P_n'(\cos\theta)\sin\theta\}^2 \tag{73}$$

and if either $j_n(\omega R)$ or $j_n'(\omega R)$ vanishes expression (73) vanishes and the disturbance will be stable.

Thus in general the geon considered will be unstable, but will, however, be stable for certain perturbations.

REFERENCES

CHAMBERS, LL. G. 1959. Can. J. Phys. **37**, 433.
MINORSKY, N. 1947. Non-linear mechanics (J. W. Edwards, Ann Arbor, Mich.), p. 12.
STRATTON, J. A. 1941*a*. Electromagnetic theory (McGraw-Hill Book Co., Inc., New York), p. 24.
——— 1941*b*. Electromagnetic theory (McGraw-Hill Book Co., Inc., New York), p. 415.
——— 1941*c*. Electromagnetic theory (McGraw-Hill Book Co., Inc., New York), p. 404.

ON "PLASTIC" WAVES IN SOLIDS[1]

JOHN M. BOWSHER[2]

ABSTRACT

The study of the propagation of "plastic" waves in solids has reached a stage where it is necessary to consider which direction future research should take. In the past 90 or so years many experiments, mostly designed to elucidate certain points of engineering significance, and a few attempts at a theoretical study have cast some light on the subject and revealed it as one of formidable difficulty.

Nearly all the experiments have of necessity relied on rather dubious theories for their interpretation, and part of the present paper will be devoted to a description of an apparatus which gives results capable of being interpreted with a very minimum of theory. The remainder of the paper is devoted to a short review of past work with particular emphasis on basic phenomena and to a brief discussion on the most pressing problems still remaining. The experiments described in the present paper bring to light a factor in the propagation of "plastic" waves that seems to have been overlooked in previous work.

INTRODUCTION

Most work on the subject of the propagation of stress waves in solids has been devoted to the limiting cases of what shall be called here Low Amplitude and Very High Amplitude waves. In low amplitude waves, the stress amplitude is assumed to be much less than the elastic limit so that, after the passage of the wave, the specimen practically regains its original form. In other words, low amplitude waves are merely elastic or sound waves. When the stress amplitude is so great that the conventional elastic constants cease altogether to have any meaning and the specimen material flows like a fluid, the wave motion is referred to as very high amplitude.

In High Amplitude stress wave propagation, however, the stress amplitude is comparable with (say 1 to 100 times) the elastic limit, and is not so large that the detailed mechanisms governing the flow of solids can be ignored as with very high amplitude waves. The chief characteristic of propagation in the high amplitude range is the very large amplitude dispersion the input signal suffers. Frequency dispersion has long been familiar in the low amplitude range where the concepts of group and phase velocity have been thoroughly explored and meaningful values of the physical constants of the specimen may now be given after measurements of the group velocities only. In the high amplitude range nothing has been found in the literature on frequency dispersion and this is, therefore, a problem which should be tackled soon. Amplitude dispersion is not so well known since it is an effect of very small importance in low amplitude work, but in high amplitude waves the velocity of a stress increment situated above the yield stress of the specimen material may, in certain cases, be as little as 10% of the elastic wave velocity (Wood 1952).

An input signal consisting of a step-function-like stress pulse thus rapidly

[1]Manuscript received April 22, 1959.
Contribution from the Imperial College of Science and Technology, London, England.
[2]Postdoctorate Fellow in the Radio and Electrical Engineering Division, National Research Council, Ottawa, Canada.

loses its initial shape and becomes transformed according to the properties of the propagating medium and the amplitude of the initial pulse. For convenience, we shall use the word profile to describe the shape assumed by an initially step-function-like pulse. Mathematically, the profile may be considered as the σ', u, ϵ, or ρ versus C curve, where

σ' is the engineering stress
u the particle velocity
ϵ the strain
ρ the density
C the stress wave velocity,

and the present paper is devoted entirely to consideration of the profiles of high amplitude pulses.

Previous work on the profiles of high amplitude waves is wholly theoretical and is typified by the figures (1, 2, 3) to be found in von Kármán and Duwez

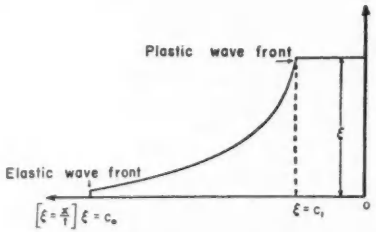

FIG. 1. Typical theoretical profile of a stress pulse propagating in a wire (after von Kármán and Duwez 1950, used with permission).

(1950), Taylor (1946), and Broberg (1956). The profiles by von Kármán and Taylor are for a medium having a stress–strain curve always concave downwards, and, moreover, having no strain–time effects. Broberg's profile applies to a medium exhibiting the delayed yield phenomenon and also applies to stresses large enough for the stress–strain curve to be concave upwards leading to the development of shock fronts.

Since so many assumptions had to be made to derive these profiles it appeared valuable to design an apparatus capable of obtaining directly the profile of a stress pulse propagating through a medium. The apparatus, which is to be described later, obtains the u–C profile directly but it has proved possible (Appendix) to derive some simple, but approximate, correction terms to the well-known relation from elasticity, $\sigma = \rho C u$, where σ is the stress. The corrected equation may then be applied to a high amplitude pulse propagating in a medium with an unknown stress–strain curve. The corrections are based on the Lagrangian formulation of "plastic" waves by von Kármán but are independent of strain–time effects since all measurements are reduced to those capable of being made while the pulse is actually being propagated.

The particle velocity u is measured by assuming that the free surface

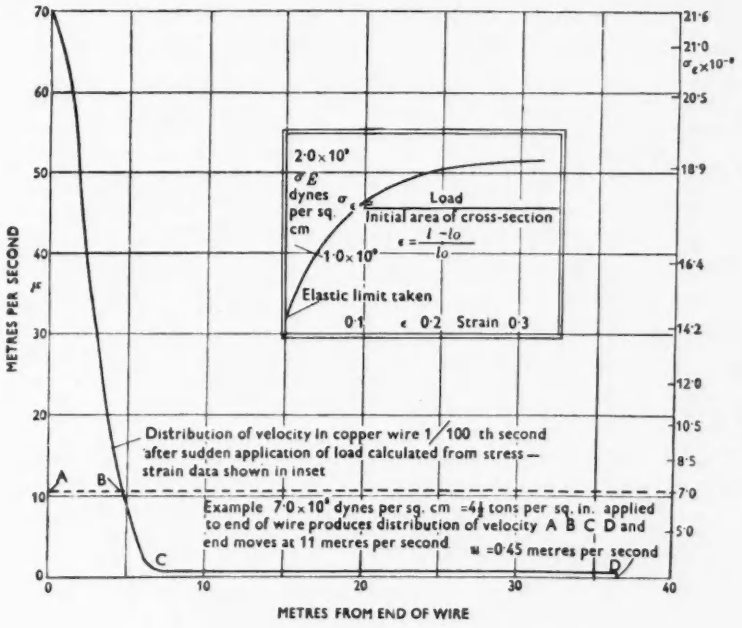
METRES PER SECOND
METRES FROM END OF WIRE
2·0×10⁹
dynes per sq. cm
Load
Initial area of cross-section
1·0×10⁹
Elastic limit taken
0·1
0·2 Strain 0·3
Distribution of velocity in copper wire 1/100 th second after sudden application of load calculated from stress—strain data shown in inset
Example 7·0×10⁸ dynes per sq. cm =4½ tons per sq. in. applied to end of wire produces distribution of velocity A B C D and end moves at 11 metres per second
=0·45 metres per second
A
B
C
D

PLASTIC WAVE IN COPPER $\frac{1}{100}$ SECOND AFTER APPLYING LOAD

FIG. 2. Typical theoretical profile of a stress pulse propagating in a copper wire. *U* corresponds to our *v* (after Taylor 1946, used with permission).

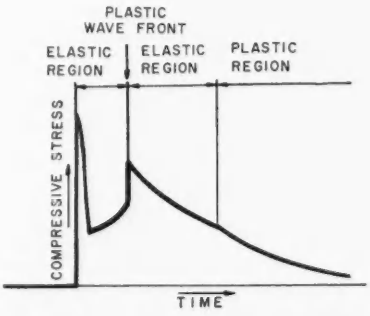

FIG. 3. Typical theoretical profile of a stress pulse propagating in a medium exhibiting a stress-dependent time delay for yielding (after Broberg 1956, used with permission).

velocity after a normal reflection of the pulse is $2u$, which assumption has been shown to be valid within very small error up to stresses much in excess of those used in the present apparatus (Walsh and Christian 1955).

A NOTE ON PLASTIC AND "PLASTIC" WAVES

Since nothing is yet known about the front separating the elastic and plastic regions in the medium through which the wave is propagating, the term "plastic" wave is used here throughout. It is felt that the term plastic wave is inappropriate as the region is not plastic but is an intermediate stage between elastic and plastic.

LOW AMPLITUDE WAVES

It was estimated recently by Davies that well over 1000 papers have been published since World War II on the subject of stress waves in solids; obviously it has become well nigh impossible to survey the field in any detail, and this section is intended to be just an introduction to give the reader some references where he may find further bibliography. We shall discuss briefly papers on the particular problem of the impact of two bars only since results obtained from experiments on impacting bars give information on some of the phenomena of importance in high amplitude stress wave propagation.

The first papers, by Cauchy (1826) and Poisson (1833), are not of much value at present and it was undoubtedly de St-Venant (1867) who gave the first satisfactory solution of the problem of the impact of bars with plane ends. Simultaneous impact over a plane end is virtually impossible to realize in practice, however (Schneebeli 1871; Hamburger 1885), and Sears (1908, 1912) in his work used a combination of de St-Venant's theory and Hertz's (1882) formula for the deformation resulting from the compressive contact of two surfaces with radii of curvature R_1 and R_2. Hertz himself did briefly consider the problem of impact in the appendix to his paper and obtained results similar to those of Davies (1949) but that work seems to have been forgotten until recently.

The experimental arrangement of two bars, one being hit by the other, is extremely suited to the study of short, large, stress pulses and considerable understanding of plastic flow has been gained by using the Hopkinson Bar, as a refinement of the two-bar apparatus is known. Hopkinson (1914) estimated the time integral of a pressure pulse by measuring the momentum transferred to a detachable "time-piece" at the end of a pressure bar, but recently Davies (1948) has applied modern techniques to the bar and an illustration of their use may be found in Taylor and Davies (1942), where the dynamic yield stress of Cordite was measured. Flow of the pressure bar material takes place quite frequently in Hopkinson bar experiments.

HIGH AMPLITUDE STRESS WAVES

The subject of high amplitude wave propagation is intimately bound up with that of plasticity and yield phenomena, and a favorite method of investigating plastic phenomena is to impact the specimen and study the resulting "plastic" waves and/or flow. Any study of "plastic" waves must, therefore, be preceded by some study of plastic flow and the various effects found. These will not be discussed in detail but the references quoted give typical results and also lead the reader to a greater bibliography.

Let us first list which effects are of importance in the study of "plastic" waves: (*i*) strain rate, (*ii*) temperature, (*iii*) pressure, (*iv*) delayed yield, (*v*) attenuation.

(*i*) *Strain Rate*

For many years it has been realized that for many metals, particularly iron and steel, a different set of mechanical constants applies when the strain rate is high, and very many experimental investigations have been performed to elucidate the difference. As early as 1872, Hopkinson (1872*a* and *b*), the father of the inventor of the Hopkinson Bar, found that an iron wire could withstand a momentary stress of almost double the elastic limit without any noticeable impairment of elastic properties and since then there have been many experiments devoted to attempts to evaluate the differences between static and dynamic properties. The best general reference is Rinehart and Pearson (1954) and a typical result for iron has been found by Whiffin (1948) to be $D/S = 3$ for $S = 20$ tons/in^2, and $D/S = 1$ for $S = 120$ tons/in^2 where D is the dynamic yield stress and S the static; these results show that the problem is of considerable complexity. Many attempts have been made to explain the strain-rate effect on the basis of an "incubation" period for yield but they overlook a paper by Edwards, Phillips, and Jones (1940) in which it is reported that for iron at very low strain rates, the yield stress begins to rise again.

The strain-rate phenomenon is not only important in metals; in plastics also it is found that the response to a stress depends on the rate of loading, which is important now with the steadily increasing use of rubbers and high polymers for vibration isolation. The physical properties of high polymers with long chain molecules with, perhaps, various degrees of cross-linking may, fortunately, be represented by a relatively simple "memory" function and may now be calculated with some confidence (cf. Alfrey 1948 for example).

(*ii*) *Temperature*

Increasing strain rate and decreasing temperature have qualitatively similar effects on many mechanical properties of metals but no simple relation has yet been found between increase of strain rate and decrease of temperature since every metal and every alloy has a different behavior. Attempts have been made by Holloman (1946), however, to obtain a single-valued function that will express the behavior of a metal under various conditions of strain, strain rate, and temperature but his equations have only a limited application.

A fairly comprehensive survey of the effects of low temperatures on the mechanical properties of metals has been given by Russell (1931), who gives the following summary.

With decrease of temperature for common metals, the

yield point	increases,
yield strength	increases,
reduction of area	decreases,
impact resistance	decreases,
hardness	increases,
and the endurance limit	increases;

the close similarity with rapid loading effects may clearly be seen.

There are, though, many exceptions to the above summary, notably the stainless steel alloys (Krivobok 1952), which exhibit greater ductility at low temperatures.

The effect of temperature on the mechanical properties of a metal must therefore be established for each metal and also as far as possible under the conditions for which knowledge of the property is desired, since present knowledge is inadequate to allow a reliable prediction from data obtained under one set of conditions to another.

(*iii*) *Pressure Effects*

The effect of pressure on the elastic constants of solids is not very great in the range of pressures of present concern. Hughes and Kelly (1953) and Cook (1957) give examples of the use of Murnaghan's (1937) theory to the calculation of the velocity of low amplitude waves in a solid under hydrostatic stress, and the reader is referred to those papers for further details.

(*iv*) *Delayed Yield*

With some materials, there is an appreciable time delay before yield takes place when the specimen is loaded to a stress above its yield point. This delay depends on the conditions and may be as much as 6 or more seconds and is of great importance in impact problems since the mechanical response of the material to a transient load is going to depend very strongly on the time constants associated with that load.

A great deal of both experimental and theoretical work has been carried out on the delayed yield phenomenon, chiefly because it occurs to such a large extent in those materials, such as iron and steel, which are of great use in engineering. The basic theoretical paper is that by Cottrell and Bilby (1949) which, together with annotations by Yokobori (1952*a* and *b*), describes a mechanism of yielding in terms of dislocations in the crystal lattice of iron and dislocation atmospheres round each iron atom formed by the disturbing effect of the smaller carbon atoms which tend to cluster in the low-potential regions around the iron atoms. In this theory a time delay in yielding is predicted. Typical experimental results are quoted by Wood and Clark (1949, 1951) and Vreeland, Wood, and Clark (1953), who measured the time of yielding by the number of repeated short-duration pulses required before yielding took place. The 1951 Wood and Clark investigation found that the effect of temperature upon time delay for mild steel confirmed the theory of Cottrell and Bilby.

The properties of crystals which are likely to be of importance in high amplitude pulse propagation and which have not been discussed above are fully dealt with by Cottrell (1953), whose work includes a comprehensive bibliography.

(*v*) *Attenuation*

For some reason the fact that the "plastic" wave will suffer attenuation during propagation and that this will affect conditions at the front between the plastic and elastic regions quite markedly seems to have escaped attention until now, and it is believed, therefore, that the discussion following is the first in print.

PROPAGATION OF HIGH AMPLITUDE WAVES

The present theories of the propagation of high amplitude waves such as those by Taylor, von Kármán, and Rakhmatulin are treated in standard works (for example, Kolsky 1953), and will not be discussed here save to emphasize that they are only extensions of ordinary elasticity theory to finite strains; there has not yet appeared in the literature a rigorous definition of a plastic wave and a subsequent analysis of its behavior for a given set of conditions. A physical interpretation of plastic waves presents grave conceptual difficulties which, we feel, are very inadequately considered in the literature and for this reason all references here to high amplitude waves are to "plastic" waves and not the loose term plastic waves which can lead to confusing and possibly inaccurate assumptions on the modes of displacement taking place during the passage of the wave.

The three theories mentioned above apply only in cases where the stress–strain curve is always concave downwards. When the curve may become concave upwards further difficulties arise due to the formation of shock fronts (see, for example, White and Griffis 1947, 1948).

If the strain-rate phenomenon is included the problem becomes still more complicated and quite complex mathematics have to be employed to obtain solutions to the simplest case (Alter and Curtis 1956; Malvern 1951; Rubin 1954). A profile calculated by Alter and Curtis is shown in Fig. 4; note that in a

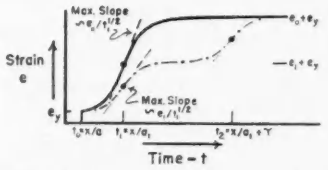

FIG. 4. Typical theoretical profile of a stress pulse propagating in a medium exhibiting the strain-rate effect. The dotted curve shows the result of a two-step application of the same pulse amplitude (after Alter and Curtis 1956, used with permission).

material exhibiting the strain-rate effect plastic strain components can travel with the velocity of sound, C_0, in contrast to the rate-independent model.

Experimental investigations into "plastic" waves are very few and are rather too strongly dependent on a particular theory to be entirely satisfying (see Kolsky 1953). A puzzling paper by McReynolds (1949) describes a type of "plastic" wave unlike the usual type considered here; it is difficult to explain McReynold's waves but they may be an experimental artifact.

In the very high amplitude range the stress amplitude is so great that the specimen material may be treated as a fluid with a considerable simplification of the theory. It is not uncommon for measurements to be made on two parameters of the motion simultaneously in very high amplitude work (Walsh and Christian 1955; Doran, Fowles, and Peterson 1958), which enables the equations of the motion to be solved without having to assume an equation of state.

In high amplitude work, on the other hand (Duwez 1947; Duwez and Clark 1947), no experiments on propagation involving the simultaneous measurement of two parameters had been reported when this work was begun (but see Bell 1959). It seemed, therefore, that an attempt should be made to record the profile of a high amplitude stress pulse in a way which would be independent of a particular theory, and could be said to mean something by itself. To do this, two parameters at least must be measured simultaneously.

APPARATUS

Let us first list the techniques that are available to one wishing to measure high amplitude waves. The problem divides naturally into two parts: (*a*) generating devices, and (*b*) receiving devices.

(*a*) *Generating Devices*

The only really convenient method to generate a high amplitude stress wave in a solid is to hit the solid with a suitably designed hammer. The use of high explosives is unnecessary because the stress amplitudes will then usually be far too large. Methods based on using the pressure developed by the passage of an electric spark through sea water contained in a small volume are rather too inflexible for experimental work where a wide range of pressures is desired.

The design of a hammer depends on many circumstances, some of which have no scientific significance. In the present work, for example, the commonest method of driving a hammer (allowing it to fall freely under gravity) was not available for the simple reason that the laboratory ceiling was not high enough. The device actually used was a high-speed pneumatic hammer (Fearon 1953), as this was thought to be a more flexible and reproducible tool than a catapult in which the hammer is accelerated by rubber bands. The hammer used was shaped with a spherical end of 5-ft radius of curvature, large enough to ensure essentially plane waves over the measuring area. A flat-ended hammer cannot be used because the alignment difficulties become too acute (*vide supra*).

(*b*) *Receiving Devices*

Most techniques are ill-suited to the measurement of two variables at once, but some worth considering are:

1. Walsh and Christian's method (1955).—This will not work in its original form in the high amplitude field, but the basis of the method is capable of adaptation (see later).

2. Pins.—This is the conventional technique for very high amplitude work but is not suitable for high amplitude work because the setting-up tolerances become too fine. Another disadvantage is that the apparatus is destroyed after each experiment.

3. Piezoelectric transducers: (A) accelerometer type, (B) pressure-sensitive type.—The main difficulty with these devices lies in their calibration. They are known to become increasingly non-linear as the stress amplitude increases, but as yet no one has found a way to calibrate over the whole range of amplitudes since at the top of the range the crystal fractures and is lost. Minshall

(1955) has reported the use of Z-cut tourmaline crystals for very high amplitude work and it appears that they would be usable in the high amplitude range. Only one parameter is measured, though, $\sigma(t)$.

4. Resistance strain gauges.—These are too large for the sort of measurements at present of interest.

5. Diffraction gratings.—This extremely elegant method has been described by Bell (1956). The main disadvantage is that a lathe accurate to optical standards is required to prepare the specimens.

6. Condenser microphones.—The condenser microphone is immediately attractive as there are no problems of bonding the specimen to the microphone (as in 3); it is merely necessary to have a conducting plate a short distance away from and parallel to the specimen surface. The use of a condenser microphone to record the surface motion of a specimen is well known but another parameter was needed. Obviously, one cannot measure the stress or density directly with a condenser microphone, so a way must be found of measuring the velocity of the stress pulse itself as it moves through the specimen.

Following the method of Walsh and Christian a technique involving the use of a small inclined groove cut in the surface of the specimen was devised for the present work; this is the first time any such method has been attempted.

Thus the receiving device used consisted of two condenser microphones—one measuring the surface displacement of the specimen, and the other the stress wave velocity in the body of the specimen by means of an inclined groove.

Calibration was performed in the following way.

(*a*) The surface motion (W)* system. The associated electronic circuitry was designed so that the response extended to direct current and the microphone was calibrated directly by comparing the amplitude of the movements of the surface after the passage of a stress wave with movements of the microphone plate measured by a micrometer. Thus the calibration is independent of linearity or distortions in the recording apparatus (both electronic and optical) and is referred directly to a micrometer screw.

(*b*) The stress wave velocity (C) system is calibrated in an entirely different way. It is necessary to get some clear indication of the time the stress wave reaches various points in its traverse of the specimen. This was done in the following manner: let there be on the conducting surface of the microphone some regions extending transversely right across the surface where the conducting layer is removed and let the microphone surface be inclined so that it is parallel to the face of the groove. As the stress pulse reaches the groove, the voltage on the microphone will start to change due to the change in capacitance produced by the reduced plate–specimen spacing and will continue to change until the "front" of the pulse has reached the first break in the conducting surface. When the front of the pulse reaches the next effective region, there will be a change in the working area of the microphone and the output voltage will have a sudden change in slope. Thus if the breaks in the conducting surface are at accurately known intervals and the times between the

*The letter used for displacement in the present work is w.

discontinuities on the record can be measured, the velocity of the stress pulse can be determined directly.

A disadvantage of this arrangement is that for accuracy a very large bandwidth is required. The microphone used was made with two breaks in the surface about 3 mm apart (see Fig. 5), and the groove and microphone were

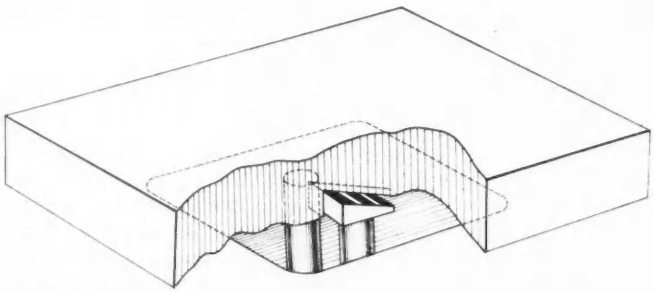

FIG. 5. Diagram showing the arrangement of the two condenser microphones under the surface of a specimen.

inclined to the surface of the specimen at an angle of about 10°. Thus the two breaks are roughly 0.4 mm apart in the direction of travel and since a typical longitudinal stress pulse velocity is approximately 5 mm/μsec the separation in time of the breaks in the recorded trace is about 0.1 μsec. To obtain 1% accuracy of measurement, therefore, a system rise time of about 1 nanosecond is needed. It was not possible to construct such a system but the method was thought to be sufficiently promising to be worth developing and a trial apparatus was constructed with a time resolution of about 30 nanoseconds. Thus the *C* system measurements made are subject to considerable error but are mainly of interest in establishing the feasibility of the method.

The rise time of the *W* system was under 1 μsec and was low enough to be of no concern.

EFFECTS ON "PLASTIC" WAVE PROPAGATION OF THE VARIOUS PHENOMENA DISCUSSED ABOVE

Various profiles may be predicted qualitatively by assuming reasonable values for the parameters and then drawing out successive phases of the motion. It is virtually impossible to predict the profiles quantitatively because so little is known about such factors as attenuation, strain rate, velocity of unloading waves, frequency dispersion of high amplitude waves, etc. Another difficulty is that some materials exhibit a polymorphic transition at certain stress amplitudes; these transitions are well known in both static and very high amplitude work and there is no reason to assume their absence in high amplitude work *ab initio*. A series of experiments on ice may, perhaps, be of value in a study of the effects of polymorphic transitions on the propagation of high amplitude waves.

The author (Bowsher 1958) has drawn some profiles qualitatively and initial results on lead show that some of his predictions have been confirmed. In particular, it was found that when the effects of attenuation are considered for an amplitude dispersive medium (as all media are above the yield point) the elastic front preceding the "plastic" one is "maintained" by the latter at the yield point and suffers no apparent attenuation until the "plastic" front has decayed to a value only slightly above the yield point. This comes about in the following way: for a "plastic" front to propagate in a stable manner, the specimen material immediately in front of it must be prestressed to the yield point. In a medium where the stress–strain curve is composed of two straight lines joining at an angle at the yield stress (case 01000 of Bowsher) the "plastic" front travels at a fixed velocity ($<C_0$) and, therefore, can only maintain the necessary prestress by "sending" out small elastic waves every time the attenuation has reduced the amplitude of the elastic front sufficiently. An unloading wave is sent back towards the impact point every time this happens to maintain momentum balance. Thus the profile of the elastic precursor is changed because the regions behind the front are maintained at stresses above those which would pertain if simple attenuation were the only mechanism effective. Similarly, the region behind the "plastic" front is at a lower stress than simple attenuation would predict. It appears on the profile that the "plastic" front is maintaining the elastic one.

When attenuation and dispersion are present (i.e. the σ'–ϵ curve is curved above the yield point, case 01100 of Bowsher), "plastic" waves of small amplitude can travel at velocities approaching C_0 and the "plastic" front can maintain a stable condition without having to generate elastic-maintaining waves to precede it. The velocity of the "plastic" front gradually increases as the wave becomes attenuated.

When an attenuating medium also exhibits the strain-rate effect as formulated by Malvern, plastic strains can travel at C_0 and the elastic front is maintained at the yield point (case 11000 of Bowsher). In his experiments the author was not able to obtain a "plastic" front with a velocity greater than about $2C_0/3$, which indicates that strain rate has much less effect than dispersion in his experimental arrangement and suggests that the reciprocal of the strain-rate parameter for the material investigated is somewhat less than the value suggested by Malvern of 1 μsec, and may be as small as 0.1 μsec. The attenuation measurements show, though, that the strain-rate effect is not entirely absent since the elastic front is maintained at the yield stress (see Fig. 9).

EXPERIMENTAL RESULTS

Some results have already been mentioned above in the discussion on attenuation phenomena of "plastic" waves.

The value of an apparatus that can measure two parameters simultaneously is shown by the profiles in Figs. 6 and 7; the latter, the u–C profile, is entirely experimentally obtained and is not dependent on the assumptions of any theory (other than that the free surface velocity is $2u$).

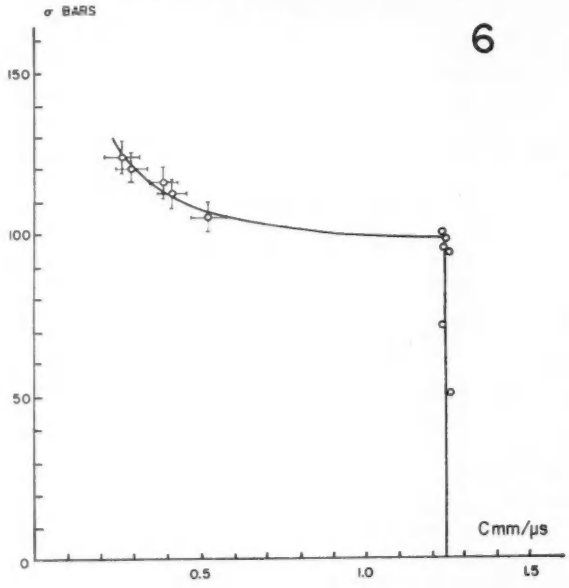

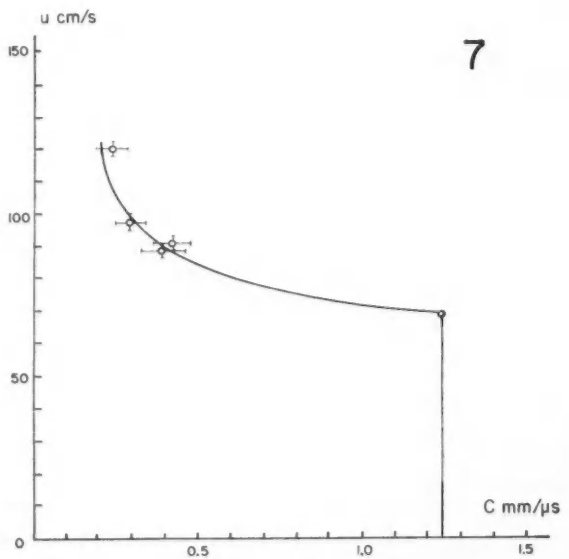

FIG. 6. Experimental σ–C profile for lead.
FIG. 7. Same results as for Fig. 6, plotted as a u–C profile.

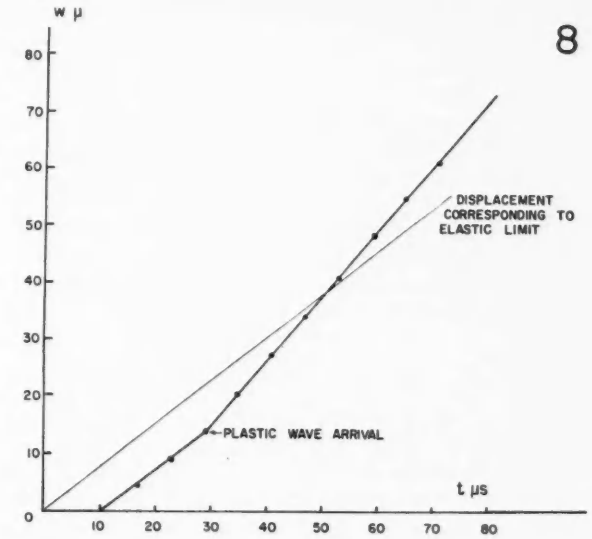

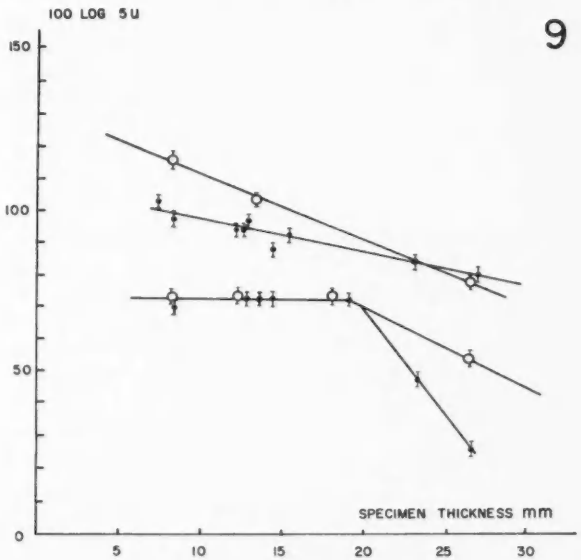

FIG. 8. Typical experimental w–t curve. The point marked "plastic wave arrival" shows the arrival at the free surface of the elastic wave reflected from the "plastic" front.

FIG. 9. Attenuation curves for elastic and "plastic" waves in lead. The upper lines are for "plastic" waves, and the lower for elastic. Points marked ● are for measurements made at +20° C and points marked ○ for measurements at −30° C.

The C system measurements are not of very great accuracy since, as mentioned above, the equipment was designed merely to test the feasibility of such an experimental approach. The results show that the method can be used provided a short rise time for the impact is achieved—this is chiefly a matter of experimental technique. The accuracy of the system depends almost entirely on the resolving time of the electronic circuitry following the condenser microphone and may be very great indeed if the latest developments in subnanosecond rise time amplifiers are used. The accuracy obtained in the present experiment is only $\pm 15\%$ but this is sufficient to show the worth of the method.

The W system was found to be capable of measuring u to within less than 3% error which is sufficient for the determinations of profiles in the present work. On the experimental w–t curve shown (Fig. 8) the errors are too small for inclusion on the graph, but are: $w \pm 1\ \mu$, $t \pm 0.1\ \mu$sec.

The profile shown (Fig. 6) was obtained for lead specimens cast from a sheet of "chemical" lead and it may be seen that the yield stress is 97 ± 10 bars, and the elastic wave velocity 1.25 ± 0.1 mm/μsec.

It is not meaningful to give attenuation results numerically as the effects discussed above tend to obscure the simple attenuation phenomenon. The results obtained (Fig. 9) show clearly that the elastic front is indeed maintained at the yield stress until the "plastic" front is no longer able to do so. This occurs at a specimen thickness of 20 mm for the lead and impact velocity used. It is interesting that the only difference found between experiments performed at $+20°$ C and those at $-30°$ C is expressed in the attenuation results. In all other respects the specimens behaved in a closely similar way at the two temperatures; it will be valuable to extend the scope of the temperature effect measurements to elucidate this point.

CONCLUSIONS

A discussion has been presented on the propagation of "plastic" waves in solid specimens. The main intent has been to summarize the main effects for the benefit of other workers in the field and to attempt a study of the physical aspects of "plastic" wave propagation.

An apparatus has been described which obtains results independent of theoretical assumptions and helps one establish which of the many phenomena are likely to be of importance for any particular specimen material.

The work presented here shows that there are many factors of "plastic" wave propagation about which virtually nothing is known experimentally. Among these are:

1. Velocity of unloading waves in a solid. This is always assumed to be the same as that of elastic waves (C_0). There is no a priori reason for this assumption though static stress–strain measurements do indicate that the velocity may be C_0.
2. The detailed microphenomena in a "plastic" front.
3. Attenuation. The author's experiments are exploratory in nature but do seem to confirm his mechanism in which the amplitude of the elastic precursor is maintained at the expense of the "plastic" front amplitude.

4. Temperature effects. The author's experiments are once again only a beginning and a detailed study would be most valuable.

5. A confirmatory series of experiments on other profiles, e.g. ρ–C or ϵ–C, would be of interest.

6. Frequency dispersion of high amplitude waves. Nothing is reported in the literature on this and in the author's experiments the specimen length was deliberately kept short (<30 mm) to minimize any frequency dispersion and so no information was gained on this topic.

7. The present experiments have only been on lead; other solid materials should, of course, be investigated. It would be of particular interest if experiments on a material like solid argon were performed since this is one of the few solids whose lattice structure is very simple and amenable to theoretical calculation.

ACKNOWLEDGMENTS

The work described above was carried out under the supervision of Dr. R. W. B. Stephens in the Acoustics Group of the Royal College of Science, Imperial College, University of London; the author would like to thank him and Dr. G. G. Parfitt for help and discussions. The author would also like to express his appreciation to the Admiralty for the provision of a Research Grant.

REFERENCES

ALFREY, T. 1948. Mechanical behaviour of high polymers (Interscience Publishers, Inc., New York).
ALTER, B. E. K. and CURTIS, C. W. 1956. J. Appl. Phys. **27**, 1079.
BELL, J. F. 1956. J. Appl. Phys. **27** (10), 1109.
——— 1959. J. Appl. Phys. **30** (2), 196.
BOWSHER, J. M. 1958. Ph.D. Thesis, University of London, London, England.
BROBERG, K. B. 1956. Kgl. Tek. Högskol. Avhandl. No. 111.
CAUCHY, A. L. 1826. Bull. soc. philomat. **180**.
COOK, R. K. 1957. J. Acoust. Soc. Am. **29** (4), 445.
COTTRELL, A. H. 1953. Dislocation and plastic flow in crystals (The Clarendon Press, Oxford).
COTTRELL, A. H. and BILBY, B. A. 1949. Proc. Phys. Soc. A, **62**, 49.
DAVIES, R. M. 1948. Phil. Trans. Roy. Soc. London, A, **240**, 375.
——— 1949. Proc. Roy. Soc. A, **197**, 416.
——— 1956. Stress waves in solids, *in* Surveys in mechanics, *edited by* G. K. Batchelor and R. M. Davies (Cambridge University Press, London).
DORAN, D. G., FOWLES, G. R., and PETERSON, G. A. 1958. Phys. Rev. Letters, **1** (11), 402.
DUWEZ, P. 1947. Publs. assoc. ingrs. fac. polytech. Mons. **95** (4), 1.
DUWEZ, P. and CLARK, D. S. 1947. Proc. Am. Soc. Testing Materials, **47**, 502.
EDWARDS, C. A., PHILLIPS, D. L., and JONES, H. N. 1940. J. Iron Steel Inst. **142** (11), 199.
FEARON, J. 1953. Compressed Air Engineering, November (only reprint seen).
FELTHAM, P. and MEAKIN, J. D. 1957. Phil. Mag. **2** (8), 1237.
HAMBURGER, H. 1885. Inaugural Dissertation, Breslau.
HERTZ, H. R. 1882. Wied. Ann. **19**.
HOLLOMAN, J. H. 1946. J. Met. Technol. **13**, 6.
HOPKINSON, B. 1914. Phil. Trans. Roy. Soc. London, A, **213**, 437.
HOPKINSON, J. 1872*a*. Mem. Proc. Manchester Lit. & Phil. Soc. **11**, 40.
——— 1872*b*. Mem. Proc. Manchester Lit. & Phil. Soc. **11**, 119.
HUGHES, D. S. and KELLY, T. L. 1953. Phys. Rev. **92**, 1145.
VON KÁRMÁN, T. and DUWEZ, P. 1950. J. Appl. Phys. **21**, 987.
KOLSKY, H. 1953. Stress waves in solids (The Clarendon Press, Oxford).
KRIVOBOK, V. N. 1952. Natl. Bur. Standards Circ. No. 520.
MALVERN, L. E. 1951. J. Appl. Mechanics, **18**, 203.
MINSHALL, S. 1955. J. Appl. Phys. **26** (4), 46.
MURNAGHAN, F. D. 1937. Am. J. Math. **59**, 259.

POISSON, S. D. 1833. Traité de mécanique, Vol. II, p. 331.
MCREYNOLDS, A. W. 1949. J. Metals, **1** (1), 32.
RINEHART, J. S. and PEARSON, J. 1954. The behaviour of metals under impulsive loads (American Society for Metals, Cleveland).
RUBIN, R. J. 1954. J. Appl. Phys. **25** (4), 528.
RUSSELL, H. W. 1931. Symposium on Effect of Temperature on Metals (Am. Soc. Mech. Engrs.), p. 658.
SCHNEEBELI, H. 1871. Poggendorff's Ann. Physik, **143**, 239.
SEARS, J. E. 1908. Proc. Cambridge Phil. Soc. **14**, (III), 257.
——— 1912. Trans. Cambridge Phil. Soc. **21**, 49.
TAYLOR, G. I. 1946. J. Inst. Civil Engrs. **26**, 486.
TAYLOR, G. I. and DAVIES, R. M. 1942. The mechanical properties of cordite during impact stresses, *in* G. I. Taylor Scientific Papers, 1958 Vol. I *edited by* G. K. Batchelor (Cambridge University Press, London).
DE ST-VENANT, A. J. C. B. 1867. J. de Liouville, **12**, 237.
VREELAND, T., WOOD, D. S., and CLARK, D. S. 1953. Trans. Am. Soc. Metals, **45**, 620.
WALSH, J. M. and CHRISTIAN, R. H. 1955. Phys. Rev. **97** (6), 1544.
WHIFFIN, A. C. 1948. Proc. Roy. Soc. A, **194**, 300.
WHITE, M. P. and GRIFFIS, L. 1947. J. Appl. Mechanics, **14**, 337.
——— 1948. J. Appl. Mechanics, **15**, 256.
WOOD, D. S. 1952. J. Appl. Mechanics, **19**, 521.
WOOD, D. S. and CLARK, D. S. 1949. Proc. Am. Soc. Testing Materials, **49**, 571.
——— 1951. Trans. Am. Soc. Metals, **43**, 571.
YOKOBORI, T. 1952*a*. Phys. Rev. **88**, 1423.
——— 1952*b*. J. Phys. Japan, **7**, 44.

APPENDIX

DERIVATION OF A RELATION BETWEEN STRESS AND PARTICLE VELOCITY IN AN ELASTIC–PLASTIC MEDIUM

Let us consider a material having a stress–strain relation like that shown in Fig. A. Let the elastic limit be at P with co-ordinates (σ'_e, ϵ_e) and let the input stress have amplitude σ'_p resulting in a strain ϵ_p. Note that the $\sigma'-\epsilon$ curve is the

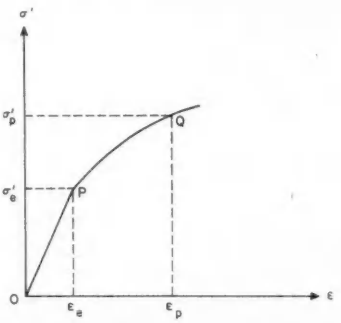

FIG. A. Stress–strain curve for an arbitrary medium.

one applying in the dynamic state of the material under the influence of the pulse, and also that, in general, it is different to the one used by von Kármán since we shall be assuming an infinite extent of medium.

In Lagrangian co-ordinates the particle velocity u is given by

$$u = \int_0^{\epsilon} \sqrt{\frac{1}{\rho}\frac{d\sigma'}{d\epsilon}}\, d\epsilon$$

where ρ is the density of the medium (assumed constant). This relation, strictly, only applies at the end of the medium where it is impacted but to the present accuracy it is sufficient to assume that it applies throughout the extent of travel of the pulse.

Let $T(\epsilon)$ be the slope of the region between P and Q,
M be the slope of the region between O and P;

then

$$u_e = \int_0^{\epsilon_e} \sqrt{M/\rho}\, d\epsilon$$

and

$$u_p = \int_0^{\epsilon_e} \sqrt{M/\rho}\, d\epsilon + \int_{\epsilon_e}^{\epsilon_p} \sqrt{T/\rho}\, d\epsilon.$$

Now

$$\sigma_p' = \int_0^{\epsilon_e} \rho C_0^2\, d\epsilon + \int_{\epsilon_e}^{\epsilon_p} \rho C_1^2\, d\epsilon,$$

where

$$\rho C_0^2 = M; \qquad \rho C_1^2 = T; \qquad C_1 = C_1(\epsilon),$$

and

$$u_p = \int_0^{\epsilon_e} C_0\, d\epsilon + \int_{\epsilon_e}^{\epsilon_p} C_1\, d\epsilon$$

$$= C_0\epsilon_e + \int_{\epsilon_e}^{\epsilon_p} C_1\, d\epsilon,$$

$$\sigma_p' = \rho C_0^2\epsilon_e + \int_{\epsilon_e}^{\epsilon_p} \rho C_1^2\, d\epsilon.$$

Thus

$$\rho C_1 u_p = \rho C_1 C_0\epsilon_e + \rho C_1 \int_{\epsilon_e}^{\epsilon_p} C_1\, d\epsilon$$

and

$$\frac{\sigma_p' - \rho C_1 u_p}{\rho} = C_0\epsilon_e(C_0 - C_1) + \left[\int_{\epsilon_e}^{\epsilon_p} C_1^2\, d\epsilon - C_1\int_{\epsilon_e}^{\epsilon_p} C_1\, d\epsilon\right].$$

If the region of the stress–strain curve from P to Q is linear, the term in square brackets becomes

$$C_1^2(\epsilon_p - \epsilon_e) - C_1^2(\epsilon_p - \epsilon_e) = 0,$$

i.e. the first term in the right-hand side is the correction term to allow for the change in slope at P. Therefore the second term is the additional correction factor allowing for the curvature from P to Q.

To get an approximate evaluation of the term in square brackets let us assume DeJuhasz's stress–strain law. We have already assumed ρ = constant so that ϵ must remain fairly small.

We assume

for

$$0 < \epsilon < \epsilon_e, \qquad \sigma' = M\epsilon$$

$$\epsilon_e < \epsilon < \epsilon_p, \qquad \sigma' = B\sqrt{\epsilon}$$

at ϵ_e,

$$\sigma_e' = M\epsilon_e = B\sqrt{\epsilon_e},$$

therefore,

$$\epsilon_e = B^2/M^2.$$

Now, the velocity of "plastic" waves is

$$C_1 = \sqrt{\frac{1}{\rho}\frac{d\sigma'}{d\epsilon}}$$

$$= \sqrt{\frac{B}{2\rho\sqrt{\epsilon}}} = \sqrt{\frac{B}{2\rho}}\,\epsilon^{-\frac{1}{4}}.$$

Thus [ ] becomes

$$\int_{\epsilon_e}^{\epsilon_p} \frac{B}{2}\,\epsilon^{-\frac{1}{2}}\,d\epsilon - \sqrt{\frac{B}{2\rho}}\int_{\epsilon_e}^{\epsilon_p}\sqrt{\frac{B}{2\rho}}\,\epsilon^{-\frac{1}{4}}\,d\epsilon = \sqrt{\frac{\epsilon_e C_0^4}{4}}\int_{\epsilon_e}^{\epsilon_p}\epsilon^{-\frac{1}{2}}\,d\epsilon - \sqrt{\frac{\epsilon_e C_0^4}{4}}\int_{\epsilon_e}^{\epsilon_p}\epsilon^{-\frac{1}{4}}\,d\epsilon$$

substituting for B,

i.e. $$[\ ] = C_0^2\epsilon_e^{\frac{1}{2}}\left[\epsilon_p^{\frac{1}{2}} - \epsilon_e^{\frac{1}{2}} - \frac{2}{3}\epsilon_p^{\frac{3}{4}} + \frac{2}{3}\epsilon_e^{\frac{3}{4}}\right].$$

Now $$\epsilon_e = u_e/C_0$$

therefore $$[\ ] = C_0^{3/2}u_e^{\frac{1}{2}}\left[\epsilon_p^{\frac{1}{2}}\left(1-\frac{2}{3}\epsilon_p^{\frac{1}{4}}\right)+\left(\frac{u_e}{C_0}\right)^{\frac{1}{2}}\left\{\frac{2}{3}\left(\frac{u_e}{C_0}\right)^{\frac{1}{4}}-1\right\}\right].$$

ϵ_p is given by $\sigma_p' = B\sqrt{\epsilon_p}$;

$$\epsilon_p = \frac{\sigma_p'^2}{B^2} = \frac{\sigma_p'^2}{\epsilon_e\rho^2C_0^4} = \frac{\sigma_p'^2}{u_e\rho^2C_0^3}$$

therefore $$[\ ] = C_0^{3/2}u_e^{\frac{1}{2}}\left[\frac{\sigma_p'}{u_e^{\frac{1}{2}}\rho C_0^{3/2}}\left(1-\frac{2}{3}\frac{\sigma_p'^{\frac{1}{2}}}{u_e^{1/4}\rho^{\frac{1}{2}}C_0^{3/4}}\right)+\left(\frac{u_e}{C_0}\right)^{\frac{1}{2}}\left\{\frac{2}{3}\left(\frac{u_e}{C_0}\right)^{\frac{1}{4}}-1\right\}\right].$$

Thus

$$\sigma_p' - \frac{\rho\sigma_p'C_0^{3/2}u_e^{\frac{1}{2}}}{u_e^{\frac{1}{2}}\rho C_0^{3/2}}\left(1-\frac{2}{3}\frac{\sigma_p'^{\frac{1}{2}}}{u_e^{1/4}\rho^{\frac{1}{2}}C_0^{3/4}}\right) = \rho C_1u_p + \rho u_e(C_0-C_1) + \rho C_0u_e\left\{\frac{2}{3}\left(\frac{u_e}{C_0}\right)^{\frac{1}{4}}-1\right\},$$

$$\sigma_p' = \rho C_0u_e + \left(\frac{3}{2}\right)^{2/3}\rho C_1^{2/3}C_0^{\frac{1}{3}}u_e^{1/6}(u_p-u_e)^{2/3}.$$

SUMMARY

Thus for an elastic wave we have

$$\sigma_e = \rho C_0u_e,$$

for a "plastic"wave with a stress–strain curve consisting of two linear portions

(1) $$\sigma_p' = \rho C_0u_e + \rho C_1(u_p-u_e),$$

whilst for a parabolic stress–strain curve

(2) $$\sigma_p' = \rho C_0u_e + \left(\frac{3}{2}\right)^{2/3}\rho C_1^{2/3}C_0^{\frac{1}{3}}u_e^{1/6}(u_p-u_e)^{2/3}.$$

To compare these formulas we substitute some figures given by DeJuhasz—these may not necessarily be correct but they give some idea of the magnitudes of the corrections to be expected.

Let us take

$$\rho = 8.9 \text{ g/cm}^3,$$
$$C_0 = 4.5 \text{ mm}/\mu\text{sec},$$
$$C_1 = 0.9 \text{ mm}/\mu\text{sec},$$
$$u_e = 100 \text{ cm/sec},$$
$$u_p = 150 \text{ cm/sec}.$$

Then the terms become

$$\rho C_0 u_e = 401 \text{ bars},$$
$$\rho C_1 (u_p - u_e) = 40 \text{ bars},$$
$$\left(\frac{3}{2}\right)^{2/3} \rho C_1^{2/3} C_0^{\frac{1}{3}} u_e^{1/6} (u_p - u_e)^{2/3} = 20.5 \text{ bars}.$$

Thus eq. (1) gives 441 bars, and eq. (2) gives 421.5 bars, a difference of 5%.

A recent paper by Feltham and Meakin (1957) leads one to suppose that the linear relation, eq. (1), might be more appropriate for copper in the present stress range, and we use it throughout.

When the stress amplitude is large enough for a shock wave to develop the Rankine–Hugoniot equations apply, and it is found that stress and particle velocity for a "plastic" wave are related by the formula

$$\sigma_p' = \rho C_1 u_p. \tag{3}$$

Let us rewrite eq. (1) as

$$\sigma_p' = \rho C_1 u_p + \rho u_e (C_0 - C_1).$$

It may thus be seen that eq. (3) is a limiting case of eq. (1) for $u_p \gg u_e$ and $C_1 \to C_0$ the conditions applying in a shock wave. For example, using typical figures we have $u_p = 10u_e$, $C_1 - C_0 = C_0/10$.

Whence

$$\sigma_p = \rho C_1 u_p + \frac{\rho C_1 u_p}{100},$$

i.e. only a 1% change is introduced by our correction terms.

NOTE ADDED IN PROOF.—An interesting mathematical treatment of this problem by L. W. Morland (1959. Phil. Trans. Roy. Soc. London, A, **251** (997), 341) has just appeared.

ROTATIONAL STATES OF EVEN–EVEN NUCLEI[1]

G. R. DEMILLE, T. M. KAVANAGH, R. B. MOORE, R. S. WEAVER, AND W. WHITE

ABSTRACT

Rotational energy levels of axially asymmetric nuclei have been calculated in the manner of Davydov and Filippov, and a comparison with experiment shows good quantitative agreement. It is suggested that agreement may be improved by introducing the Bohr–Mottelson vibration–rotation interaction and a centrifugal stretching correction analogous to the type used in molecular spectra. The D–F method seems to be particularly useful for nuclei in the transition regions between "rotational" and "near-harmonic" modes of collective excitation.

Bohr and Mottelson (1953) have shown that even–even nuclei with spheroidal shapes may be expected to exhibit rotational states with energy levels given by

$$E_{\text{rot}} = \frac{\hbar^2}{2\Im} I(I+1), \qquad I = 0, 2, 4, 6, \ldots$$

where $\Im$ is the effective moment of inertia and I the total nuclear angular momentum. The ratios of the energies represented in this simple level scheme are, $E(4+)/E(2+) = 3.33$, $E(6+)/E(2+) = 7.00$, $E(8+)/E(2+) = 12.00$.

Davydov and Filippov (1958) have extended the treatment to include nuclei with ellipsoidal shapes, i.e. nuclei not possessing axial symmetry. Deviations from axial symmetry may be characterized by the nuclear shape parameter γ, a quantity which varies between 0 and $\pi/3$. Values of γ of 0 and $\pi/3$ characterize prolate and oblate spheroids respectively. The Hamiltonian operator for rotational motion is given by

$$\mathbf{H} = \frac{\hbar^2}{4B\beta^2} \sum_{i=1}^{3} \frac{\mathbf{I}_i^2}{2\sin^2\{\gamma-(2\pi/3)i\}}$$

where B is the mass transport parameter, β is the nuclear quadrupole deformation parameter, and the $\mathbf{I}_i$ are operators of the projections of the total angular momentum along the body-fixed axes of the nucleus. The Hamiltonian is symmetric about $\gamma = \pi/6$ and consequently a prolate ellipsoid of deformation γ ($<\pi/6$) will exhibit the same rotational spectrum as an oblate ellipsoid of deformation $\pi/3-\gamma$.

The energy equations of Dennison (1931) for an asymmetric top may be applied. The symmetry conditions of Bohr (1952) exclude certain energy levels. Resultant curves of relative energy vs. γ are given in Figs. 1 and 2. The 2+, 4+, 6+, 8+, ... spin sequence appears and, as long as γ is small, the relative spacing of these levels does not differ appreciably from that of a spheroidal rotor. New levels, of energy $E(2'+)$, $E(3+)$, $E(4'+)$, ..., appear,

[1]Manuscript received June 29, 1959.
Contribution from the Radiation Laboratory, McGill University, Montreal, Que.

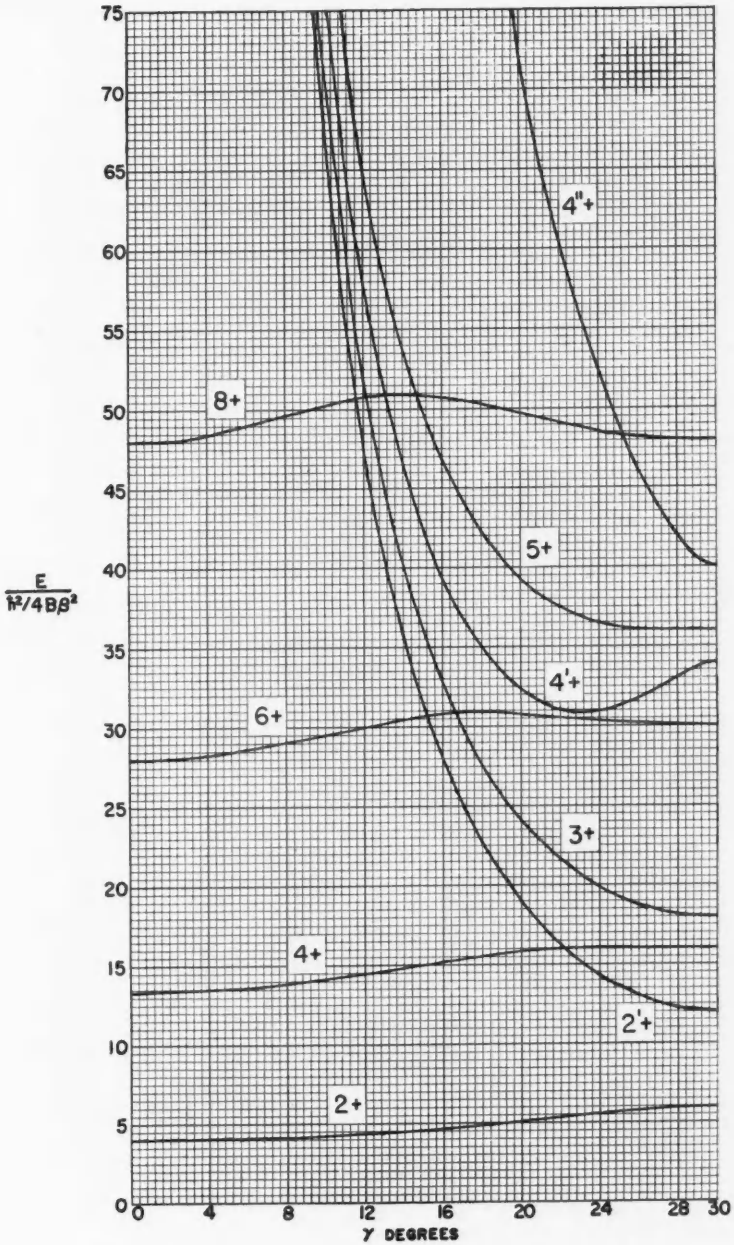

FIG. 1. Rotational energy levels of axially asymmetric even–even nuclei.

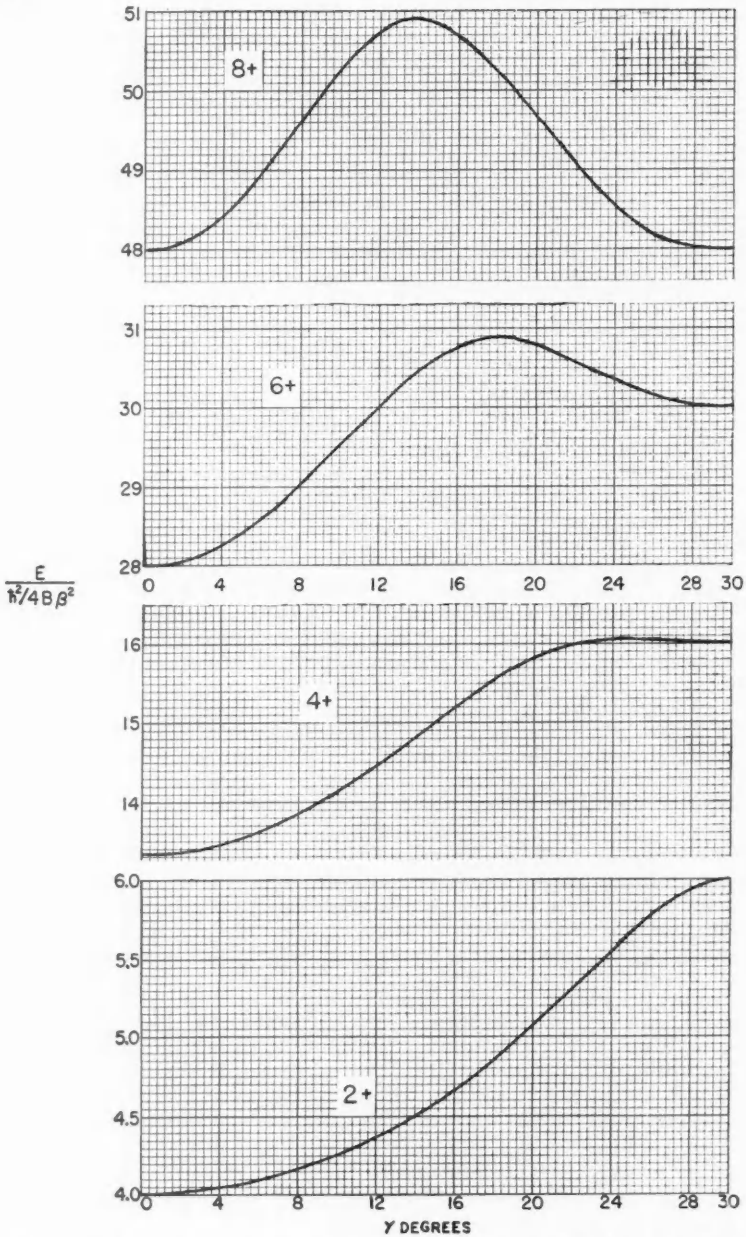

FIG. 2. Rotational energy levels of the "ground state band" of axially asymmetric even-even nuclei.

TABLE I

Rotational energy levels of some even–even nuclei. Theoretical values are for γ determined from $E(2'+)/E(2+)$

Nucleus	$E(2+)$	$E(2'+)$	γ	$E(3+)$		$E(4+)$		$E(6+)$		$E(8+)$		$E(4'+)$		$E(5+)$		$E(6'+)$		References
				Expt.	Theor.	Expt.	Theor.	Expt.	Theor.	Expt.	Theor.	Expt.	Theor.	Expt.	Theor.	Expt.	Theor.	
$_{62}Sm^{152}$	121.8	1092	13.2	1240	1214	367	402											
$_{64}Gd^{154}$	123.1	998	13.9	1130	1121	371	406											
$_{66}Dy^{160}$	86.5	966	11.9	1049	1052	283	287					1156	1165					Grigor'ev (1958)
$_{74}W^{182}$	100.1	1222	11.4	1332	1322	329	332	677	690			1501	1439	1620	1612	1810	1770	Gallagher (1958)
$_{74}W^{184}$	111.2	904	13.8	1006	1015	364	367											
$_{76}Os^{186}$	137.2	768	16.6			434	445	869	896									Diamond (1958)
$_{76}Os^{188}$	155.0	633	19.1			478	490											Diamond (1958)
$_{76}Os^{190}$	186.7	558	22.2	754	745	548	560	1048	1070	1670	1716	956	1084					Diamond (1958) Nielsen (1959)
$_{76}Os^{192}$	205.8	489	25.0	691	695													
$_{78}Pt^{192}$	316.5	613	~30	921	929	785	844											Kawamura (1958)
$_{90}Th^{228}$	57.5	965	9.7	1017	1022	186	191											
$_{94}Pu^{238}$	44.1	1030	~8	1071	1074	146	147	304	307	514	525							
$_{94}Pu^{240}$	42.9	1017	~8	1060	1060	142	143	292	299									Davydov (1958)

NOTE: Experimental energy values have been taken for the most part from Strominger, Hollander, and Seaborg (1958). Additional references are given in the last column. Energies are given in kev and γ in degrees.

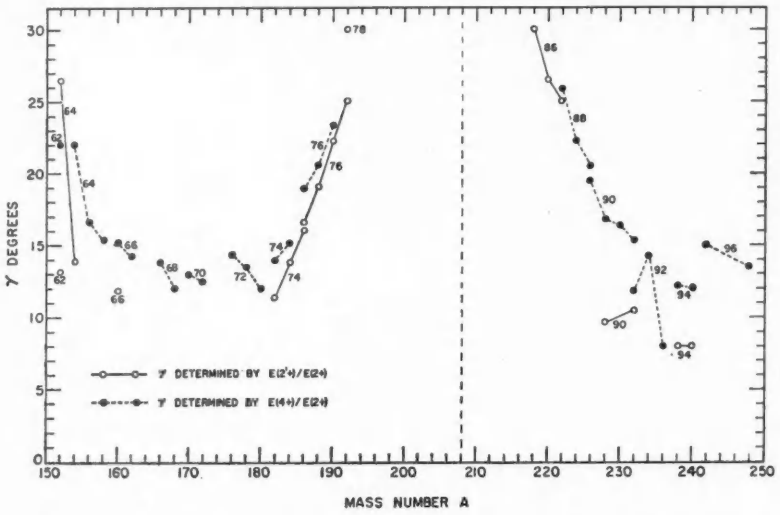

FIG. 3. Variation of the nuclear shape parameter γ with mass number A. Figures indicate proton number.

however, as a direct consequence of axial asymmetry. If, as proposed by Davydov, γ is determined from the ratio $E(2'+)/E(2+)$ and the experimental value of $E(2+)$ assumed, the energies of the remaining levels may be predicted for even–even nuclei with large quadrupole deformations. A comparison of these predictions with experimental data in the range $150 < A < 250$ is shown in Table I. All spin assignments are those given by the authors of the reference quoted. In general, agreement is good—especially in the tungsten–osmium transition region and in the region of heavy nuclei. In these regions discrepancies are typically of the order 1 to 3%, with the exception of the $4'+$ level of Os^{190} where the discrepancy is 13%.

Figure 3 shows the variation of γ with mass number A for the range $150 < A < 250$. Since the $2'+$ level is not always known, γ has been calculated from the ratio $E(4+)/E(2+)$ in some cases. γ calculated in this manner is always somewhat larger than that given by the $E(2'+)/E(2+)$ ratio. The three transition regions from "rotational" to "near-harmonic" level schemes (Scharff-Goldhaber *et al.* 1958) are clearly shown for $A \sim 150$, 190, and 220. The samarium–gadolinium group ($A \sim 150$) exhibits a very fast transition, whereas the tungsten–osmium group ($A \sim 190$) and the radon–radium–thorium group show a more gradual transition.

Qualitative arguments indicate that the minimum finite value of γ for a stable deformation cannot be small, since the frequencies of vibration and rotation would then be comparable, and separation into rotational and vibrational levels meaningless. The data in Fig. 3 would seem to support this. However, most of the low values of γ were obtained from the $E(4+)/E(2+)$ ratio. It is well to keep in mind that low values of γ obtained from

TABLE II

Energy levels of some even–even nuclei. Theoretical values are for γ determined from levels within the "ground state rotational band"

Nucleus	$E(2+)$	γ	$E(4+)$		$E(6+)$		$E(8+)$		$E(2'+)$		References
			Expt.	Theor.	Expt.	Theor.	Expt.	Theor.	Expt.	Theor.	
$_{72}Hf^{176}$	88.4	14.4	290.5*	—	596	596					
$_{72}Hf^{178}$	93.1	13.5	306.8*	—	633	633	1060	1060			
$_{72}Hf^{180}$	93.3	11.9	308.8	308.8	642	642	1085*	—			Scharff-Goldhaber (1957)
$_{74}W^{182}$	100.1	14.1	329.3	329.6	677.1*	—			1222	794	Gallagher (1958)
$_{76}Os^{188}$	137.2	18.3	434.1	438	869*	—			768	618	Diamond (1958)
$_{76}Os^{190}$	186.7	23.2	547.9	549.5	1048	1042	1670*	—	558	510	Diamond (1958) Nielsen (1959)
$_{92}U^{232}$	47.2	13.5	156.3	156	321*	—					
$_{92}U^{234}$	43.5	13.1	143	144	296	297	499*	—			
$_{92}U^{236}$	45.3	10.9	151	150	313*	—					
$_{94}Pu^{238}$	44.1	11.6	145.9	145.7	303.5*	—	514	515	1030	517	
$_{94}Pu^{240}$	42.9	12.0	142*	—	292	295			1017	466	Davydov (1958)
$_{96}Cm^{248}$	42.1	14.4	138	139	284*	—					

NOTE: γ has been determined from the ratio of the energy of the level marked with an asterisk to that of the first 2+ level. The choice of level takes into account the relative sensitivities of the various ratios to changes in γ, as well as the experimental accuracy of the energy measurements.

Experimental energy values have been taken for the most part from Strominger, Hollander, and Seaborg (1958). Additional references are given in the last column. Energies are given in kev and γ in degrees.

ratios of the energies $E(2+)$, $E(4+)$, $E(6+)$, $E(8+)$ do not necessarily prove the existence of a stable deformation of this magnitude. For values of γ up to approximately 15°, the effect of assuming a γ is equivalent to introducing the Bohr–Mottelson vibration–rotation interaction correction of the form $-bI^2(I+1)^2$. Values of γ obtained from the $E(2'+)/E(2+)$ ratio are not subject to this objection.

Table II gives the results of calculations of energies of what has been termed the "ground state rotational band", $2+$, $4+$, $6+$, $8+$, ... If γ is determined not from the ratio $E(2'+)/E(2+)$ but rather from any two members of the "ground state band", then the energies of the remaining two levels of this band may be predicted to an accuracy usually well within 1%. However, energies of the $2'+$, $3+$, $4'+$, . . . levels cannot then be predicted with any precision. The data is consistent with assuming a higher value of γ for the "ground state band" than for the $2'+$, $3+$, $4'+$, . . . levels.

A qualitative argument may help to clarify this point. Two corrections which may be of importance in the Davydov–Filippov treatment are the vibration–rotation interaction correction and a centrifugal stretching correction. As in molecular spectra these corrections have the form $-bI^2(I+1)^2$ and become more important as the equilibrium deformation decreases. For the "ground state band" it is the β deformation that is important and for the $2'+$, $3+$, $4'+$, . . . levels it is the γ deformation that is important. The effect of this correction to the energies of the levels of the "ground state band" is equivalent to an upward shift of γ of several degrees. Since γ is relatively insensitive to the ratio $E(2'+)/E(2+)$, the correction which must be applied to the $2'+$ level does not appreciably affect γ as determined from this level. Thus the difference between γ calculated from the "ground state band" energies and γ calculated from the $E(2'+)/E(2+)$ ratio is quite naturally accounted for by the type of correction arrived at by analogy with molecular spectra.

This paper has shown that the Davydov and Filippov treatment can successfully account for a large number of nuclear energy levels. It cannot, however, predict all the low-lying excited levels, for it is known that other $0+$ and $2+$ levels exist which cannot arise as excited states of a rigid asymmetric rotor. This point has been clearly shown in a recent paper by King and Johns (1959) concerning the energy levels of Os^{188}.

ACKNOWLEDGMENTS

The authors express thanks to the National Research Council for scholarships held during the course of this work.

REFERENCES

BOHR, A. 1952. Kgl. Danske Videnskab. Selskab, Mat.-fys. Medd. **28**, No. 14.
BOHR, A. and MOTTELSON, B. R. 1953. Kgl. Danske Videnskab. Selskab, Mat.-fys. Medd. **27**, No. 16.
DAVYDOV, A. S. and FILIPPOV, G. F. 1958. Nuclear Phys. **8**, 237.
——— 1958. Acta Phys. Acad. Sci. Hung. **9**, 169.
DENNISON, D. 1931. Revs. Modern Phys. **3**, 280.

DIAMOND, R. M. and HOLLANDER, J. M. 1958. Nuclear Phys. **8**, 143.
GALLAGHER, C. J., JR., and RASMUSSEN, J. O. 1958. Phys. Rev. **112**, 1730.
GRIGOR'EV, E. P., ZOLOTAVIN, A. V., and KRATSIK, B. 1958. Izvest. Akad. Nauk S.S.S.R. Ser. Fiz. **22**, 785.
KAWAMURA, M., AOKI, A., and HAYASHI, T. 1958. J. Phys. Soc. Japan, **13**, 1071.
KING, W. J. and JOHNS, M. W. 1959. Can. J. Phys. **37**, 755.
NIELSEN, O. B., POULSEN, N. O. R., SHELINE, R. K., and JENSEN, B. S. 1959. Nuclear Phys. **10**, 475.
SCHARFF-GOLDHABER, G. 1957. Proceedings of the University of Pittsburgh Conference on Nuclear Structure.
SCHARFF-GOLDHABER, G., ALBURGER, D. E., HARBOTTLE, G., and MCKEOWN, M. 1958. Phys. Rev. **111**, 913.
STROMINGER, D., HOLLANDER, J. M., and SEABORG, G. T. 1958. Revs. Modern Phys. **30**, 585.

NOTE ADDED IN PROOF.—The authors are pleased to note that Davydov and Rostovsky (Nuclear Phys. **12**, 58, 1959) in a paper on transition probabilities give energy levels nearly identical with the above values.

IRREVERSIBLE THERMODYNAMICS AND KINETIC THEORY IN THE DERIVATION OF THERMOELECTRIC RELATIONS[1]

J. W. LEECH[2]

ABSTRACT

The variety of experimental behavior found in thermoelectricity at low temperatures provides an incentive for extending the theoretical treatment. In the past, irreversible thermodynamics has been used to provide a satisfactory derivation of the Thomson relations. It appears that what one might call a general "primary equation" of thermoelectricity can be derived from irreversible thermodynamics, and that this should be of direct use in kinetic discussions. The form of the equation suggests that an even more direct approach to the thermoelectric problem should be possible.

1. INTRODUCTION

The phenomenon of thermoelectricity has for a long time furnished a convenient method for temperature measurement. It is less well known as a means for investigating the solid state though recent experimental investigations (see for example MacDonald *et al.* 1958*a*, *b* and 1959; cf. also MacDonald 1959) have revealed a variety of new phenomena, particularly at low temperatures. There have been two main theoretical approaches to the subject. On the one hand, irreversible thermodynamics has been used (see for example Onsager 1931; Callen 1948; de Groot 1951; Domenicali 1954) to provide a satisfactory derivation of the fundamental Thomson relations; on the other hand, kinetic theory based on the Boltzmann equation has been used for detailed calculation of the various thermoelectric quantities (see for example Wilson 1953). If, however, we combine these approaches there results an appreciable simplification of the kinetic calculations. The generality of the irreversible thermodynamic argument suggests that it may always be profitable to use it as a check in the development of the kinetic explanation of the more complicated thermoelectric phenomena.

We believe it worth while to summarize both treatments using a common notation before combining them to obtain a simplified expression for the calculation of the Thomson coefficient. This should obviate the rather surprising misidentifications and unphysical statements which are to be found in the literature of the subject* and which can usually be resolved by an understanding of both forms of argument.

[1]Manuscript received May 13, 1959.
Contribution from the Division of Pure Physics, National Research Council, Ottawa, Canada.
Issued as N.R.C. No. 5300.

[2]Now at the Department of Physics, Queen Mary College, University of London, London, England.

*Mott and Jones (1936, p. 309), for instance, appear to identify the Peltier heat with the contact potential difference between two media and ter Haar (1956) writes down expressions for the electric and heat currents (his equations (38) and (39)) which depend on the thermoelectric power in an obviously wrong manner.

2. IRREVERSIBLE THERMODYNAMICAL TREATMENT

We wish to take into account the simultaneous flow of heat and electricity through a medium which, in general, contains both thermal and electric potential gradients. It is supposed that, although the medium is in a non-equilibrium state, it is nevertheless possible to define regions small on a macroscopic scale but large on a microscopic one whose instantaneous states may be specified using thermodynamic co-ordinates.

Irreversible thermodynamics can be approached from a number of different directions and at a number of levels (see de Groot 1951; Denbigh 1951; Prigogine 1955; Davies 1957). Entropy plays a dominant part in all these approaches, particularly its creation and transport. We propose to introduce the irreversible thermodynamic postulates in the form of an equation linking the entropy flow $\mathbf{J}^{(s)}$ and the entropy density s by means of the balance equation:

$$\frac{\partial s}{\partial t} = -\nabla . \mathbf{J}^{(s)} + \frac{1}{T} \sum_i \mathbf{J}_i . \mathbf{X}_i. \tag{1}$$

Here, the $\mathbf{J}_i$ are flow vectors (in our case the electric and heat currents) and the $\mathbf{X}_i$ are thermodynamic "forces" giving rise to these flows. The term

$$\frac{1}{T} \sum_i \mathbf{J}_i \mathbf{X}_i$$

obviously represents the rate of creation of entropy per unit volume.

It is further assumed that, for conditions not too far removed from equilibrium, we may write:

$$\mathbf{J}_i = \sum_j l_{ij} \mathbf{X}_j \tag{2}$$

where the l_{ij} are functions of temperature and of the constitution of the medium which obey the Onsager relations:

$$l_{ij} = l_{ji}. \tag{3}$$

Assumptions (1) to (3) appear in most treatments of the subject though in many cases they are deduced from more fundamental postulates. In particular the Onsager relations (3) are usually held to be based ultimately on the principle of detailed balancing.

There is considerable choice in the precise form of either the flow vectors $\mathbf{J}_i$ or of the appropriate conjugate quantities $\mathbf{X}_i$. However, once one set has been chosen there is no longer any arbitrariness in the other.

In the case of thermoelectricity the choice of the electric current density $\mathbf{J}$ and the heat current density $\dot{\mathbf{Q}}$ as flow vectors is clearly indicated since they play a major role in the kinetic treatment. The corresponding conjugate quantities, the thermodynamic forces $\mathbf{X}_i$, will be identified by setting up an entropy balance equation based on first- and second-law considerations.

Restricting attention to one-dimensional flow, the time variation of the

internal energy density of the electrons in a conducting medium is, from the first law of thermodynamics:

$$\frac{\partial u}{\partial t} = -\frac{\partial \dot{Q}_x}{\partial x} - \frac{\partial}{\partial x}(J_x \phi) \tag{4}$$

where ϕ is the electrostatic potential at the point in question.

The second law leads us to write (see Sommerfeld 1956):

$$T\frac{\partial s}{\partial t} = \frac{\partial u}{\partial t} - \mathbf{e}(\phi + g)\frac{\partial N}{\partial t}, \tag{5}$$

where g is the chemical potential per unit conduction charge in the neutral medium, $\mathbf{e}$ the electronic charge (in sign and magnitude), and N is the electron density.

It will be seen that consideration has been restricted to a single type of charge carrier but that no specific mechanism has been assumed for the process of heat conduction.

Combining (4) and (5) and allowing for the continuity of charge we find after some rearrangement:

$$\frac{\partial s}{\partial t} = -\frac{\partial}{\partial x}\left\{\frac{\dot{Q}_x - gJ_x}{T}\right\} + \frac{1}{T}\left\{\dot{Q}_x\left[T\frac{\partial}{\partial x}\left(\frac{1}{T}\right)\right] + J_x\left[\mathfrak{E}_x - T\frac{\partial}{\partial x}(g/T)\right]\right\} \tag{6}$$

where $\mathfrak{E}_x = -\partial\phi/\partial x$ is the electrostatic field acting on the electrons.

The following identifications may now be made:

$$\text{(7)}\quad \text{the entropy flow } J_x^{(s)} = \frac{1}{T}\{\dot{Q}_x - gJ_x\},$$

$$\text{(8)}\quad \begin{aligned} &\text{the thermodynamic "force" conjugate to } J_x \text{ is } X_J = \mathfrak{E}_x - T\frac{\partial}{\partial x}(g/T), \\ &\text{the thermodynamic "force" conjugate to } \dot{Q}_x \text{ is } X_Q = T\frac{\partial}{\partial x}\left(\frac{1}{T}\right); \end{aligned}$$

hence, assuming near equilibrium:

$$\text{(9)}\quad \begin{aligned} J_x &= l_{JJ}\left[\mathfrak{E}_x - T\frac{\partial}{\partial x}(g/T)\right] + l_{JQ}\left[T\frac{\partial}{\partial x}\left(\frac{1}{T}\right)\right], \\ \dot{Q}_x &= l_{QJ}\left[\mathfrak{E}_x - T\frac{\partial}{\partial x}(g/T)\right] + l_{QQ}\left[T\frac{\partial}{\partial x}\left(\frac{1}{T}\right)\right] \end{aligned}$$

where the Onsager relations (3) show that:

$$l_{JQ} = l_{QJ}. \tag{10}$$

This completes the statement of the postulates of irreversible thermodynamics in a form relevant to our considerations. It remains to identify the various thermoelectric quantities and to determine their necessary interrelations.

3. IDENTIFICATION OF THERMOELECTRIC QUANTITIES AND RELATIONSHIPS

Equations (9) may be rewritten in a form more appropriate to the later kinetic discussion as:

$$
\begin{aligned}
J_x &= l_{JJ}\left[\mathfrak{E}_x-\frac{\partial' g}{\partial x}\right]-\left[l_{JJ}\,T\,\frac{\partial}{\partial T}\,(g/T)+\frac{l_{JQ}}{T}\right]\frac{dT}{dx} \\
&= \sigma\left[\mathfrak{E}_x-\frac{\partial' g}{\partial x}\right]+\alpha\,\frac{dT}{dx} \\
\dot{Q}_x &= l_{QJ}\left[\mathfrak{E}_x-\frac{\partial' g}{\partial x}\right]-\left[l_{QJ}\,T\,\frac{\partial}{\partial T}\,(g/T)+\frac{l_{QQ}}{T}\right]\frac{dT}{dx} \\
&= \beta\left[\mathfrak{E}_x-\frac{\partial' g}{\partial x}\right]+\gamma\,\frac{dT}{dx}
\end{aligned}
\tag{11}
$$

where the symbol $\partial' g/\partial x$ denotes change of g at constant temperature, i.e. it allows for the possibility of a non-homogeneous medium. In terms of the newly defined coefficients the Onsager reciprocal relation (10) becomes:

$$
\beta = -\sigma T\left\{\frac{\alpha}{\sigma}+T\,\frac{\partial}{\partial T}\,(g/T)\right\}. \tag{12}
$$

We also note that the thermal conductivity is given by:

$$
\kappa \equiv -\left[\dot{Q}_x \Big/ \frac{dT}{dx}\right]_{J_x=0} = \left(\frac{\alpha\beta}{\sigma}-\gamma\right) \tag{13}
$$

and that for a *homogeneous* medium:

$$
\sigma = [J_x/\mathfrak{E}_x]_{dT/dx=0}, \tag{14}
$$

which justifies our use of this particular symbol.

The identification of the Thomson and Peltier coefficients is made by considering $\partial q/\partial t$, the rate of heat absorption by the electrons per unit volume. Under steady-state conditions J_x = const. and $\partial q/\partial t = \partial u/\partial t$; hence from (4):

$$
\frac{\partial q}{\partial t} = \mathfrak{E}_x J_x - \frac{\partial \dot{Q}_x}{\partial x}. \tag{15}
$$

For a homogeneous medium ($\partial' g/\partial x = 0$) we get using (11) and (15):

$$
\frac{\partial q}{\partial t} = \frac{J_x^2}{\sigma} - J_x \frac{dT}{dx}\left[\frac{\alpha}{\sigma}+\frac{\partial}{\partial T}\,(\beta/\sigma)\right]+\frac{d}{dx}\left[\kappa\,\frac{dT}{dx}\right]. \tag{16}
$$

The *Thomson coefficient* μ is defined as the reversible heat absorbed per unit volume when unit electric current flows down unit temperature gradient. This immediately gives:

$$
\mu = \frac{\alpha}{\sigma}+\frac{\partial}{\partial T}\,(\beta/\sigma) \tag{17}
$$

from the realization that reversing the electric current *or* the temperature distribution leaves the first and third terms of (16) unchanged but alters the sign of the second. This is essentially the identification made by Mott and Jones (1936) though they made it by assuming the term $d/dx\ [\kappa(dT/dx)]$ to be negligible.

The identification is in fact a precise one and involves no assumptions beyond those basic to irreversible thermodynamics.

Equation (17) has been used in the kinetic approach to calculate the Thomson coefficient. In that form no explicit use has been made of the Onsager relation. If this is now remedied by combining (12) with (17) we get:

$$\mu = T\frac{\partial}{\partial T}\left\{-\frac{\alpha}{\sigma}-\frac{\partial g}{\partial T}\right\}. \tag{18}$$

This result does not seem to have appeared previously. It represents a useful practical advance on the form (17) since the quantity β has been replaced essentially by g. Whereas in the kinetic approach the determination of β requires the evaluation of a separate integral, g is to be identified with the Fermi energy and can be assumed known.

The *Peltier coefficient* Π_{AB} is defined as the reversible heat absorbed at the junction between two media A and B when unit electric current passes from A to B. Our formulation cannot be used to deal with a strictly discontinuous boundary but we may consider the more realistic case of a continuous merging of medium A into B under isothermal conditions. For such a region, again assuming a steady state, we obtain using (11) and (15):

$$\frac{\partial q}{\partial t} = \frac{J_x^2}{\sigma} - J_x\frac{d}{dx}[\beta/\sigma - g]. \tag{19}$$

Or, integrating from an interior point of A to an interior point of B:

$$\int\frac{\partial q}{\partial t}\,dx = J_x^2\int\frac{dx}{\sigma} - J_x\left\{\left[\frac{\beta}{\sigma}-g\right]_B-\left[\frac{\beta}{\sigma}-g\right]_A\right\}. \tag{20}$$

The division into reversible and irreversible parts again occurs (this time solely in terms of current reversibility) and the Peltier coefficient is identifiable as:

$$\Pi_{AB} = [\beta/\sigma - g]_A - [\beta/\sigma - g]_B \tag{21}$$

which, using the Onsager relation (12), becomes:

$$\frac{\Pi_{AB}}{T} = \left[\frac{\alpha}{\sigma}+\frac{\partial g}{\partial T}\right]_B-\left[\frac{\alpha}{\sigma}+\frac{\partial g}{\partial T}\right]_A. \tag{22}$$

Combining (18) and (22) now gives the familiar Thomson relation:

$$\frac{d}{dT}\left[\frac{\Pi_{AB}}{T}\right] = \frac{\mu_A-\mu_B}{T}. \tag{23}$$

From the derivation it is clear that the Peltier heat is associated with the

transfer of charge from the *interior* of one medium to the *interior* of the other and is *not*, as sometimes asserted, directly connected with surface charges or contact potentials.

Finally it is necessary to obtain expressions for the thermoelectric power. To do this we must first evaluate the open-circuit potential difference between two points such as X and Y of Fig. 1, which represents the usual arrangement

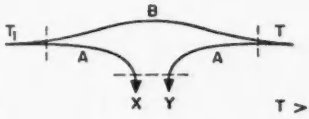

FIG. 1. Basic thermoelectric circuit. The region including the contacts X, Y below the dashed line is supposed to be isothermal, as are also the corresponding contact regions at temperatures T_1 (supposed fixed) and T.

for measuring thermal electromotive forces. This is done by integrating the electric field between X and Y along a path through the media A and B. The temperature T_1 is supposed fixed in what follows while T may be varied.

The integration is effected by again considering boundary regions as continuous. The transition region from the interior to the exterior of medium A at X produces an effect equal and opposite to that at Y since they are both uniformly at the temperature. This leaves integrations over the temperature range T_1 to T in media A and B and over the transition regions from A to B at temperatures T_1 and T. We define the thermoelectric force of the couple as

$$E_B - E_A = E_Y - E_X \text{ in Fig. 1 (and we note that } T > T_1)$$

$$= -\int_X^Y \mathfrak{E}_x dx.$$

Using (11) with the restriction $J_x = 0$ we find after some working:

$$E_B - E_A = \Pi_{AB}(T) - \Pi_{AB}(T_1) + \int_{T_1}^{T} (\mu_B - \mu_A)\, dT. \tag{24}$$

The thermoelectric power of the couple is given by

$$S_B - S_A \equiv \frac{d}{dT}(E_B - E_A) \tag{25}$$

and we can then show using (23) and (24) that

$$T\left(\frac{dS_B}{dT} - \frac{dS_A}{dT}\right) = (\mu_B - \mu_A) \tag{26}$$

and that

$$\Pi_B - \Pi_A = T(S_B - S_B), \text{ writing } \Pi_{BA} \equiv \Pi_B - \Pi_A.$$

It is then obviously consistent with these relations to define an absolute

thermoelectric power S, and Peltier heat, Π, for a single medium related to the Thomson coefficient, μ, by the equations

$$\mu = T\frac{dS}{dT}. \tag{27}$$

and

$$\Pi = TS.$$

This completes the derivation of the Thomson relations. It should be emphasized again that all the results are independent of special assumptions regarding the boundary regions of the media and rest upon distinguishing between reversible and irreversible heat production. The somewhat artificial nature of the latter distinction should also be noted. For observational reasons J_x and dT/dx are regarded as independent variables in the above argument but any two of J_x, dT/dx, $\mathfrak{E}_x$, and $\dot{Q}_x$ could, in principle, be so chosen and each pair would lead to a different division of the heat production into reversible and irreversible parts.

4. THE KINETIC APPROACH

The simplest calculations of the magnitudes of thermoelectric quantities are based on a kinetic approach which starts from the Boltzmann equation and takes into account only electron transport processes (see Wilson 1953, Chapter 8).

We suppose it possible to divide the medium into elementary regions which contain sufficient electrons to be characterized by a distribution function $f(x, y, z, p_x, p_y, p_z)$ giving the distribution of electrons in phase space. This function then obeys the Boltzmann equation:

$$\frac{\partial f}{\partial t}+\mathbf{v}\,.\,\nabla f+\dot{\mathbf{p}}\,.\,\nabla_{\mathbf{p}} f = \left(\frac{\partial f}{\partial t}\right)_{\text{coll}}. \tag{28}$$

The following additional assumptions are now made:

(a) there is local equilibrium, i.e.

$$\frac{\partial f}{\partial t} = 0; \tag{29}$$

(b) there exists a unique relaxation time τ such that:

$$\left(\frac{\partial f}{\partial t}\right)_{\text{coll}} = -\frac{f-f_0}{\tau}, \tag{30}$$

where f_0 is the distribution function corresponding to over-all equilibrium when no gradients or flows are present;

(c) the only forces acting on the electrons other than random collision forces are those due to the electric field, i.e.

$$\dot{\mathbf{p}}_i = \mathbf{e}\mathfrak{E}. \tag{31}$$

With these and assuming a variation in f in the x direction only, the Boltzmann equation may be rewritten:

$$f = f_0 - \tau v_x \frac{\partial f}{\partial x} - \frac{\tau \mathbf{e} \mathfrak{E}_x}{m} \frac{\partial f}{\partial v_x}. \tag{32}$$

The electric and heat current densities may be written in terms of f as:

$$\begin{aligned} J_x &= \mathbf{e} \int v_x f \, d^3v \\ \dot{Q}_x &= \int \tfrac{1}{2} m v^2 v_x f \, d^3v. \end{aligned} \tag{33}$$

Using (32) and (33) in conjunction with the properties:

$$\begin{aligned} \int v_x f_0 d^3v &= \langle v_x \rangle = 0 \\ \int v_x \frac{\partial f}{\partial v_x} d^3v &= \int f \, d^3v = N = \text{electron density}, \end{aligned} \tag{34}$$

we find:

$$\begin{aligned} J_x &= \frac{N\mathbf{e}^2\tau}{m} \mathfrak{E}_x - \mathbf{e}\tau \int v_x^2 \frac{\partial f}{\partial x} d^3v \\ \dot{Q}_x &= -\frac{\mathbf{e}\tau}{2} \mathfrak{E}_x \int v_x v^2 \frac{\partial f}{\partial v_x} d^3v - \frac{m\tau}{2} \int v_x^2 v^2 \frac{\partial f}{\partial x} d^3v. \end{aligned} \tag{35}$$

It is difficult to determine f explicitly, but approximate values for the integrals in (35) can be obtained by assuming $f \approx f_0$, the equilibrium value of the distribution function. A second approximation is necessary in this determination. Since f_0 is known only as a function of T it is required to assume a value for the temperature at the point in question before evaluating the integrals. However, since true thermodynamic equilibrium does not exist there is no strict meaning to temperature. The difficulty may be overcome by assuming a temperature equal to that which would exist in the same body in true thermodynamic equilibrium if it had the same mean value for some such property as the kinetic energy of the electrons. With this sort of assumption (35) becomes:

$$\begin{aligned} J_x &= \frac{N\mathbf{e}^2\tau}{m} \mathfrak{E}_x - \mathbf{e}\tau \frac{\partial}{\partial T} \int v_x^2 f_0 \, d^3v \cdot \frac{dT}{dx} \\ \dot{Q}_x &= -\frac{\mathbf{e}\tau}{2} \int v_x v^2 \frac{\partial f_0}{\partial v_x} d^3v \, \mathfrak{E}_x - \frac{m\tau}{2} \frac{\partial}{\partial T} \int v_x^2 v^2 f_0 \, d^3v \cdot \frac{dT}{dx}. \end{aligned} \tag{36}$$

In this form contact is made with the irreversible formulation since equations (36) are of the form (11) with $(\partial' g / \partial x) = 0$. The irreversible method is, of course, more general than the kinetic one though the main conclusions still hold and, in particular, it is possible to identify the Thomson coefficient as in (18):

$$\mu = T\frac{\partial}{\partial T}\left\{-\frac{\alpha}{\sigma}-\frac{\partial g}{\partial T}\right\}$$

with

$$\sigma = \frac{N\mathbf{e}^2\tau}{m}$$

$$\alpha = -\mathbf{e}\tau\frac{\partial}{\partial T}\int v_x^2 f_0\, d^3v = -\frac{2\mathbf{e}\tau}{3m}NC_{el} \tag{37}$$

where C_{el} is the electronic specific heat per electron, i.e.

$$\mu = T\frac{\partial}{\partial T}\left\{\frac{2}{3}\frac{C_{el}}{\mathbf{e}}-\frac{\partial g}{\partial T}\right\}. \tag{38}$$

The thermoelectric power for the medium is similarly:

$$S = \left(\frac{2C_{el}}{3\mathbf{e}}-\frac{\partial g}{\partial T}\right). \tag{39}$$

5. PARTICULAR CASES

Two elementary cases may be considered:

(*a*) *Metallic conductors.*—For these g is the Fermi energy of the electrons *per unit positive charge*; hence, $g = \zeta/\mathbf{e}$ where ζ is the Fermi energy per electron.

Now,

$$\zeta = \zeta_0 - \frac{\pi^2k^2T^2}{12\,\zeta_0}\cdots$$

where

$$\zeta_0 = \frac{h^2}{8m}\left(\frac{3N}{\pi}\right)^{2/3}$$

its value at $T = 0$, and

$$C_{el} = \frac{\pi^2k^2T}{2\zeta_0},$$

therefore,

$$S = \frac{\pi^2k^2T}{2\mathbf{e}\,\zeta_0} \quad \text{and} \quad \mu = \frac{C_{el}}{\mathbf{e}}. \tag{40}$$

(*b*) *Semiconductors.*—Here

$$\zeta = kT\ln\left\{\frac{1}{2}N\,h^3(2\pi\,mkT)^{-3/2}\right\}$$

and $C_{el} = 3k/2$, assuming a Maxwellian electron distribution, hence:

$$S = \left(\frac{5k}{2\mathbf{e}}-\frac{\zeta}{\mathbf{e}T}\right) \quad \text{and} \quad \mu = \frac{3k}{2\mathbf{e}} = \frac{C_{el}}{\mathbf{e}}. \tag{41}$$

MacDonald (1958) has previously shown that the result $\mu = C_{el}/\mathbf{e}$ follows quite generally from the kinetic argument with the condition of eq. 30 but *without* specific assumptions concerning the electron statistics. The order of magnitude of the result is correct over a wide range of conditions both for metals and semiconductors, showing that the assumptions introduced in the kinetic treatment are reasonably valid. The relevance of Thomson's remark (Thomson 1854) to the effect that μ may be called the specific heat of electricity is readily apparent.

So far the electron transport process has been supposed unaffected by the crystal lattice through which the electrons move. It has been suggested (Gurevich 1945, 1946) that the electrons may receive directed momentum from the lattice waves. The effect on the thermoelectric power may be seen by a small modification of the above simple kinetic argument.

Let us, following MacDonald (1954), assume that the lattice waves exert a pressure, p, on the conduction electrons proportional to u_L, the energy density associated with the lattice waves, i.e. $p = \epsilon u_L$, where ϵ is of order unity. The net force density is therefore given by

$$-\frac{\partial}{\partial T}(\epsilon u_L)\frac{dT}{dx}$$

for a homogeneous medium. Assuming a fraction λ of this force acts on the electrons then the accelerating force per electron becomes:

$$F_x = \mathbf{e}\mathfrak{E}_x - \frac{\lambda}{N}\frac{\partial}{\partial \tau}(\epsilon u_L)\frac{dT}{dx}\,; \tag{42}$$

substituting this in the Boltzmann equation leaves the coefficient σ unchanged but modifies α to:

$$\alpha = -\frac{\mathbf{e}\tau N}{m}\left[\frac{2}{3}C_{el} + \frac{\lambda}{N}\frac{d}{dT}(\epsilon u_L)\right]. \tag{43}$$

On the assumption that no net increase in the internal energy of the electrons results from the electron/lattice wave interaction the irreversible thermodynamic argument remains unchanged and the thermoelectric power becomes:

$$S = \left\{\frac{2}{3}\frac{C_{el}}{\mathbf{e}} - \frac{\partial g}{\partial T} + \frac{\lambda}{N\mathbf{e}}\frac{\partial}{\partial T}(\epsilon u_L)\right\}. \tag{44}$$

6. CONCLUSIONS

It has been shown how irreversible thermodynamic considerations simplify the determination of the various thermoelectric coefficients using kinetic theory arguments based on the Boltzmann equation. In particular an expression for the Thomson coefficient is derived (equation (18)) which does not seem to have appeared previously in explicit form. Although only the simplest models have been considered, the extension to more complex ones is reasonably straightforward. It is immediately apparent, for instance, from equation (11) that the same formal kinetic relationships must hold for a

non-homogeneous material as for a homogeneous one if $\mathfrak{E}_x$ is replaced by $\{\mathfrak{E}_x - (\partial' g/\partial x)\}$. The restriction to a single type of charge carrier can also readily be removed.

ACKNOWLEDGMENTS

The author is indebted to Dr. D. K. C. MacDonald for initiating this study and to both him and Dr. J. S. Dugdale for much helpful discussion in the course of its preparation.

REFERENCES

CALLEN, H. B. 1948. Phys. Rev. **73**, 1349.
DAVIES, R. O. 1957. Repts. Progr. in Phys. **19**, 326.
DE GROOT, S. R. 1951. Thermodynamics of irreversible processes (North-Holland Pub. Co., Amsterdam).
DENBIGH, K. G. 1951. Thermodynamics of the steady state (Methuen & Co. Ltd., London).
DOMENICALI, C. A. 1954. Revs. Modern Phys. **26**, 167.
GUREVICH, L. 1945. J. Phys. U.S.S.R. **9**, 477.
——— 1946. J. Phys. U.S.S.R. **10**, 67.
MACDONALD, D. K. C. 1954. Physica, **20**, 996.
——— 1958. Z. physik. Chemie, **16**, 310.
——— 1959. Science, **129**, 943.
MACDONALD, D. K. C., PEARSON, W. B., and TEMPLETON, I. M. 1958*a*. Phil. Mag. **3**, 657, 917.
——— 1958*b*. Proc. Roy. Soc. A, **248**, 107.
——— 1959. Phil. Mag. **4**, 380.
MOTT, N. F. and JONES, H. 1936. Theory of properties of metals and alloys (Oxford University Press).
ONSAGER, L. 1931. Phys. Rev. **37**, 405; **38**, 2265.
PRIGOGINE, I. 1955. Introduction to thermodynamics of irreversible processes (Blackwell, Oxford).
SOMMERFELD, A. 1956. Thermodynamics and statistical mechanics (Academic Press, Inc., New York).
TER HAAR, D. 1956. Physica, **22**, 61.
THOMSON, W. 1854. Trans. Roy. Soc. Edinburgh, **21**.
WILSON, A. H. 1953. Theory of metals, 2nd ed. (Cambridge University Press).

THE ENERGIES AND RELATIVE PAIR PRODUCTION CROSS SECTIONS FOR Zn^{65} AND Na^{22} GAMMA RAYS

P. P. SINGH, H. W. DOSSO, AND G. M. GRIFFITHS

For gamma rays just above 1.02 Mev a three-crystal pair spectrometer of even moderate resolution can be used to determine the gamma-ray energies very accurately. Since exactly the rest mass of the pair electrons is subtracted from each incident photon by pair production, a measurement of the small remaining kinetic energy of the pair electrons establishes the energy of the gamma rays with considerably greater accuracy than that of the kinetic energy measurement. This method has been used to determine the energies of the gamma rays from Zn^{65} and Na^{22} sources. The spectrometer consists of three sodium iodide (ThI) crystals as shown in Fig. 1. The annihilation of the

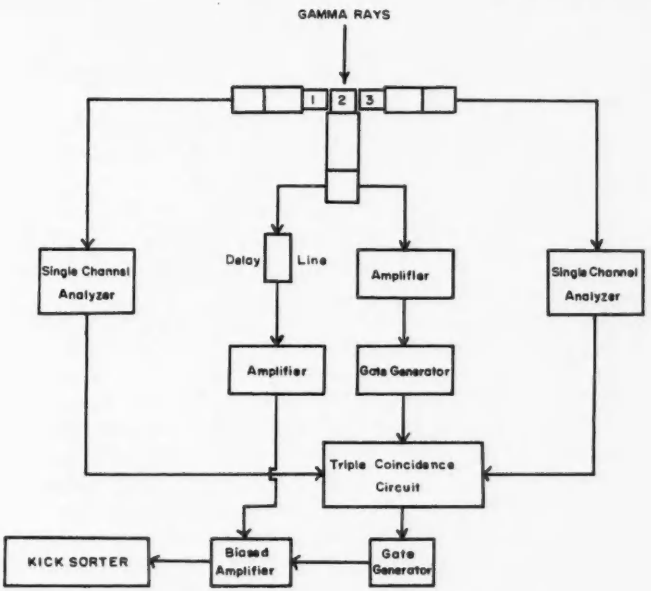

FIG. 1. Block diagram of the three-crystal spectrometer.

positron after the pair event in the center crystal (1.75 cm × 4 cm × 4 cm) gives two .51-Mev quanta which leave the center crystal in opposite directions. The colinear .51-Mev annihilation quanta are detected in coincidence in the

side crystals (2 in. long and $1\frac{3}{4}$ in. diameter). The pulses produced in the side channels enter single-channel differential discriminators which select only those pulses which correspond to .51-Mev absorption in the side crystals. The output from the side-channel analyzers and the pulses from the center channel pass into a triple coincidence circuit. The triple coincidence output pulses open a gate which allows coincident center channel pulses to enter the 30-channel kicksorter. The differential discrimination in the side channels greatly reduces the background due to coincidences from multiple scattering, double Compton events, and cascade gamma rays and so increases the resolution of the apparatus.

The three NaI (ThI) crystals were mounted on RCA 6342 photomultipliers and had a resolution of about 8.3% for 1.3-Mev gamma rays. A 0.2-in. diameter collimated beam of radiation, obtained with a 31-cm long lead collimator, was incident along the center crystal axis. The collimation improved the resolution significantly. Photomultiplier gain changes were kept to a minimum by using stabilized power supplies and relatively low counting rates. No significant gainshifts were recorded over a period of 1 day. The kicksorter spectrum was recorded after every 2 to 3 hours and thus a regular check was kept on the gainshifts. Linearity of the center crystal was established to better than 0.1% for the energy range from 40 kev to 500 kev by the use of a standard pulse generator and gamma-ray sources of known energies from Cs^{137}, Eu^{155}, and Na^{22}.

Typical spectra produced by Co^{60} alone, and by Co^{60} with Na^{22}, and by Co^{60} with Zn^{65} are shown in Fig. 2. Since the Co^{60} γ-rays have been established to better than 1 kev (1.3325±.0003 and 1.1728±.0005 Mev), using a double-focusing spectrometer (Lindstrom 1953) to compare the Co^{60} lines with the accurately known RaC 1.4158±.0002 Mev transition, the energies of the Na^{22} and Zn^{65} γ-rays can be obtained from the present experiment to better than 2 kev.

The individual peaks for each of the gamma rays were isolated graphically by subtracting the typical Co^{60} spectrum and the background from the composite spectra as shown in Fig. 2. Assuming a Gaussian shape for the peaks, the mean energy and the variance of each peak was computed with the help of the University of British Columbia Alwac IIIE Computer. The statistical uncertainty in the mean energy for each peak was also calculated from the variance and total number of counts in the peak; in all cases this uncertainty was not greater than 1 kev. A more realistic estimate of the uncertainty in the mean gamma-ray energies was obtained by calculating the standard deviation in the measured means from seven runs for the Na^{22} and Zn^{65} sources. Since the Na^{22} and Zn^{65} gamma-ray energies were determined by simultaneous measurement with respect to the Co^{60} gamma rays, gainshifts and other systematic errors were effectively cancelled out. The final results of the present experiment are

Zn^{65} gamma-ray energy 1.1124±.0019 Mev,

Na^{22} gamma-ray energy 1.2736±.0018 Mev.

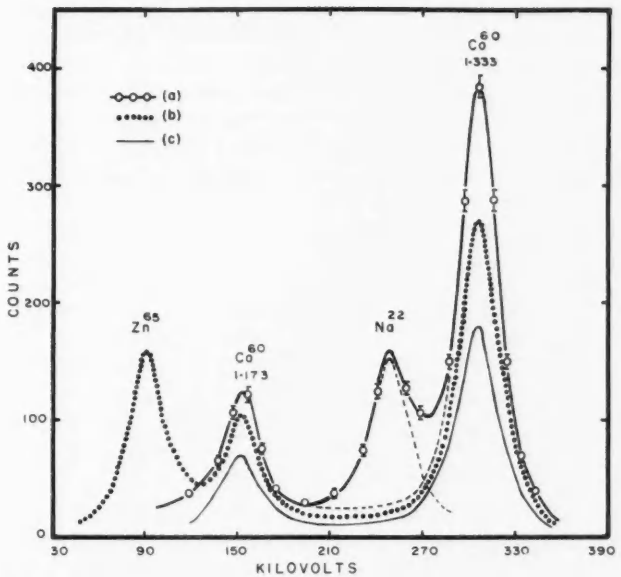

FIG. 2. Typical spectra obtained with three-crystal pair spectrometer. Curve (*c*) is for Co^{60}, curve (*b*) for Co^{60} and Zn^{65}, and curve (*a*) for Co^{60} and Na^{22} gamma rays.

The present results for Zn^{65} gamma rays agree, to within the errors, with those reported by Johanson (1956), 1.112±.003 Mev, and Waggoner (1950), 1.112±.007 Mev; and they are significantly different from those of Hedgran (1950), 1.125 Mev, and Good (1951), 1.127±.009. The Na^{22} gamma-ray energy agrees with that of P. Marmier as reported by Ajzenberg (1955), 1.275±.005. In both cases our estimated errors are less than those reported earlier.

Relative Pair Production Cross Sections

We have also measured the relative pair production cross sections for γ-rays of Zn^{65}, Na^{22}, Co^{60}, and RdTh, using the pair spectrometer. For a source of cascade gamma rays such as Co^{60} the relative pair production cross section is simply obtained from the ratio of the number of counts in the two pair peaks since the number of gamma rays of each energy is the same. This method has been used by Griffiths and Warren (1952) for Co^{60} and Na^{24} gamma rays. West (1956), with much-improved apparatus and a detailed study of the overall efficiency of the three-crystal spectrometer, was able to obtain absolute pair cross sections for the same gamma-ray cascades in both sodium iodide and anthracene. In the present work we have extended the energy range of the measurements of the relative pair production cross sections in sodium iodide by using Zn^{65}, Na^{22}, Co^{60}, and RdTh sources of known strength in exactly the same geometry. Since some of these sources emit only single gamma rays above

1.02 Mev it was necessary to know the relative strengths of the sources in order to obtain relative pair production cross sections. The strength of the sources was independently measured to better than 5% with a sodium iodide scintillation counter employing a crystal $2\frac{1}{2}$ in. in diameter by $3\frac{1}{2}$ in. long whose efficiency as a function of gamma-ray energy had been studied in some detail in this energy range. (Details of this work will be published.) The ratio of pair production cross sections obtained for the gamma-ray energies given in brackets are:

$$\frac{\sigma(2.62)}{\sigma(1.33)} = 16.8 \qquad \frac{\sigma(1.33)}{\sigma(1.17)} = 5.1 \qquad \frac{\sigma(1.17)}{\sigma(1.11)} = 4.22$$

If we take the absolute cross section for the 1.33-Mev gamma rays of Co^{60} from the work of West (1956) as $(6.81 \pm .17) \times 10^{-26}$ cm^2 then these ratios lead to the following absolute pair production cross sections in sodium iodide:

$$(1.11) = (0.32 \pm .03) \times 10^{-26} \text{ cm}^2$$
$$(1.17) = (1.34 \pm .12) \times 10^{-26} \text{ cm}^2$$
$$(2.62) = (116 \pm 10) \times 10^{-26} \text{ cm}^2$$

The errors of about 10% include that quoted by West for the 1.33-Mev gamma ray (about 2.5%) plus statistical and estimated systematic errors introduced by our ratios. The ratios obtained here for pair production by Co^{60}, Na^{22}, and RdTh gamma rays are in good agreement with the results collected by West (1956) and the Zn^{65} result combined with the absolute values given by West for Co^{60} gamma rays provides a measurement of the pair production cross section in sodium iodide at an energy about 90 kev above the pair production threshold.

We are pleased to acknowledge the help of Mr. G. Jones of this laboratory for his assistance with the computer programing. One of us (P.P.S.) gratefully acknowledges the receipt of a National Research Council Studentship.

AJZENBERG, F. and LAURITSEN, T. 1955. Revs. Modern Phys. **27**, 77.
GOOD, M. L. 1951. Phys. Rev. **81**, 891.
GRIFFITHS, G. M. and WARREN, J. B. 1952. Proc. Phys. Soc. A, **65**, 1050.
HEDGRAN, A., SIEGBAHN, K., and SVARTHOLM, N. 1950. Proc. Phys. Soc. A, **63**, 960.
JOHANSON, K. E. 1956. Arkiv Fysik, **10**, 247.
LINDSTROM, G., HEDGRAN, A., and ALBURGER, D. E. 1953. Phys. Rev. **89**, 1303.
WAGGONER, M. A., MOON, M. L., and ROBERTS, A. 1950. Phys. Rev. **80**, 420.
WEST, H. I. 1956. Phys. Rev. **101**, 915.

RECEIVED MAY 19, 1959.
DEPARTMENT OF PHYSICS,
UNIVERSITY OF BRITISH COLUMBIA,
VANCOUVER, B.C.

POSSIBLE CHEMICAL REACTION OF ORTHOPOSITRONIUM WITH OXYGEN

D. A. L. PAUL

It has been shown previously (Paul 1958) that the effect of traces of oxygen in quenching orthopositronium in liquid argon is much greater than was observed by Deutsch (1953) when oxygen was introduced as the impurity in argon gas.

In concluding the above-mentioned experiments (1958) two further measurements were made of the quenching of orthopositronium by oxygen at lower temperatures in liquid nitrogen. As before, the reciprocal of the τ_2 lifetime is plotted against oxygen concentration and a straight line can be fitted to the experimental points, which, however, are subject to rather large uncertainties. From the slope of the line the volume rate, λ^*/n, for the quenching process is obtained, λ^* being the increased annihilation rate due to the presence of n molecules/cm^3 of O_2. When a simple gas–kinetic picture of the quenching process may be assumed, one writes

$$\frac{\lambda^*}{n} = \sigma v \ (\text{cm}^3/\text{sec})$$

where σ is the cross section for the quenching process and v the velocity of positronium. In liquids, however, it would seem plausible to make comparisons of volume rate rather than to use gas–kinetic ideas, where it is clear that they cannot be entirely appropriate. The new results together with the previous results are given in Table I.

TABLE I

Medium	Temperature, °K	Volume rate per molecule O_2, 10^{-13} cm^3/sec units	Author
Argon gas	~300	3.1	Calculated from Deutsch (1953)
Argon liquid	87.5	9.7	Paul (1958)
Nitrogen liquid	77.5	4.0	
Nitrogen liquid	64.7	2.6	

NOTE: The relative values of volume rates in liquid argon and liquid nitrogen are estimated to be accurate to within 20%. Absolute values are probably good to ±20%.

An electron exchange mechanism has been proposed by Ferrell (1958) to account for the high volume rate observed by Deutsch. It is probable, however, that some additional mechanism must be invoked to explain the strong temperature dependence in the neighborhood of 80° K.

A mechanism which would account for the more rapid quenching in liquid than in gaseous argon is the formation of the chemical compound $(e^+ e^-)O_2$. That it is plausible that this positronium compound should be formed may be seen by considering its hydrogen analogue, hydroperoxo, the HO_2 radical. Hydroperoxo, a stable but highly reactive compound, is readily formed from molecular oxygen and atomic hydrogen and has been detected with a mass spectrometer by Foner and Hudson (1953) and by Robertson (1954). Robertson

estimates furthermore that HO_2 formed through bimolecular association would dissociate in about 5×10^{-12} second unless a collisional de-excitation should follow within that time. In three-body collisions, however, it would generally be possible for HO_2 to be formed in the ground state. If these arguments are applied to $(e^+ e^-)O_2$ it is readily seen that a chemically stable compound would be formed much more abundantly, for example, in liquid argon with oxygen impurity than in the gas of identical composition, since the three-body reaction,

$$(e^+ e^-)+O_2+X \Rightarrow (e^+ e^-)O_2+X,$$

would be quite rare in the gas, but probably every collision of $(e^+ e^-)$ and O_2 could be considered to be of this type in the liquid. In the gas phase positronium would generally have undergone annihilation before a three-body collision would occur to form $(e^+ e^-)O_2$ in the ground state; and an excited state of $(e^+ e^-)O_2$ would generally dissociate before annihilation took place, if one allows that the dissociation will not take longer, on the average, than a few times 10^{-12} second. To account for the enhanced quenching in liquid argon, it must then be assumed that the ground state of $(e^+ e^-)O_2$ is short-lived with respect to annihilation, having $\tau \sim 10^{-10}$ second, so that the three-body chemical reaction is in effect competing directly with other modes of annihilation. This condition would surely be fulfilled, since the electron density at the positron must be at least as great in the compound as it is for free positrons in liquid oxygen.

The total volume rate may thus be thought of as made up of a part due to annihilations which are consequent upon free collisions of oxygen and positronium, and the rest a chemical reaction rate. The strong temperature dependence in the neighborhood of 80° K suggests fitting the data to an exponential function, and in fact the three experimental points will yield the constants in an expression of the type

$$\frac{\lambda^*}{n} = A+Be^{-\phi/kT}.$$

It is tempting to identify the second term with the reaction rate, and obtain a value of $\phi \sim 0.09$ ev, i.e., 2000 cal/mole. This quantity is a plausible activation energy for the formation of $(e^+ e^-)O_2$. The value of A obtained is then $2.5\pm0.5\times10^{-12}$ cm^3/sec, less than but hardly different from Deutsch's value for the quenching of orthopositronium by oxygen in argon gas. This last observation suggests that the term A arises from an electron exchange mechanism (Ferrell 1958) and that there is very little, if any, temperature dependence in the quenching arising from this mechanism.

DEUTSCH, M. 1953. Progr. in Nuclear Phys. **3**, 131.
FERRELL, R. A. 1958. Phys. Rev. **110**, 1355.
FONER, S. N. and HUDSON, R. L. 1953. J. Chem. Phys. **21**, 1608.
PAUL, D. A. L. 1958. Can. J. Phys. **36**, 640.
ROBERTSON, A. J. B. 1954. Applied mass spectrometry (The Institute of Petroleum, London), p. 112.

RECEIVED JANUARY 19, 1959.
DEPARTMENT OF PHYSICS,
ROYAL MILITARY COLLEGE OF CANADA,
KINGSTON, ONTARIO, CANADA.

NOISE TRAINS

N. C. GERSON* AND W. H. GOSSARD†

A study of atmospheric noise in the frequency range 1–30 Mc/s was undertaken employing a dynamic spectrograph. The spectrograph included a set of R.F. comb filters whose outputs activated a moving strip recorder. The equipment thus provided an acceptance bandwidth of 500 kc/s with which noise bursts have been studied. During the investigation, it was found that some bursts appear to drift completely through the 500 kc/s frequency interval available. This note describes several of the preliminary results already noticed. Because of the frequency sweep of the atmospherics, the phenomena have been termed "sweepers."

When examined aurally with normal receiving equipment, the passage of a sweeper produces an audible swish, chirp, whistle, etc. The type of sound presented to the ear depended upon the bandwidth acceptance of the receiver and the rate of change of frequency with time ($\Delta f/\Delta t^2$).

The rate of sweeper occurrence in the range 24.0–24.5 Mc/s has been found to equal about 1250/hour between sunrise and sunset. The rate seems variable, and on other occasions the maximum rate exceeded 2300/hour and 4200/hour, respectively. Generally it seems that sweepers at frequencies below 20 Mc/s are received mostly during darkness, while those between 20 and 30 Mc/s, mainly during daylight.

Sweepers already observed in the 500 Mc/s spectrograph cover frequency ranges greater than 75 kc/s. The total duration of an individual sweeper varies from 4 to 18 seconds and undoubtedly greater durations may yet be found. Sweepers may drift through 500 kc/s in less than 0.1 second. On an f–t graph, a typical sweeper begins as t = constant, assumes a value of $\Delta f/\Delta t^2 > 0$, and terminates as f = constant. The time spent by the sweeper in each of these regions is variable. (Values of $\Delta f/\Delta t^2 = 5000$ Mc/sec^2 have already been noted.) The great majority of sweepers drift from high to low frequencies although a few travel in the reverse direction.

It has been found that sweepers appear in trains separated by a somewhat constant time interval. Trains composed of 50 to 100 individual sweepers in 10 minutes have already been noted. Some trains appear to persist for hours. The resolution of the equipment has not permitted detection of significant changes in the dispersion of one sweeper relative to others in the same train.

Sweepers probably originate as solar noise bursts although terrestrial electrical discharges or cosmic noise pulses must also be considered. The repetitive nature of sweepers in a train implies (if they are of solar origin) the existence of some relaxation process in the chromosphere.

*Vice Chairman, Arctic Committee, United States National Committee for the International Geophysical Year.
†Department of Defence.

If sweepers are of terrestrial origin, they may become trapped after radiation, by different magnetic force lines and be reflected successively between the northern and southern hemispheres. In this case, they become an extension of whistlers, except that they occur at much higher frequencies. The periodic radiation of energy may occur from bunched electrons (either in the earth's atmosphere or in interplanetary space) moving in crossed electric and magnetic fields.

RECEIVED MAY 1, 1959.
PRIVATE CONTRIBUTION.

AUTOCORRELATION OF QUANTUM-MECHANICAL WAVE FUNCTIONS

RICHARD BOURRET

I. CORRELATION FIELD THEORIES*

In recent years autocorrelation functions have received a great deal of attention in such disparate studies as statistics, the theory of turbulence, electrical filter analysis, optics, and acoustics. One of the early proposed applications was by Richardson (1926), who suggested the use of the autocorrelation of diffusate concentration instead of concentration itself in the differential equation governing turbulent diffusion. In an equation for turbulent diffusion recently advanced by the author autocorrelation functions play a central role, but in this case they are autocorrelation functions of turbulent velocity fluctuations rather than of the concentration of the diffusate. These velocity autocorrelations are the basic variables in the modern theory of turbulence (e.g. Batchelor 1956). In acoustics the autocorrelation of the pressure field has been usefully employed where noise contamination has been present (e.g. Lyon 1950). In the optical theory of partially coherent radiation autocorrelation functions of the electrical and magnetic fields have been used by Wolf (1954, 1956) and later by the author (Bourret 1959). In these studies the autocorrelation functions are shown to satisfy "field" equations formally identical with the Maxwell equations.

In view of this variety of applications of correlation functions to physical theory, it seems worth while to consider the possibility of a quantum-mechanical autocorrelation function constructed from the state function of a system.

II. DEFINITION OF AUTOCORRELATION FIELD IN QUANTUM MECHANICS

We begin with a definition of the autocorrelation field of a system in an eigenstate of the energy. Designating the associated wave function by $\psi_E(x)$ we define the complex autocorrelation field by

*This material was done under contract Nonr 840(oi) and is contribution No. 235 from the Marine Labaratory, the University of Miami.

$$\phi_E(\eta) = \int \psi_E^*(x)\psi_E(x+\eta)\,dx. \tag{1}$$

Some obvious properties of this function are:

$$\phi_E(-\eta) = \phi_E^*(\eta) \tag{2}$$

$$\phi_E(\eta) \to 0 \qquad \eta \to \pm\infty \tag{3}$$

and

$$\phi_E(0) = 1 \tag{4}$$

on account of the assumed normalization of the wave function. An interesting consequence of our definition is that shifts in the co-ordinate origin of the wave function will leave the autocorrelation function unchanged. Since both quantum mechanics and relativity forfeit classical information in exchange for applicability to non-classical problems, and since general relativity, in particular, forfeits "co-ordinate knowledge" altogether, it may be hoped that the information lost in the transition to the autocorrelation function may be physically inessential.

More knowledge is lost, however, in this transition than mere knowledge of the co-ordinate origin as can be seen from the following: from the usual relation between the wave function and its momentum transform

$$\chi_E(p) = h^{-\frac{1}{2}} \int \psi_E(x) e^{-ipx/\hbar} dx \tag{5}$$

we obtain by inversion and substitution into equation (1)

$$\phi_E(\eta) = \int |\chi_E(p)|^2 e^{ip\eta/\hbar} dp. \tag{6}$$

In the absence of a magnetic field the wave function may be chosen real, and so equation (5) implies that

$$\chi_E(-p) = \chi_E^*(p). \tag{7}$$

We can, therefore, invert (6) and express it as

$$\chi_E(p)\chi_E(-p) = \hbar^{-1} \int \phi_E(\eta) e^{-ip\eta/\hbar} d\eta. \tag{8}$$

Because of our specialization to energy eigenstates $\psi_E(x)$ can be recovered from $\phi_E(\eta)$ providing only that the Hamiltonian be reflection invariant, for in that case the wave function must have even or odd parity (Schiff 1949) and hence, by equation (5), so must $\chi_E(p)$. Equation (8) then shows that $\psi_E(x)$ is determined to within a constant phase factor.

III. OTHER PROPERTIES OF THE AUTOCORRELATION FIELD

From equation (6) it is clear that $\phi_E(\eta)$ is simply the expectation value of the dynamical variable $e^{ip\eta/\hbar}$. This can also be seen by expressing the defining relation, equation (1), in the form

$$\phi_E(\eta) = \int \psi_E^*(x) e^{i\eta p/\hbar} \psi_E(x) dx = \langle e^{i\eta p/\hbar} \rangle_E \tag{9}$$

and regarding p as an operator. From this last relation we see that $\phi_E(\eta)$ can be employed to evaluate the expectation value of any function of the momentum by the operation

$$\langle f(p) \rangle_E = f\left(\frac{\hbar}{i}\frac{d}{d\eta}\right) \phi_E(\eta)|_{\eta=0}. \tag{10}$$

Because the preceding formula can readily be used to obtain the moments of the momentum distribution we see that $\phi_E(\eta)$ corresponds to what is called the moment-generating function in statistics.

An interesting feature of the interpretation of $\phi_E(\eta)$ as an expectation value of a dynamical operator is that it enables us to construct its exact classical analogue. If $P(p)$ is the *classical* momentum distribution, we can for the classical "autocorrelation function equivalent" by forming the function

$$\phi_E(\eta) = \int e^{i\eta p/\hbar} P(p) dp. \tag{11}$$

We may, alternatively, construct it as a time average by the formula

$$\phi_E(\eta) = \frac{1}{T}\int_0^T e^{i\eta p(t)/\hbar} dt \tag{12}$$

where T has been suitably defined.

The preceding definitions of quantum-mechanical autocorrelation function for systems in an energy eigenstate can readily be generalized to general state functions. Consider the general time-dependent state function

$$\psi(x, t) = h^{-\frac{1}{2}} \int c(E) \psi_E(x) e^{-iEt/\hbar} dE \tag{13}$$

where $|c(E)|^2$ is the probability density of the energy states. We generalize our definition simply by including an autocorrelation over time, i.e.

$$\phi(\eta, \tau) = \int_{-\infty}^{+\infty} dt \int dx\, \psi^*(x, t) \psi(x+\eta, t+\tau). \tag{14}$$

Substitution of (13) into (14) yields

$$\phi(\eta, \tau) = \int |c(E)|^2 \phi_E(\eta) e^{-iE\tau/\hbar} dE. \tag{15}$$

This can be replaced by a sum when discrete energy levels are to be used. The case in which $\tau = 0$ takes the specially simple form of a weighted average of the $\phi_E(\eta)$. The classical analogue of (15) is obtained by replacing E with the Hamiltonian for the system and integrating over phase space. The weighting function $|c(E)|^2$ is then replaced by the normalized Gibbsian expression

$$\exp[-H(p, q)/\theta] \tag{16}$$

to give the *canonical* autocorrelation function analogue. θ, as usual, is the modulus of the distribution and is defined by

$$\theta = kT. \tag{17}$$

IV. EXAMPLE OF THE AUTOCORRELATION FIELD, QUANTUM AND CLASSICAL

The harmonic oscillator provides a convenient illustrative example of the autocorrelation field. Using the abbreviations

$$\beta^2 = m\omega/\hbar \tag{18}$$

and

ω = classical angular frequency of oscillator,

we write the wave functions corresponding to the energy

$$E_n = \hbar\omega\,(n+\tfrac{1}{2}) \tag{19}$$

as

$$\psi_n(x) = (2^n n!)^{-\frac{1}{2}}(\beta^2/\pi)^{\frac{1}{4}}\, e^{-\beta^2 x^2/2} H_n(\beta x), \tag{20}$$

where the H_n are Hermite polynomials. Using these functions in the defining equation (1), and employing an expansion theorem for Hermite functions (Morse and Feshbach 1953) we obtain for the autocorrelation field of the nth eigenstate

$$\phi_n(\eta) = \frac{1}{n!}\, e^{-\beta^2\eta^2/4} L_n(\beta^2\eta^2/2) \tag{21}$$

where L_n is the Laguerre polynomial of order n. It is interesting to note that these functions are the axially symmetric solutions of the *two*-dimensional Schrödinger equation

$$\nabla^2\phi + \frac{2m}{\hbar^2}\left(E - \frac{m\omega^2}{2} r^2\right)\phi = 0 \tag{22}$$

with the radial distance r replaced by $\eta/2$, and with the normalization appropriate to autocorrelation functions. This relation to the two-dimensional harmonic oscillator gives some additional insight into the quality of the information lost in the transition from the wave to the autocorrelation function.

The classical autocorrelation function equivalent may be derived from expression (12), taking T to the oscillatory period. For the harmonic oscillation described by

$$x = x_0 \sin\omega\,(t+\delta) \tag{23}$$

and

$$p = mx_0\omega\cos\omega\,(t+\delta)$$

where x_0 and δ are arbitrary, equation (12) readily yields

$$\phi_E(\eta) = J_0\left[\left(\frac{2mE}{\hbar^2}\right)^{\frac{1}{2}}\eta\right] \tag{24}$$

where we have used

$$E = \tfrac{1}{2}m\omega^2 x_0, \tag{25}$$

and J_0 is the Bessell function of order zero.

The *canonical* autocorrelation function for a one-dimensional assembly of harmonic oscillators with a Boltzmann distribution in energy (the Einstein solid) is constructed from equation (15), rewritten as a discrete sum, with the weighting factors

$$Z^{-1}e^{-E_n/\theta} \quad \text{where} \quad Z = \sum e^{-E_n/\theta}. \tag{26}$$

Using the notations

$$\frac{1}{\theta(\tau)} = \frac{1}{\theta} + \frac{i\tau}{\hbar} \quad \text{and} \quad \Delta(\tau) = \tanh\frac{\hbar\omega}{2\theta(\tau)} \tag{27}$$

the calculation yields

$$\phi(\eta, \tau) = \frac{\sinh(\hbar\omega/\theta)}{\sinh\{\hbar\omega/\theta(\tau)\}}\exp\left[-\frac{m\omega\eta^2}{4\hbar\Delta(\tau)}\right]. \tag{28}$$

The special case with $\tau = 0$ and with high temperature will be of interest. It is simply

$$\phi(\eta, 0) = e^{-m\theta\eta^2/2\hbar^2} \tag{29}$$

where

$$\frac{\hbar\omega}{2\theta} \ll 1.$$

The corresponding classical canonical function is obtained from equation (15) by using Gibbsian weights and replacing the energy integral with an integral over phase space. We have:

$$\phi(\eta, \tau) = Z^{-1}\int\int dx dp\, e^{-H(p,x)/\theta(\tau)} J_0\left[\frac{\eta}{\hbar}\sqrt{2mH(p, x)}\right] \tag{30}$$

where Z now has the classical significance

$$Z = \int\int dx dp\, e^{-H(p,x)/\theta}. \tag{31}$$

Substituting the harmonic oscillator Hamiltonian

$$H(p, x) = \frac{p^2}{2m} + \frac{m\omega^2}{2}x^2 \tag{32}$$

into equation (30) we obtain

$$\phi(\eta, \tau) = \frac{\theta(\tau)}{\theta}\exp\left[-\frac{m\theta(\tau)\eta^2}{2\hbar^2}\right]. \tag{33}$$

For $\tau = 0$ this becomes identical with the high-temperature result for quantum-mechanical assemblies.

V. CONCLUSION

From the foregoing it is clear that the autocorrelation function for a quantum-mechanical system is intermediate between the state function and the partition function in the amount of physical information which it carries. If, therefore, further investigations should provide us with a means of calculating it directly (i.e., not via the wave function nor, classically, via the solutions of the equations of motion) it might prove a useful tool when the complete wave-mechanical description is inaccessible and the partition function inadequate.

BATCHELOR, G. K. 1956. The theory of homogeneous turbulence (Cambridge University Press, London).
BOURRET, R. C. 1959. A covariant generalization of the Stokes parameters. J. Optical Soc. Am. (in press).
LYON, R. H. 1956. J. Acoustical Soc. Am. **28**, 76.
MORSE, P. M. and FESHBACH, H. 1953. Methods of theoretical physics (McGraw-Hill Book Co., Inc.), p. 787.
RICHARDSON, L. F. 1926. Proc. Roy. Soc. A, **110**, 209.
SCHIFF, L. I. 1949. Quantum mechanics (McGraw-Hill Book Co., Inc.), p. 139.
WOLF, E. 1954. Nuovo cimento, **12**, 884.
——— 1956. Proceedings of a symposium on astronomical optics and related subjects (North-Holland Publishing Co., Amsterdam), p. 177.

RECEIVED MAY 5, 1959.
THE MARINE LABORATORY,
UNIVERSITY OF MIAMI,
CORAL GABLES, FLORIDA.

ANHARMONIC FORCES AND THE EINSTEIN MODEL OF A CRYSTAL*

J. W. LEECH†

At temperatures near the melting point the specific heats of crystals are sometimes found to exceed the classical values predicted by the harmonic model (see for example Blackman 1955; Berg and Morrison 1957). Such anomalous values have been attributed to the action of anharmonic forces.

The mathematical problem of allowing for anharmonic forces is a formidable one and it is not surprising to find their effect calculated in an approximate manner using the simple Einstein model of a solid (see Henkel 1955; Zucker 1958).

The validity of such an extended Einstein model could be estimated by comparing its predictions with experimental observations. It is doubtful, however, whether existing experimental data are sufficiently accurate in view of alternative explanations in terms of lattice defect formations (see for example Carpenter 1953; MacDonald 1953). The predictions could also be compared with those of a fuller mathematical analysis based on a more

*Issued as N.R.C. No. 5299.
†Now at the Department of Physics, Queen Mary College, University of London, London, England.

obviously justifiable model. There have been such theoretical approaches (see for example Born and Brody 1921; Schrödinger 1922; Peierls 1929; Born 1933; Hooton 1955; Ludwig 1958; Stern 1958) but the conclusions, aside from general predictions concerning temperature dependence, are not yet in a conveniently usable form. In the absence of direct checks on the validity of the anharmonic Einstein model it is useful to make an indirect one by considering the one-dimensional case, which, though unrealistic, has the merit of being mathematically manageable.

An exact classical statistical mechanical analysis of the anharmonic linear chain model, considering only nearest-neighbor interaction, has been made by Damköhler (1935), by Dugdale and MacDonald (1954), by MacDonald and Roy (1955), and by Leibfried (1955). Their values for the excess specific heat at constant length may be expressed as:

$$\Delta C_L = \frac{3Nk^2T}{4D}(\lambda_3{}^2-2\lambda_4)+0(T^2) \approx CT(\lambda_3{}^2-2\lambda_4) \tag{1}$$

where D is the mutual P.E. of two atoms at their equilibrium separation r_0, and the potential energy at separation $r = (r_0+x)$ relative to that at r_0 is given by

$$V = D\{(ax)^2+\lambda_3(ax)^3+\lambda_4(ax)^4+\ldots\}.$$

Damköhler's result differs from the others in the coefficient of the second-order term, but this is immaterial in the present analysis.

In the Einstein model approximation each atom of the chain moves in the field of its two nearest neighbors considered frozen at their equilibrium positions. Effects due to odd-order terms of the potential series cancel out and a short analysis shows that to first order in T:

$$\Delta C_L = CT(-2\lambda_4).$$

In the specific forms normally assumed for the interatomic potential (Morse and Lennard Jones–Mie types) λ_4 is positive and comparable in magnitude to $\lambda_3{}^2$. If we regard (1) as the standard result for the one-dimensional problem, it follows that the cancelling out of the odd-order terms in the analysis of the anharmonic Einstein model leads to serious error in ΔC_L.

There is no guarantee that one-dimensional considerations have any bearing on the three-dimensional problem, but some sort of parallel would be expected. On this basis it appears unlikely that the anharmonic Einstein model will provide reasonable values for the specific heat. This conclusion is at variance with the apparent agreement with experiment of the conclusions of Henkel and Zucker. Domb (private communication) has suggested that one would expect a 'mean' field approximation to be reasonable in three dimensions since the number of nearest neighbors is relatively large. In support he points out that in the corresponding approximation for the Ising model the results are quite wrong in one dimension but reasonable in three dimensions. If this suggestion can be justified in detail it points to the need for caution in extrapolating from conclusions based on one-dimensional analysis. Meanwhile

there still seems to be doubt whether the observed excess specific heats can be attributed to anharmonic forces.

BERG, W. T. and MORRISON, J. A. 1957. Proc. Roy. Soc. A, **242**, 467.
BLACKMAN, M. 1955. Handbuch der Physik, **7** (1), 370.
BORN, M. 1933. Handbuch der Physik, **24** (2), 675.
BORN, M. and BRODY, E. 1921. Z. Physik, **6**, 132.
CARPENTER, L. G. 1953. J. Chem. Phys. **21**, 2244.
DAMKÖHLER, G. 1935. Ann. Physik, **24**, 1.
DUGDALE, J. S. and MACDONALD, D. K. C. 1954. Phys. Rev. **96**, 57.
HENKEL, J. H. 1955. J. Chem. Phys. **23**, 681.
HOOTON, D. J. 1955. Phil. Mag. **46**, 422, 433.
LEIBFRIED, G. 1955. Handbuch der Physik, **7** (1), 269.
LUDWIG, W. 1958. J. Phys. Chem. Solids, **4**, 283.
MACDONALD, D. K. C. 1953. J. Chem. Phys. **21**, 177, 2097.
MACDONALD, D. K. C. and ROY, S. K. 1955. Phys. Rev. **97**, 673.
PEIERLS, R. 1929. Ann. Physik, **3**, 1055.
SCHRÖDINGER, E. 1922. Z. Physik, **11**, 170.
STERN, E. A. 1958. Phys. Rev. **111**, 786.
ZUCKER, I. J. 1958. Phil. Mag. **3**, 987.

RECEIVED MAY 13, 1959.
DIVISION OF PURE PHYSICS,
NATIONAL RESEARCH COUNCIL,
OTTAWA, CANADA.

THERMAL CONDUCTIVITY OF SOLID ARGON AT 80° K

D. J. LAWRENCE, A. T. STEWART, AND E. W. GUPTILL

We have measured the thermal conductivity of solid argon by a simple technique which is suitable for about 10% accuracy. Figure 1 shows a schematic

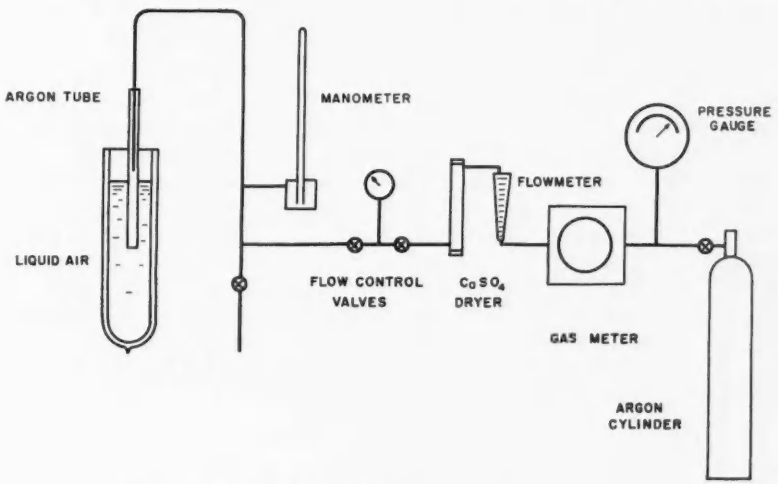

FIG. 1. Schematic diagram of the experimental arrangement.

diagram of the apparatus. Commercial argon flows at a constant rate through a wet-type gas meter and a drying tube into a 2.5-cm diameter precision bore glass tube immersed about 26 cm in liquid air. The argon freezes in a clear polycrystalline layer of uniform thickness on the inside of the glass tube. The heat of sublimation is conducted away through the solid argon and glass layers.

The heat flow, $\dot{Q}$, in a radial direction through a uniform cylindrical shell of thermal conductivity, k, and length, h, is given by

$$\dot{Q} = -k2\pi rh\, dT/dr$$

where dT/dr is the temperature gradient at a distance r from the axis. Integration of this equation through the glass tube and the solid argon shell and elimination of the interface temperature gives

$$\frac{2\pi h\Delta T}{\dot{Q}} = \frac{1}{k_A}\ln(r_1/r)+\frac{1}{k_G}\ln(r_2/r_1)$$

where ΔT is the temperature difference between the solid argon inner surface and the bath. The second term on the right is constant involving only the dimensions and conductivity of the glass, so the solid argon conductivity, k_A, can be obtained from the slope of a graph of $2\pi h\Delta T/\dot{Q}$ versus $\ln(r_1/r)$. The heat, Q, which flows through the solid argon is obtained mostly from the heat of sublimation of solid argon. We used a value of 189 joules/g, which is obtained from the Clausius–Clapeyron equation using the vapor pressure measurements of Clark *et al.* (1951). The remainder of $\dot{Q}$ (up to 10%) is supplied by gas cooling. The amount of heat is calculated from the thermal data of Hilsenrath *et al.* (1955) and the measured temperature change of the gas. The initial temperature was measured just above the solid argon top edge by a thermocouple suspended in the flowing gas. The final temperature of the gas was that of the inner surface of the solid argon, which was obtained by vapor pressure measurement. A plot of solid argon vapor pressure for a typical run is shown in Fig. 2. The flow was stopped three times in this run to enable the slowly changing bath temperature to be measured. The pressure fluctuations in this run are due to occasional sticking of a bath stirrer. These readings were used to calculate the values of ΔT shown in Fig. 3. The corresponding values of $\ln(r_1/r)$ were calculated from the gas meter volume measurements and the solid argon density (Dobbs and Jones 1957). From each of the three sections of Fig. 3 we obtained a value for the slope, and from the weighted average the value of thermal conductivity which is shown.

The error shown is due only to internal consistency in vapor pressure measurements. The systematic uncertainties in the experiment are of the order of 15%. The final average value from seven runs for the thermal conductivity of argon at 80° K is

$$k = 2.6\pm0.4 \text{ mw/cm deg.}$$

This is in reasonable agreement with White and Woods (1958) value, $k = 3.1\pm0.3$ mw/cm deg (taken from their graph), who used quite different techniques of formation of the solid and of measurement.

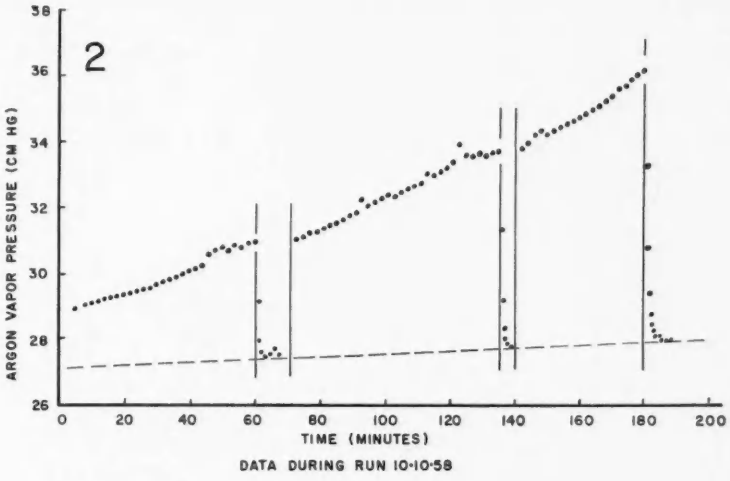

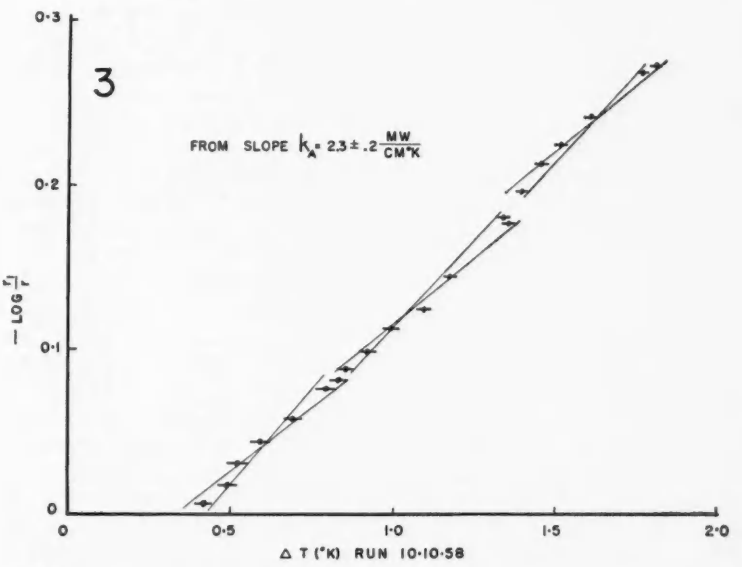

FIG. 2. Typical argon vapor pressure data for one run.
FIG. 3. Plot of log (r_1/r) is a function of ΔT. The argon conductivity k_A is obtained from the slope.

This work was supported by grants from the Defense Research Board and the National Research Council.

CLARK, A. M., DIN, F., ROBB, J., MICHELS, A., WASSENAAR, T., and SWIETERING, TH. 1951. Physica, **17**, 876.
DOBBS, E. R. and JONES, G. O. 1957. Repts. Progr. in Phys. **20**, 516.
HILSENRATH, J., BECKETT, C. W., BENEDICT, W. S., FANO, L., HOGE, H. J., MASI, J. F., NUTTALL, R. L., TOULOUKIAN, Y. S., and WOOLLEY, H. W. 1955. Tables of thermal properties of gases (National Bureau of Standards, Circular 564).
WHITE, G. K. and WOODS, S. B. 1958. Phil. Mag. **3**, 785.

RECEIVED MAY 26, 1959.
PHYSICS DEPARTMENT,
DALHOUSIE UNIVERSITY,
HALIFAX, N.S.

THE DECAY OF Mg^{23}

R. S. STOREY* AND K. G. MCNEILL

Magnesium-23 decays by positron emission with a half-life of 12 seconds. This decay has been studied by a number of authors (Hunt 1954; Boley 1951) and the energy of the beta transition to the ground state of Na^{23} has been found to be 2.95 Mev. The existence of an energy level in Na^{23} at 0.439 Mev above the ground state has been shown by work on the decay of Ne^{23} (Penning 1957) and on coulomb excitation of Na^{23} (Temmer 1956). A positron decay of Mg^{23} to this level is energetically possible, and moreover is allowed on Gamow–Teller selection rules ($(3/2)^+ \rightarrow (5/2)^+$). Such a transition should be followed by a 0.44-Mev gamma ray. In 1939 no gamma ray was observed during experiments on this nuclide (White 1939), but modern techniques are much more sensitive and discriminatory than the absorption methods used by White *et al.* In view of the recent interest in this isobar (Paul and Montague 1958), a search for the 0.44-Mev gamma ray has been made using scintillation spectrometry.

Magnesium, 99.8% pure, in the form of a cylindrical lump $1\frac{1}{4}$-in. diameter by 2 in. long, was irradiated in the bremsstrahlung beam of the 23-Mev betatron of the Ontario Cancer Institute, Toronto. After irradiation for 15 seconds, the magnesium was quickly transferred to a counting position. Here gamma rays from the magnesium could be detected by two 2 in. $\times$ $1\frac{3}{4}$ in. NaI crystals mounted on DuMont 6364 photomultipliers. The two detectors made an angle of 80° to each other, the Mg source being at the point of intersection of the axes of the photomultipliers. Scattering from one crystal to the other was prevented by lead shielding. One of the detectors fed a 100-channel pulse height analyzer (100 PHA). The other fed a single-channel PHA, set to pass pulses of 0.48 to 0.54 Mev. Output pulses from this gated the 100 PHA. Thus into the 100 PHA would pass only those gamma rays in coincidence with positron annihilation quanta. Moreover, the angular separation of the detectors prevented any true coincidences between the annihilation quanta. The resolving time of the coincidence circuit was 1.6 microseconds.

*National Research Council Postdoctorate Fellow.

Counting lasted 15 seconds. After a lapse of a further 15 seconds, a background of 15 seconds was subtracted. The sample was then reirradiated. This cycle was repeated until a sufficient number of counts was accumulated. The removal of background after each count eliminated the effect of build-up of background due to 15-hour Na^{24} made by the reaction $Mg^{25}(\gamma p)Na^{24}$. The results of one such run, as displayed on the 100 PHA, are shown in the figure.

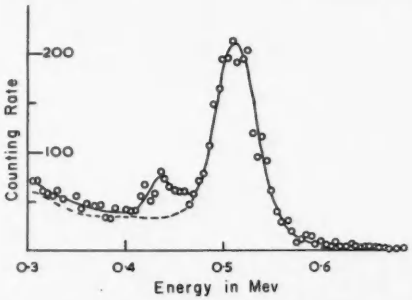

FIG. 1. The spectrum of gamma rays in coincidence with annihilation quanta. The 0.51-Mev peak is due to random coincidences. The dotted line indicates the spectrum obtained from C^{11}, a pure positron emitter, the areas of the 0.51-Mev photopeaks being the same in both cases. The energy scale is calibrated using Na^{22} and Cs^{137} sources.

In the coincidence spectra displayed on the 100 PHA, there were two photopeaks apparent. One, at 0.51 Mev, was due to random coincidences with annihilation quanta, whereas the other, at 0.44 Mev, could not be due to this cause—this fact was checked using C^{11}, a pure positron emitter. We attribute it to the decay of Mg^{23} by the emission of a 2.51-Mev positron followed by a 0.44-Mev gamma ray from the first-excited state of Na^{23}.

An estimate of the relative intensity of the 2.51-Mev positron decay compared with that of the 2.95-Mev decay was made, using the results of the coincidence measurement and the fact that without the coincidence circuit operating, only a slight distortion of the low energy tail of the 0.51-Mev peak was seen at 0.44 Mev. The result is that $0.065 \pm .025$ of the disintegrations are via the excited state of Na^{23}. The inaccuracy quoted is largely due to difficulties of beam control caused by the cycling procedure.

Magnesium-23 has a half-life of 12 seconds. Using the experimental result that 6.5% of the disintegrations are to the excited state of Na^{23}, the partial half-lives for the ground states – excited state transitions are 12.7 seconds and 185 seconds, with $\log_{10} ft$ values of 3.7 and 4.5 respectively. The first value is characteristic of a super allowed transition, caused by the fact that Mg^{23} and Na^{23} are mirror nuclei of each other in their ground states. The value of 4.5 is consistent with the expected allowed character of a 2.51-Mev positron transition.

To summarize, the existence of an allowed transition from the ground state of Mg^{23} to the 0.44-Mev excited state of Na^{23} has been demonstrated.

ACKNOWLEDGMENTS

This work was supported by the National Research Council of Canada Grant BT-84. We wish to express our thanks to Mr. D. Bowman and Mr. J. Pozhke for assisting in the measurements and to the Ontario Cancer Institute for making the betatron available to us.

BOLEY, F. I. and ZAFFARANO, D. J. 1951. Phys. Rev. **84,** 1059.
HUNT, W. A., KLINE, R. M., and ZAFFARANO, D. J. 1954. Phys. Rev. **95,** 611A.
PAUL, E. B. and MONTAGUE, J. H. 1958. Nuclear Phys. **8,** 61.
PENNING, J. R. and SCHMIDT, F. H. 1957. Phys. Rev. **105,** 647.
TEMMER, G. M. and HEYDENBURG, N. P. 1956. Phys. Rev. **104,** 989.
WHITE, M. G., DELSASSO, L. A., FOX, J. G., and CREUTZ, E. C. 1939. Phys. Rev. **56,** 512.

RECEIVED JUNE 10, 1959.
DEPARTMENT OF PHYSICS,
UNIVERSITY OF TORONTO,
TORONTO, ONTARIO.

EXCHANGE REACTION OF 90-MEV PROTONS ON DEUTERONS

D. R. FIRTH

INTRODUCTION

Exchange forces are demonstrated by the appearance of high-energy protons when hydrogen is bombarded by neutrons of energies much greater than the potential well (Fermi 1950).

In like manner one expects fast neutrons from the reaction of fast protons on deuterons. Indeed, predictions for energy and angular distributions of such neutrons are implied in the calculations of Gluckstern and Bethe (1951) and Chew (1951) on the mirror reaction at 90 Mev. Of especial interest is their prediction of a narrow peak only 1 Mev wide at the maximum neutron energy. This maximum energy decreases as the scattering angle increases.

However, the spread of at least a few million electron volts commonly found in the proton beams, as well as the relatively poor resolution of neutron detectors at 90 Mev, means that one cannot accurately check this process by looking at the neutrons. This was demonstrated in the work of Hofmann and Strauch (1953), who attributed the shape of their neutron spectrum to a spread of 25 Mev in proton beam energy.

On the other hand, one may look at the total momentum and total energy of each pair of remaining protons, and from conservation laws deduce the energy and angle of the emitted neutron. The shape of the neutron spectrum is not expected to vary much from, say, 85 Mev to 90 Mev, so that the spectrum of the total pair energy (which is the reverse of the neutron spectrum taken to the origin) will not be blurred by a spread in beam energy. If the incident energy is somewhat uncertain there will be only a small error in the calculated angle of the neutron.

The probability of this reaction, however, will be strongly influenced by

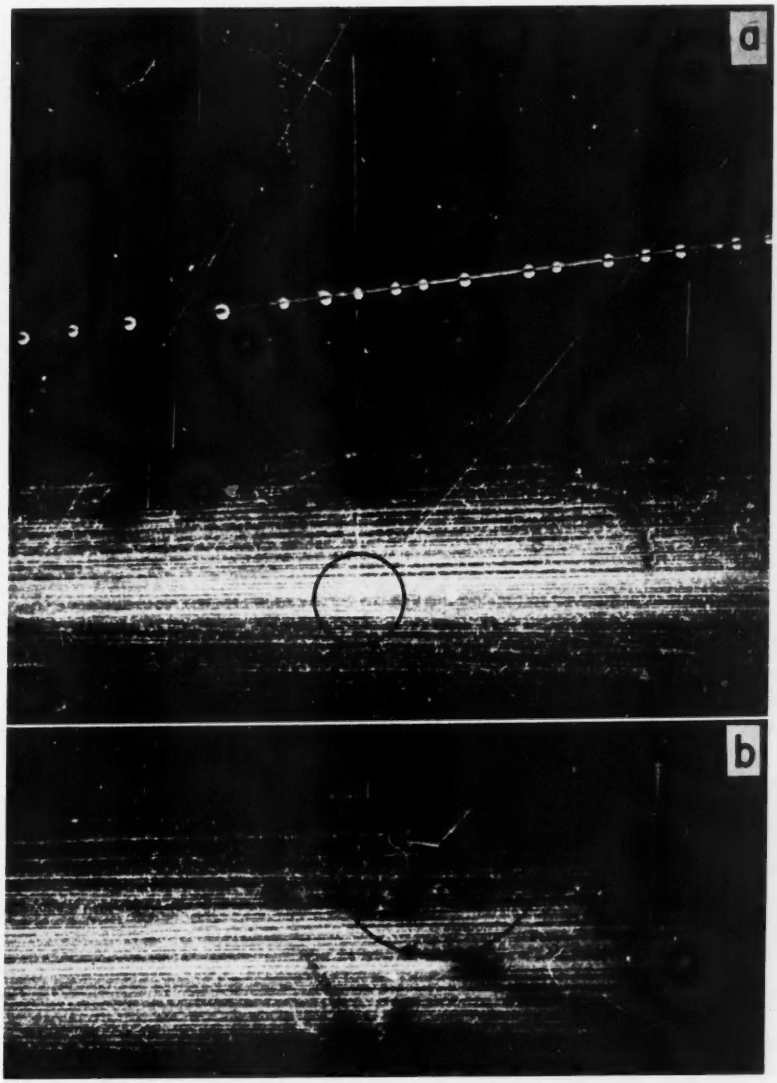

FIG. 1. As an example of the analysis, event 1*a* shows two protons of energy 5.6 Mev and 5.8 Mev. Taking the average incident proton energy as 87 Mev, one finds the neutron emitted at 29°. From Gluckstern and Bethe, for an 87-Mev proton and the neutron off at 30°, the most likely energy for the proton pair is 11.4 Mev, which agrees well with (5.6 plus 5.8) Mev. In its center of mass this proton pair has an energy of 1.4 Mev.

the final state interaction between the slow particles (Watson 1952; Migdal 1955). One can imagine, for example, a primary mechanism of charge exchange between the incident proton and the neutron, leaving two protons with low relative energy, which will therefore have $l = 0$ and $S = 0$. But in the original deuteron these two nucleons have $l = 0$ and $S = 1$, so the charge exchange interaction must also change the spin state. The final state interaction is also largely responsible for the sharpness of the neutron spectrum; final states are favored which have the two protons within p–p virtual resonance.

EXPERIMENTAL

The aim of this note is to show the feasibility of investigating this reaction by means of a diffusion cloud chamber, which was filled to 19 atmospheres with deuterium.

Pulses of protons at 90 Mev from the external beam of the McGill synchrocyclotron were sent through the cloud chamber and photographs were taken 120 milliseconds later. It was possible to use relatively intense proton beams, since the slow protons from the reaction give tracks more than 20 times as dense as 90-Mev protons, and therefore stand out among the mass of tracks.

The photographs (Fig. 1*a* and 1*b*) show two examples of the charge exchange. Preliminary results from several hundred photographs indicate that about one out of every six events is due to charge exchange.

In both figures certain bare patches appear in the beam tracks. These are caused by the passage, some seconds before the proton beam, of an ionizing particle which removes vapor from a considerable region. Another feature typical of a diffusion chamber is the uneven supersaturation throughout the sensitive region, which can cause a track to be less dense at its end than its beginning (see event on Fig. 1*b*).

It is concluded that the neutron–proton exchange force is spin dependent and can be investigated in some detail in this way.

ACKNOWLEDGMENT

The author would like to thank the National Research Council for a scholarship.

CHEW, G. F. 1951. Phys. Rev. **84**, 710.
FERMI, E. 1950. Nuclear physics (University of Chicago Press, Chicago).
GLUCKSTERN, R. L. and BETHE, H. A. 1951. Phys. Rev. **81**, 761.
HOFMANN, J. A. and STRAUCH, K. 1953. Phys. Rev. **90**, 44 p.
MIGDAL, A. B. 1955. J. Exptl. Theoret. Phys. U.S.S.R. **28**, 3.
WATSON, K. M. 1952. Phys. Rev. **88**, 1163.

RECEIVED JUNE 29, 1959.
RADIATION LABORATORY,
MCGILL UNIVERSITY,
MONTREAL, QUE.

MOMENTUM DISTRIBUTION OF ANNIHILATING ELECTRON–POSITRON PAIRS IN LiF

R. H. MARCH AND A. T. STEWART

We have determined the momentum distribution of electron–positron pairs annihilating in LiF in order to resolve the large discrepancy (see Figs. 1(B) and 1(C)) which exists between the results of Lang and DeBenedetti (1957) and Millett and Castillo-Bahena (1957). Our results agree fairly well with Lang's.

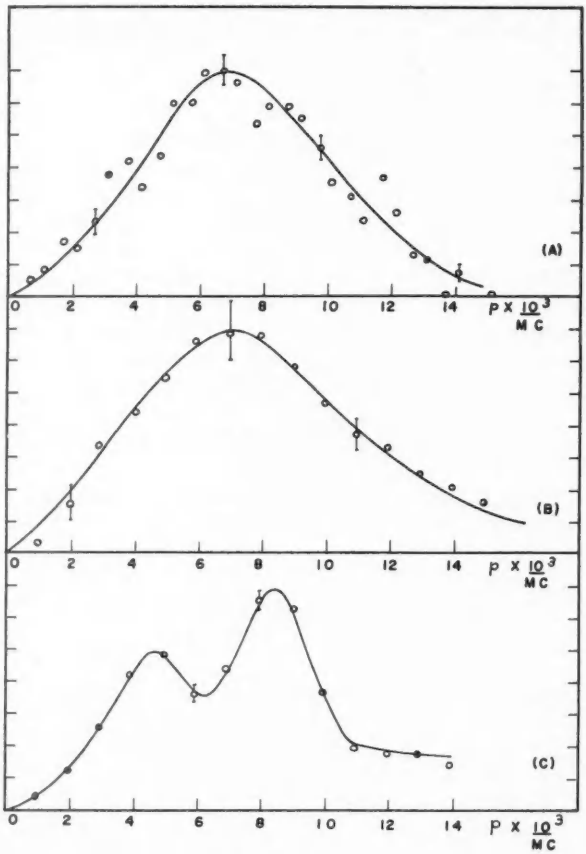

FIG. 1. Momentum distribution of electron–positron pairs annihilating in LiF: (A) this experiment, (B) the distribution obtained by us from Lang's smoothed data (1957), (C) as given by Millett (1957).

Before presenting the various data it is necessary to discuss briefly[1] the experimental arrangements. The technique is the usual one of measuring the angle between annihilation photons to determine their momentum and hence the momentum of the annihilating pair. Lang's apparatus and ours detected annihilation radiation in two scintillation counters mounted behind slits in Pb shields. The source, midway between the counters, was arranged to move at right angles to the plane of the slits. Coincidences were observed as a function of the transverse displacement of the source. The rate of coincidences between the two counters is proportional to the number of events which have a given z component of momentum, p_z, determined by the displacement of the source (taken to be along the z axis).

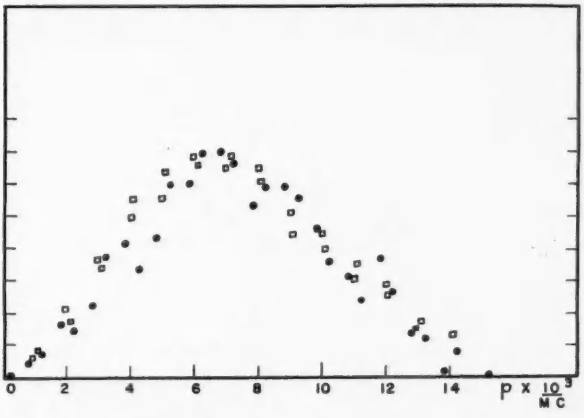

FIG. 2. Comparison of the momentum distribution of electron–positron pairs annihilating LiF and NaF. ● LiF, □ NaF (Stewart and Pope).

Millett's apparatus defined the angle between the annihilation photons by accepting in one counter a narrow pencil of radiation through a small circular aperture, and in the other a cone of radiation defined by an annular aperture in Pb shielding. The angle between accepted photons was varied by inserting annular apertures of different sizes, the relative efficiencies of which must be known. The rate of coincidences between the two counters in this experimental arrangement is proportional to the number of events that have a given radial component of momentum, determined by the angle of the cone. (The polar axis is taken to be the line joining the counters.) From both experimental arrangements the momentum distribution, $N(p)$, may be obtained by an inversion process.

Momentum distributions obtained from an inversion of our data, from an inversion of Lang's data, and by Millett are shown in Fig. 1. It is seen that

[1]A full discussion of these experimental arrangements can be found in the references and A. T. Stewart, Can. J. Physics, **35**, 168 (1957).

Lang's data gives a slightly higher momentum for the peak of the distribution than ours. There is, however, a large discrepancy between both these distributions and that obtained by Millett and Castillo-Bahena. It is possible that such a discrepancy could occur if the relative efficiencies of the various annular apertures used by Millett were not accurately known.[2] This problem is not encountered in the parallel slit arrangement because one slit is used for all angles.

The result obtained for LiF is compared with a similar result for NaF[3] in Fig. 2. The two are similar thus confirming the commonly held hypothesis that most annihilations occur with the electrons of the negative ion.

NOTE ADDED IN PROOF.—Recent data obtained by Dr. Millett is in reasonable agreement with results presented here. We are indebted to him for his courtesy in sending us the new results in advance of publication.

We are grateful to J. M. Robson for the assistance given us in connection with the shipments of Cu^{64} and thanks are due to Atomic Energy of Canada Limited for the loan of equipment.

LANG, G. and DEBENEDETTI, S. 1957. Phys. Rev. **108**, 914.
MILLETT, W. E. and CASTILLO-BAHENA, R. 1957. Phys. Rev. **108**, 257.

RECEIVED JUNE 2, 1959.
DEPARTMENT OF PHYSICS,
DALHOUSIE UNIVERSITY,
HALIFAX, N.S.

[2]It may be noted that humps occur at the same angle, about 6 milliradians in Millett's data for all materials.
[3]We are indebted to Stewart and Pope for these results in advance of publication.

NOTES TO CONTRIBUTORS

Canadian Journal of Physics

MANUSCRIPTS

General.—Manuscripts, in English or French, should be typewritten, double spaced, on paper 8½×11 in. **The original and one copy are to be submitted.** Tables and captions for the figures should be placed at the end of the manuscript. Every sheet of the manuscript should be numbered. Style, arrangement, spelling, and abbreviations should conform to the usage of recent numbers of this journal. Greek letters or unusual signs should be written plainly or explained by marginal notes. Characters to be set in boldface type should be indicated by a wavy line below each character. Superscripts and subscripts must be legible and carefully placed. Manuscripts and illustrations should be carefully checked before they are submitted. Authors will be charged for unnecessary deviations from the usual format and for changes made in the proof that are considered excessive or unnecessary.

Abstract.—An abstract of not more than about 200 words, indicating the scope of the work and the principal findings, is required, except in Notes.

References.—References should be listed **alphabetically by authors' names,** unnumbered, and typed after the text. The form of the citations should be that used in current issues of this journal; in references to papers in periodicals, titles should not be given and only initial page numbers are required. The names of periodicals should be abbreviated in the form given in the most recent *List of Periodicals Abstracted by Chemical Abstracts.* All citations should be checked with the original articles and each one referred to in the text by the authors' names and the year.

Tables.—Tables should be numbered in roman numerals and each table referred to in the text. Titles should always be given but should be brief; column headings should be brief and descriptive matter in the tables confined to a minimum. Vertical rules should not be used. Numerous small tables should be avoided.

ILLUSTRATIONS

General.—All figures (including each figure of the plates) should be numbered consecutively from 1 up, in arabic numerals, and each figure referred to in the text. The author's name, title of the paper, and figure number should be written in the lower left corner of the sheets on which the illustrations appear. Captions should not be written on the illustrations.

Line drawings.—Drawings should be carefully made with India ink on white drawing paper, blue tracing linen, or co-ordinate paper ruled in blue only; any co-ordinate lines that are to appear in the reproduction should be ruled in black ink. Paper ruled in green, yellow, or red should not be used. All lines must be of sufficient thickness to reproduce well. Decimal points, periods, and stippled dots must be solid black circles large enough to be reduced if necessary. Letters and numerals should be neatly made, preferably with a stencil (**do NOT use typewriting**) and be of such size that the smallest lettering will be not less than 1 mm high when the figure is reduced to a suitable size. Many drawings are made too large; originals should not be more than 2 or 3 times the size of the desired reproduction. Whenever possible two or more drawings should be grouped to reduce the number of cuts required. In such groups of drawings, or in large drawings, full use of the space available should be made; the ratio of height to width should conform to that of a journal page (4¾×7½ in.), but allowance must be made for the captions. **The original drawings and one set of clear copies (e.g. small photographs) are to be submitted.**

Photographs.—Prints should be made on glossy paper, with strong contrasts. They should be trimmed so that essential features only are shown and mounted carefully, with rubber cement, on white cardboard, with no space between those arranged in groups. In mounting, full use of the space available should be made. **Photographs are to be submitted in duplicate;** if they are to be reproduced in groups one set should be mounted, the duplicate set unmounted.

REPRINTS

A total of 50 reprints of each paper, without covers, are supplied free. Additional reprints, with or without covers, may be purchased at the time of publication.

Charges for reprints are based on the number of printed pages, which may be calculated approximately by multiplying by 0.6 the number of manuscript pages (double-spaced typewritten sheets, 8½×11 in.) and including the space occupied by illustrations. Prices and instructions for ordering reprints are sent out with the galley proof.

Contents

Beatrice H. Worsley—Scattering factors for some of the heavier atoms - - 967

A. G. Fenton, K. G. McCracken, D. C. Rose, and B. G. Wilson—The onset times of Forbush-type cosmic ray intensity decreases - - - - - - - - 970

J. F. Hart and Beatrice H. Worsley—Approximate wave functions of Pb^{+++} by the method of self-consistent field without exchange - - - - - - - 983

F. D. Manchester—A cryostat for measuring specific heats between 1 and 4.2° K using a mechanical thermal switch - - - - - - - - - - - 989

Lesser Blum and Nora V. Cohan—Orbital following in tetrahedral molecules - 1002

Ll. G. Chambers—The Hund gravitational equations and geons - - - - 1008

J. M. Bowsher—On "plastic" waves in solids - - - - - - - - - - 1017

G. R. DeMille, T. M. Kavanagh, R. B. Moore, R. S. Weaver, and W. White—Rotational states of even-even nuclei - - - - - - - - - - - 1036

J. W. Leech—Irreversible thermodynamics and kinetic theory in the derivation of thermoelectric relations - - - - - - - - - - - - - - 1044

Notes:

P. P. Singh, H. W. Dosso, and G. M. Griffiths—The energies and relative pair production cross sections for Zn^{65} and Na^{22} gamma rays - - - - - - 1055

D. A. L. Paul—Possible chemical reaction of orthopositronium with oxygen 1059

N. C. Gerson and W. H. Gossard—Noise trains - - - - - - - - - 1061

Richard Bourret—Autocorrelation of quantum-mechanical wave functions 1062

J. W. Leech—Anharmonic forces and the Einstein model of a crystal - - 1067

D. J. Lawrence, A. T. Stewart, and E. W. Guptill—Thermal conductivity of solid argon at 80° K - - - - - - - - - - - - - - - - - 1069

R. S. Storey and K. G. McNeill—The decay of Mg^{23} - - - - - - - 1072

D. R. Firth—Exchange reaction of 90-Mev protons on deuterons - - - - 1074

R. H. March and A. T. Stewart—Momentum distribution of annihilating electron-positron pairs in LiF - - - - - - - - - - - - - 1076

Printed in Canada *by* University of Toronto Press